VOLUME 86 NO. WW2
JUNE 1960

JOURNAL of the

Waterways and Harbors Division

PROCEEDINGS OF THE

AMERICAN SOCIETY OF CIVIL ENGINEERS

BASIC REQUIREMENTS FOR MANUSCRIPTS

Original papers and discussions of current papers should be submitted to the Manager of Technical Publications, ASCE. Authors should indicate the technical division to which the paper should be referred. The final date on which a discussion should reach the Society is given as a footnote with each paper. Those who are planning to submit material will expedite the review and publication procedures by complying with the following basic requirements:

1. Titles must have a length not exceeding 50 characters and spaces.

2. A 50-word summary must accompany the paper.

3. The manuscript (a ribbon copy and two copies) should be double-spaced on one side of 8½-in. by 11-in. paper.

4. The author's full name, Society membership grade, and footnote reference stating present employment must appear on the first page of the paper.

5. Mathematics are recomposed from the copy that is submitted. Because of this, it is necessary that letters be drawn carefully, and that special symbols be properly identified.

6. Tables should be typed (ribbon copies) on one side of 8½-in. by 11-in. paper. Specific reference and explanation must be made in the text for each table.

7. Illustrations must be drawn in black ink on one side of 8½-in. by 11-in. paper. Because illustrations will be reproduced with a width of between 3-in. and 4½-in., the lettering must be large enough to be legible at this width. Photographs should be submitted as glossy prints. Explanations and descriptions must be made within the text for each illustration.

8. Papers should average about 12,000 words in length and must be no longer than 18,000 words. As an approximation, each full page of typed text, table, or illustration is the equivalent of 300 words.

9. Papers must be written in the third person.

Reprints from this Journal may be made on condition that the full title of the paper, name of author, page reference, and date of publication by the Society are given. The Society is not responsible for any statement made or opinion expressed in its publications.

This Journal is published quarterly by the American Society of Civil Engineers. Publication office is at 2500 South State Street, Ann Arbor, Michigan. Editorial and General Offices are at 33 West 39 Street, New York 18, New York. $4.00 of a member's dues are applied as a subscription to this Journal. Second-class postage paid at Ann Arbor, Michigan.

The index for 1959 was published as ASCE Publication 1960-10 (list price $2.00); indexes for previous years are also available.

HW.IR.WW.

Journal of the

WATERWAYS AND HARBORS DIVISION

Proceedings of the American Society of Civil Engineers

WATERWAYS AND HARBORS DIVISION
EXECUTIVE COMMITTEE
Joe W. Johnson, Chairman; Richard O. Eaton, Vice Chairman;
Lawrence B. Feagin; Evan W. Vaughan; Robert J. Winters, Secretary

COMMITTEE ON PUBLICATIONS
Jay V. Hall, Jr., Chairman; W. Mack Angas; Joseph M. Caldwell;
Ellsworth I. Davis; James W. Dunham

CONTENTS

June, 1960

Papers

	Page
Shock Pressures Exerted by Breaking Waves on Breakwaters by Shoshichiro Nagai	1
Breakwaters in the Hawaiian Islands by Robert Q. Palmer	39
Prediction of Maximum Practical Berth Occupancy by Thomas J. Fratar, Alvin S. Goodman, and Austin E. Brant, Jr.	69
Navigation Model Studies of New Ohio River Locks by Eugene P. Fortson and George B. Fenwick	79
Analysis of Load Distribution in the Piles of Piers by M. A. Gouda	93
Discussion	117

Copyright 1960 by the American Society of Civil Engineers.

Journal of the
WATERWAYS AND HARBORS DIVISION
Proceedings of the American Society of Civil Engineers

SHOCK PRESSURES EXERTED BY BREAKING WAVES ON BREAKWATERS

By Shoshichiro Nagai,[1] M. ASCE

SYNOPSIS

The results of the studies from April, 1956 to March, 1959 of the shock pressures exerted by breaking waves on composite-type breakwaters are presented. Such hitherto unknown problems as relationships between wave profiles and pressures from instant to instant in plunging of breaking waves into the breakwaters, the velocities of water particles in the breakers, and the behavior of air bubbles entrained in them, were clarified by the synchronised use of a 16 mm high speed movie taken at 3,000 frames per sec and an electro-magnetic oscillograph. A formula for the prediction of the maximum shock pressures and the maximum resultant pressure per unit length of breakwaters were derived.

INTRODUCTION

Since the prediction of shock-pressures exerted by breaking waves on breakwaters is the most important thing to be known for the design of breakwaters, the problem has been studied by a number of harbor engineers and in-

Note.—Discussion open until November 1, 1960. To extend the closing date one month, a written request must be filed with the Executive Secretary, ASCE. This paper is part of the copyrighted Journal of the Waterways and Harbors Division, Proceedings of the American Society of Civil Engineers, Vol. 86, No. WW 2, June, 1960.

[1] Prof. of River and Harbor Engrg., Dept. of Civ. Engrg., Faculty of Engrg., Osaka City Univ., Osaka, Japan.

vestigators during several decades in nature as well as in models in many parts of the world. But very little information has been available in regard to both the theory and the practical data of the shock pressures obtained by measurements in seas, because of the difficulties in the experiments and actual measurements due to the high intensity and instantaneousness of the shock pressures. To the author's knowledge, it seems that there exists no generally accepted formula which is available with sufficient confidence to insure that both safe and economical designs are obtained, being established on the basis of a sufficient number of practical or experimental data.

The author has been studying this subject since 1956 and the experiments are still under way. Over two thousand tests of the shock pressures exerted by breaking waves on the vertical walls of composite-type breakwaters by the use of two or three wave-pressure-gauges have been performed, and the behavior from instant to instant of the breaking waves plunging against the breakwaters, the relationships between the wave pressures and the configuration of the breaking waves, the motion of the water particles in the breaking waves, etc., were measured by means of a 16 mm high speed movie taken at 3,000 frames per sec in synchronism with the pressure gauges. On the other hand, the mechanics of the shock pressures was also studied theoretically. From the results of the theoretical considerations and the experimental data, the new formulas of the maximum shock pressure as well as the vertical distribution of maximum simultaneous shock pressures were established for the vertical walls of composite-type breakwaters.

PROMINENT PAST RESEARCH

Hiroi's Formula.[2]—Owing to I. Hiroi's formula the intensity of the pressures exerted by breaking waves on breakwaters are expressed by the equation, $p = 1.5\, w_0\, H$, in which w_0 represents the unit weight of water and H is the wave height. The pressure expressed by Hiroi's formula corresponds to a dynamic pressure exerted on a vertical wall by the fall velocity and orbital crest velocity of a water particle when the water particle falls down on the still water surface at an angle of 45° from the breaking wave crest. This formula has been used for about forty years in Japan for the calculation of the resultant of shock pressures acted on the unit length of a vertical wall by employing the conventional equation, $P = p \cdot h$, in which h is the height from the top to the bottom of the vertical wall of a breakwater. As is seen from this equation, it is assumed that the shock pressures are uniformly distributed with an average value of p over the total height of the vertical wall. This assumption was obtained from actual experience in a number of composite-type breakwaters in Japan where the tops of the vertical walls of breakwaters have generally been constructed as high as 2 m to 2.5 m above the high water level of the ordinary spring tide. Owing to the experimental results, it was proved that the values of P determined by the conventional method were acceptable in a rough approximation for such low composite-type breakwaters as have been constructed in Japan.

Larras' Experiments.[3]—J. Larras probably gave the first information concerning the time variation of shock pressures exerted by breaking waves

2 "The Force and Power of Waves," by Isamu Hiroi, Engineering, August, 1920.

3 "Le déferlement des lames sur les jetée verticales," by J. Larras, Ponts et Chaussees, May, 1937.

on vertical walls built on slopes. The pressure-time curves obtained in his experimental wave tank were the same types as those shown subsequently in Figs. 10 (a) and (b).

Bagnold's Study.[4]—R. A. Bagnold measured the shock pressures of breaking waves exerted on a vertical wall by a single wave made to break by means of a sloping beach. But he did not investigate the relationships between the shock pressures and the characteristics of waves, as well as the vertical distribution of pressure. After assuming that the shock pressure is caused by an adiabatic compression of the cushion of air enclosed between a vertical wall and the front face of a breaking wave, he established an equation which describes the relationships between the shock pressure and time. It was proved, theoretically as well as empirically, that his equation did not truly describe the phenomenon of shock pressure.[5]

Minikin's Equation.[6]—Using Bagnold's assumption, R. R. Minikin derived the following equation for maximum shock pressures in tons per sq m caused by breaking waves on the vertical breakwaters:

$$p_{max.} = 102.4\ h_1 \left(1 + \frac{h_1}{h_o}\right)\frac{H}{L} \quad \ldots\ldots\ldots\ldots \quad (1)$$

He assumed the maximum pressure $p_{max.}$ to occur always at the still water surface and the vertical distribution of shock pressures exerted on the vertical wall in the same occurrence as $p_{max.}$ to be expressed by

$$p_y = p_{max.} \left(1 - \frac{2y}{H}\right)^2 \quad \ldots\ldots\ldots\ldots\ldots \quad (2)$$

in which p_y is a pressure intensity at a distance y above or below the still water surface.

Eq. 1 is considered to be inadequate in its derivation,[5] and Eqs. 1 and 2 seem to have been derived mostly from Minikins experience with damage in actual breakwaters. As will be shown later, the author's experimental results proved that the values calculated by Eq. 1 from the experimental values were within $\pm$ 60% for the ordinary shock-pressures of breaking waves, but Eq. 1 indicated very great discrepancies for the extraordinary high shock-pressures. The pressure-distribution expressed by Eq. 2 was proved the same as the A-type distribution defined by the author.

The resultant of the total pressures exerted on the unit length of a vertical wall, P, is calculated by the equation

$$P = \frac{1}{3}\, p_{max.}\ H + w_o \frac{H}{2}\left(h_1 + \frac{H}{4}\right) \quad \ldots\ldots\ldots \quad (3)$$

in which the first term in the right hand side of Eq. 2 expresses the dynamic wave-pressure and the second the hydrostatic pressure corresponding to the depth of water at the crest position of the wave.

---

4 "Interim Report on Wave-Pressure Research," by R. A. Bagnold, Journal of the Inst. of Civ. Engrg., Vol. 2, 1938-1939.

5 "Researches of the Shock Pressures of Breaking Waves on Breakwaters," by S. Nagai, Interim Report, Proceedings, 5th Conference of Coastal Engrg., Japan, November, 1958.

6 "Winds, Waves and Maritime Structures," by R. R. Minikin, London, 1950.

EXPERIMENTAL EQUIPMENT AND PROCEDURE

The experiments were carried out in a concrete channel with an overall length of 25m, a width of 2m, and a depth of 1m, at the Field Hydraulic Laboratory of the Osaka City University, as shown in Fig. 1. In order to permit visual observation as well as photographic measurement, the one side of the wave channel in the neighborhood of breakwater-models was made of 10-mm plate-glass. The experimental waves were generated by a flap-type wave-generating machine, and the periods of the waves were changed $T \fallingdotseq 1.2$ to 1.3 sec., 1.5 to 1.6 sec., and 1.9 to 2.0 sec., the heights $H \fallingdotseq 6$ to 22 cm., and the lengths $L \fallingdotseq 2.0$ to 4.5 m. These waves were made to break in front of the

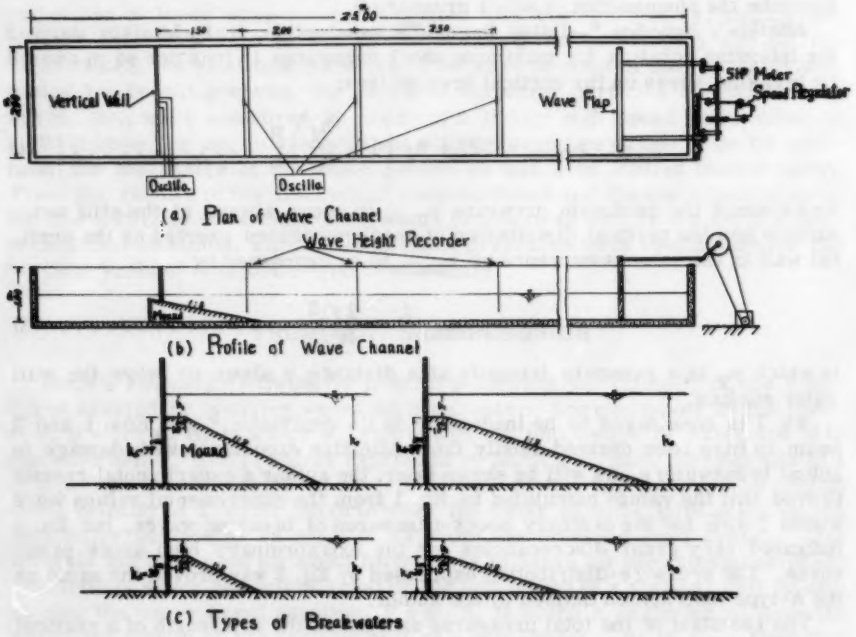

FIG. 1.—LABORATORY EQUIPMENT

breakwaters and to strike severely against the vertical walls by the slopes of rubble-mound which were constructed with wood in the inclination to the horizontal bottom of 1:2, 1:3, and 1:5 as the foundation of the vertical walls. The period, length, and height of the waves were measured by three electric wave-height gauges located at spaces of two and three meters as shown in Fig. 1. The measurement of the shock-pressures of breaking waves were performed by the use of the two or three strain-gauge type pressure-recorders devised specially for this experiment in the laboratory in 1953. The pressure-recorders, which have a phosphor-bronze thin circular plate of a 4-cm diameter, were fed by 5,000 cycles A. C. so as to measure shock-pressures changes occurring within $\frac{1}{500}$ sec.

When a 10-m horizontal width was constructed on the top of the rubble-mound (that is, in front of the vertical wall) with front slopes of 1:2 and 1:3, waves broke easier than in the case when the vertical wall was located on slopes of the same inclination with no horizontal top-width.

But when the slope of the rubble mound was 1:5, most waves broke as a plunging breaker and provided greater impact against the vertical wall than in the case of the 1:2 and 1:3 slopes. The slopes of breakwater-models and the water depths used in the experiments are summerised in Table 1.

Experiments of Solitary Wave.—As the breaker of a solitary wave has been often used for the study of the shock-pressures of breaking waves, some experiments concerned with a breaking solitary wave were performed in the wave channel as shown in Fig. 1. In order to compare the behavior of breaking waves at the instant when the breakers of the solitary wave strikes the vertical wall, the relationships between the shock-pressures and the characteristics of the solitary wave as well as the vertical distribution of the maximum

TABLE 1.—SHAPES OF BREAKWATERS AND WATER DEPTHS

h_d, in cm	Top Width of Mound, in cm	Slope 1:m	h_1, in cm	h_o, in cm	h_1/h_o	h_1/H
(1)	(2)	(3)	(4)	(5)	(6)	(7)
37	10	1:2	0 ~ 29	37 ~ 66	0 ~ 0.440	0 ~ 2.0
37	10	1:3	9 ~ 15	46 ~ 52	0.196 ~ 0.289	0.55 ~ 0.78
20	10	1:2	6 ~ 20	26 ~ 40	0.231 ~ 0.50	0.75 ~ 1.70
20	10	1:3	9 ~ 15	29 ~ 35	0.310 ~ 0.428	0.55 ~ 1.63
37	0	1:2	0 ~ 24	37 ~ 61	0 ~ 0.393	0 ~ 2.0
33 ~ 38	0	1:5	3 ~ 20	40 ~ 57	0.075 ~ 0.351	0.30 ~ 1.0

simultaneous pressures with those in the shallow-water breaking waves were examined. The solitary waves with a height of H = 15.5 cm and a wave cerelity of ω = 2.30 m per sec were made to break in front of the vertical walls by the base-mound, which had a top of a 20-cm horizontal width and a 1:10 front slope. The experiments of a solitary wave were confined to only two cases where the depths in front of the vertical wall, h_1 = 4.4 cm and 6.4 cm, and the depths above the horizontal bottom of the channel, h_o = 41.4 cm and 43.4 cm.

BEHAVIOR OF BREAKING WAVES PLUNGING INTO BREAKWATERS

Configuration of the Water Surface of Breaking Waves before and after Striking against a Vertical Wall.

The Case of Shallow-Water Waves.—The behavior and configuration of the water surface before and after breaking waves plunged into the breakwater-models as shown in Fig. 1 (c) were studied by the use of a 16 mm high speed movie taken at 3,000 frames per sec for the waves of the characteristics and the water depths shown as follows:

a. h_1 = 11.7 cm, $h_1 + h_d = h_o$ = 48.7 cm, T = 1.5 sec, H = 15 cm, L = 264, 264, 272 cm, peak pressure recorded on the pressure-gauge located at 5.7 cm

below SWL = p_{peak} = 43, 59, and 75 gr per sq cm, peak pressure recorded at 7.7 cm below SWL = p_{peak} = 66, 45, and 61 gr per sq cm.

b. h_1 = 13.7 cm, h_o = 50.7 cm, T = 1.25, 1.38, and 1.67 sec, H = 18 to 19 cm, L = 220, 234, and 317 cm, peak pressure recorded at 10 cm below SWL = p_{peak} = 62 to 67 gr per sq cm, the maximum pressure = $p_{max.}$ = 131 to 141 gr per sq cm.

These shallow-water waves struck against the vertical walls of breakwater-models as plunging breakers, accompanied by spray 1m to 1.5 m high.

In the experiments of shallow-water waves, the measurement of pressure and wave-characteristics, as well as the photography were always performed

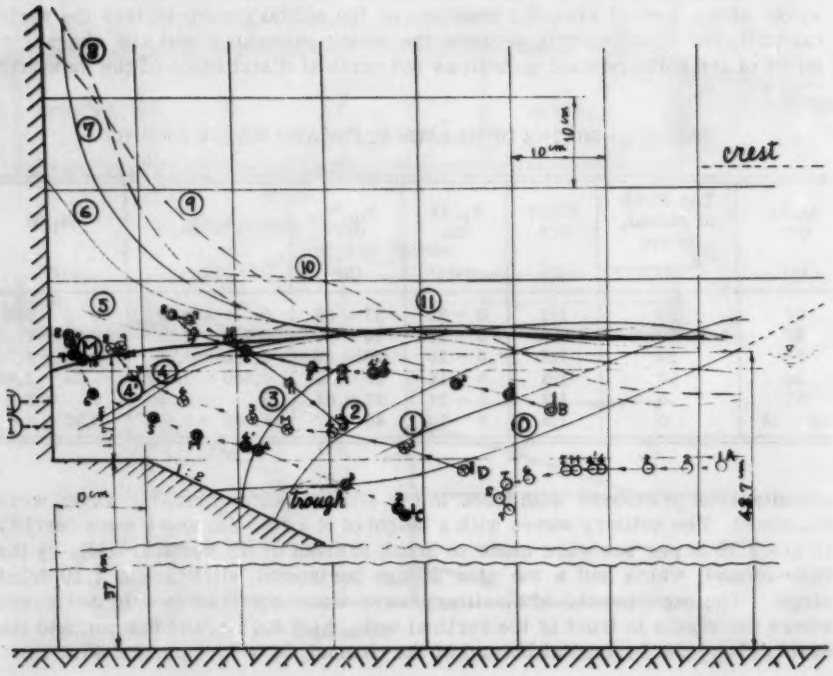

FIG. 2.—WATER SURFACE SHAPES OF A BREAKING WAVE

for several fully developed waves not effected by wave reflections from the vertical wall. The fifth wave in a series of generated waves appears to satisfy these conditions.

Fig. 2 shows the water surfaces or wave-profiles of the fifth wave at intervals of 1/10 sec obtained from the frames of the high speed movie taken for the waves indicated as (a). The paths of motion of water particles are also shown and T = 1.5 sec, L = 272 cm, and H = 15 cm. As is seen in Fig. 2, after the fourth wave which has been retrogressing from the vertical wall meets the coming fifth wave on the slope of the base-mound, it makes the wave-front of the fifth wave a bow-shaped curve with its lower part descending quickly down

on the slope and its upper part pushing up the top of the fifth wave. At the instant when the fifth wave-crest reached the highest point as possible as it can rise and the wave-trough reached the lowest point, the wave-front stops to progress, indicating a height from SWL to the wave-crest, $H_u = 20$ cm and a height from SWL to the wave-trough, $H_l = 14$ cm. Putting $H_u + H_l = H_b$ (height of the breaker), $H_b = 34$ cm, therefore the ratios are obtained

$$\frac{H_u}{H_b} \doteqdot 0.59$$

and

$$H_l/H_b \doteqdot 0.41$$

These values of the ratios are comparatively different from those of $H_u/H_b = 0.75$ and $H_l/H_b = 0.25$ obtained generally in breaking waves caused on long and gentle slopes. It seemed in general that relationships among the height of breakers, H_b, the depth at the point of breaking, h_b, and the height of deep-water waves, H_o, in the breaking waves caused on such short and steep slopes as used in this experiment were comparatively different from those in the breaking waves on long and gentle slopes.

After the wave-front progressed to the locations (0)-(1)-(2)-(3)-(4), as shown in Fig. 2, at intervals of 1/10 sec, toward the vertical wall, the wave broke and gave the hardest blow against the wall at the location of the wave-front (M). Then the wave-front ran up to (5), (6), and (7) at intervals of 1/10 sec along the vertical wall, and then went down to (8), (9), and (10).

A number of air bubbles were observed in the breaking waves before, at, and after the breaking, but the phenomenon, in which those air bubbles were compressed in the waves or the appreciably large masses of air were enclosed and pressed between the wave-front of the breaker and the vertical wall, could not be found notwithstanding Bagnold's assumption.

In the case of the waves indicated as (b), the shapes of the wave-profiles of breakers before and after striking against the vertical wall are nearly the same as in the case of the (a) waves, and the compressing of entrained air bubbles or air-bodies could never be observed.

The Case of Solitary Waves.—The behavior of a solitary wave with a height of H = 15.5 cm and a wave celerity of $\omega = 230$ cm per sec which broke in front and struck against the vertical wall of a breakwater-model, founded on a mound with a top of 20-cm width, a seaward slope of 1:10, and a height of $h_d = 37$ cm, was studied in a depth of $h_1 = 4.4$ cm by the use of a 16 mm high speed movie in order to compare it with the behavior of a breaking waves in shallow-water. The solitary wave produced the maximum pressure $p_{max} = 150$ gr per sq cm slightly above the still water surface by fully breaking just before the vertical wall.

Fig. 3 shows the state of the profile of a breaking solitary wave at various instants at intervals of 1/10 sec and $h_1 = 4.4$ cm, and H = 15.5 cm. At an instant when the water surface of the breaking solitary wave came to the location shown by a (M) line in Fig. 3, the wave pressure indicated the maximum value p_{max}. The lines (2), (3), (4), ----, and (7) show the water surface corresponding to the times (2), (3), (4), ----, and (7) in Figs. 9 (a) and (b). The lines (8), (9), (10), and (11) show the descending state of the water surface. According to these figures, it is seen that the beginning of the pressure-action occurs later on the upper pressure-gauge than on the lower one; on the contrary, the peak pressure acts earlier on the upper gauge than on the lower

one. Therefore it seemed that the masses of air might have been easily enclosed between the wave front and the vertical wall. Nevertheless, the photographs of the high speed movie could not confirm the enclosure of the masses of air as well as the compression of air bubbles entrained in the breaking wave.

Wave Cerelity and Water-Particle Velocity just before and after Striking against a Vertical Wall.

The Case of Shallow-water Waves.—The location of the water surface and of water particles in the breakers before and after shallow-water waves broke in front of and struck against the breakwater-model are shown in Fig. 2. In Fig. 2 the lines ①, ②, ----, and ⑦ show the water surfaces of a plunging

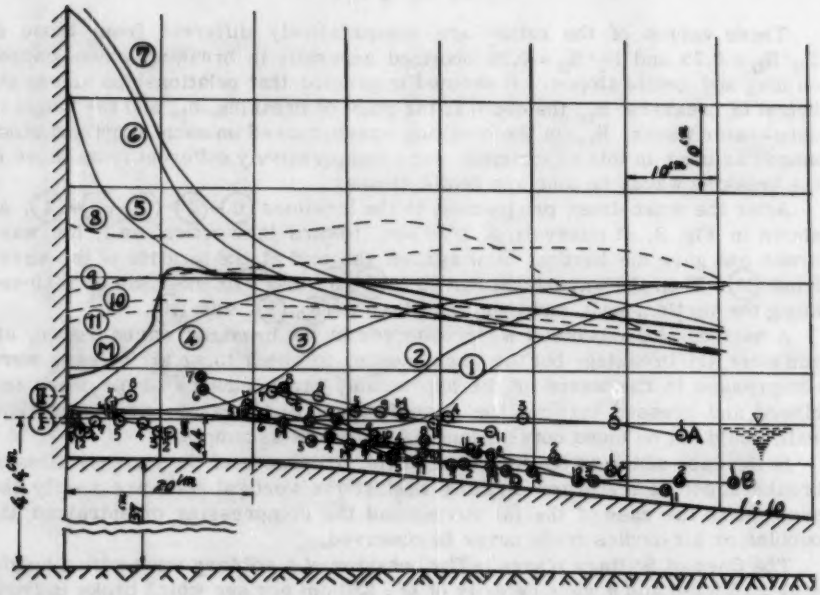

FIG. 3.—WATER SURFACE SHAPES OF A BREAKING WAVE, (SOLITARY WAVE).

breaker and the continued run-up waves at intervals of 1/10 sec and the lines ⑧, ⑨, ⑩, and ⑪ the descending wave surfaces at the same intervals. From Fig. 2 it was found that just before the breaking wave struck against the vertical wall, the wave celerity reached the maximum value, and the horizontal component of the maximum wave celerity reached 200 cm per sec which was slightly greater than $\omega = 182$ cm per sec at the horizontal bottom of the channel.

The paths and velocities of the motion of water particles in the breaking waves were measured by the use of the high speed movie, by throwing into the breakers small spheres made of synthetic resin with diameters of 1.5 cm to 1.9 cm and specific weights of 1.00 to 1.12. The results are shown in Fig. 2, as well as in Table 2.

Table 2 indicates that the velocities of the synthetic resin particles reached the maximum value just before or after the breaking waves struck against the

vertical wall. The diameters of the resin-particles were too large to rush up with the water of a thickness of several centimeters running up along the vertical wall. The path of motion of the A resin-particle shown in Fig. 2 appears to show an elliptic orbit of an underwater particle situated at the back side of the breaking wave. The velocity of the A particle from 1 to 2, u_A = 36 cm per sec can compare favorably with the theoretical maximum horizontal velocity of a water particle on an elliptic orbit at the location, $u_{max.}$ = 31 cm per sec. But the velocities from 2 to 3 and from 3 to 4 are larger than the theoretical velocities of the water particle, probably because of the effect of mass-transport due to the wave breaking.

The Case of a Solitary Wave.—The behavior of the breaking of a solitary wave is comparatively different, as shown in Fig. 3, from that of a shallow-water wave, because the progressive nature of a solitary wave is never su-

TABLE 2.—OBSERVED VELOCITIES OF RESIN PARTICLES IN A BREAKING WAVE SHOWN IN FIG. 2

Location of Particle	Velocity of Particle, in cm per sec			
	A	B	C	D
①~②	36	48	8	...
②~③	46	62	62	70
③~④	50	80	102	80
④~⑤	38	76	120	86
⑤~⑥	42	76	70	80
⑥~⑦	24	60	50	58
⑦~⑧	16	30	24	42
⑧~⑨	18	20	8	14
⑨~⑩	...	50	24	10
⑩~⑪	...	78	...	...
⑪~⑫	...	78	...	...

perimposed with a retrogressive wave reflected by a vertical wall, and the trough of a solitary wave exists always on or slightly above the still water surface.

From Fig. 3 it is known that just before striking against the vertical wall, the celerity of the solitary wave front reached the maximum value 220 to 230 cm per sec which coincided with the wave celerity before breaking, ω = 230 cm per sec. The velocities of the synthetic resin particles at the various locations of the breaking solitary wave are presented in Table 3. As is seen in Fig. 3, the particles in front of the vertical wall indicate only a slight motion, and this is considered to be the result of no retrogressive wave reflected from the wall. Figs. 4 and 5 show the state of the breaking solitary wave shown in Fig. 3 at instants when the wave pressure began to act on the pressure-gauge and when the pressure reached the maximum value respectively.

Behavior of Breaking Waves at the Instant of Peak Pressure.

The Case of Shallow-Water Waves.—The time variation curves of breaking wave pressures produced from oscillograms are shown in Fig. 1 (a) and (b), in which the lines ①, ②, ③, corresponds to the water surfaces ①, ②, ③, shown in Fig. 2, respectively. The curve of Fig. 6 (a) is the record on a lower pressure-gauge located at 7.9 cm below SWL, and the curve of Fig. 6 (b) is the record on an upper pressure-gauge located at 5.3 cm below SWL.

From Figs. 2 and 6, it is known that the wave pressure begins to act at an instant when the breaking wave comes in contact with the pressure-gauge, and reaches the peak value at a very short interval of approximately 1/30 sec to 1/60 sec and drops down at a much shorter interval of 1/100 to 1/500 sec. Fig. 7 shows the state of a breaking wave in Fig. 2 at an instant when the wave pressure began to act on the pressure-gauge. Fig. 8 shows the state of a

TABLE 3.—OBSERVED VELOCITIES OF RESIN PARTICLES IN A BREAKING SOLITARY WAVE SHOWN IN FIG. 3

Location of Particle	Time, in $\frac{1}{120}$ sec	Velocity of Particle, in cm per sec					
		A	B	C	D	E	F
①~②	12	70	60	65	45	10	0
②~③	13	92	85	83	46	7	6
③~④	12	85	70	80	70	18	10
④~⑤	16.5	73	62	69	69	20	1
⑤~⑥	14	60	56	52	43	12	17
⑥~⑦	8.5	51	42	28	21	17	17
⑦~⑧	26.5	25	23	32	41	10	...
⑧~⑨	18	47	57	47	47	31	...
⑨~⑩	17	42	67	39	35	...	...
⑩~⑪	24	33	50	28	25	...	...

breaking wave at an instant when the pressure reached the maximum value for a shallow water wave in Fig. 2. From studies due to synchronizing the oscillograph connected to 3 pressure-gauges, with the high speed movie, it was found that in shallow-water waves the peak pressures at the various elevations of the vertical wall occurred in turn from the bottom of the wall to the highest point of wave run-up.

The Case of a Solitary Wave.—Figs. 9 (a) and (b) show the time-variation curves of the breaker of a solitary wave recorded on a lower pressure-gauge located 0.6 cm below SWL and an upper gauge located 2.0 cm above SWL respectively. The peak pressures in Figs. 9 (a) and (b) are p_{peak} = 95 gr per sq cm and 89 gr per sq cm respectively, and the maximum pressure, p_{max} = 150 gr per sq cm, which occurred at 4.0 cm above SWL. According to Fig. 9, the wave pressure begins to act on the lower pressure-gauge 3/120 sec earlier than on the upper pressure-gauge. On the contrary, the peak pressure occurs on the upper gauge 1/120 sec earlier than on the lower gauge. From the re-

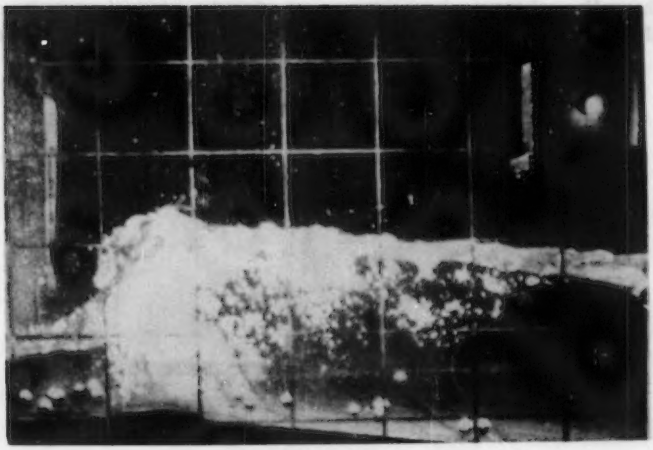

FIG. 4.—INSTANT WHEN WAVE PRESSURE BEGAN TO ACT.

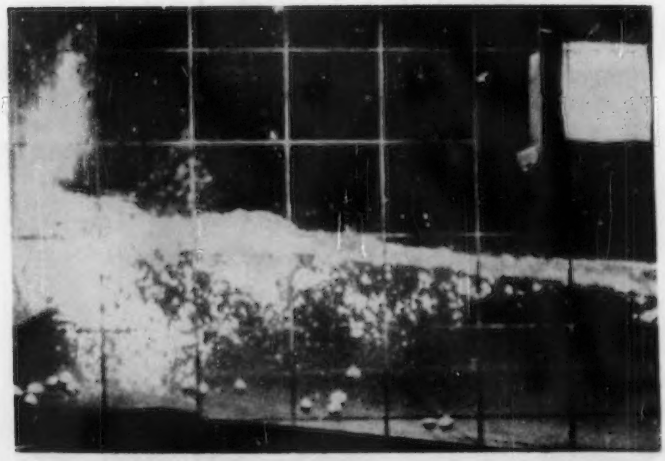

FIG. 5.—INSTANT WHEN PRESSURE INDICATED THE MAXIMUM VALUE

sults obtained in synchronism with the high speed movie and the oscillograph connected with three pressure-gauges, it was found that when a solitary wave broke in front of and struck against a vertical wall, the peak pressure occurred the earliest at a location in which the breaking wave-crest struck against the wall, and the peak pressure at the location was the maximum pressure on the wall. Since the crest of the breaking solitary wave struck at or

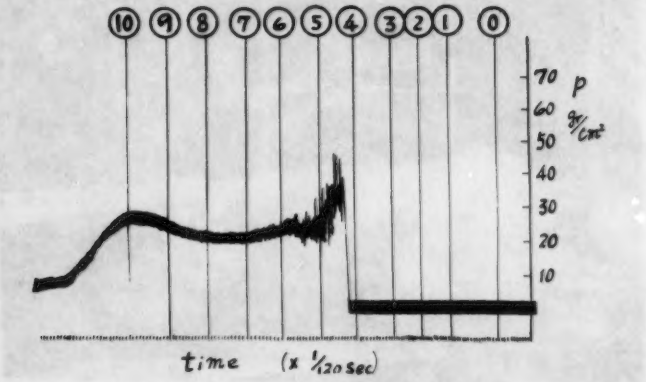

(a) RECORD ON A LOWER GAGE

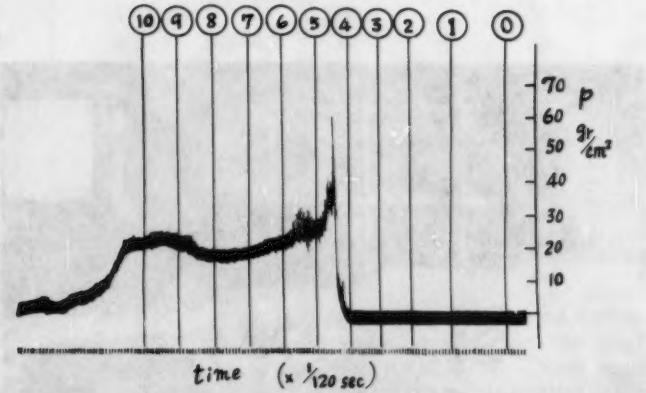

(b) RECORD ON AN UPPER GAGE

FIG. 6.—PRESSURE-TIME CURVES OF THE BREAKING WAVE OF SHALLOW WATER WAVE SHOWN IN FIG. 2.

slightly above SWL against the vertical wall, the maximum pressure occurred always at or slightly above SWL. For example, in Fig. 9 it occurred at 4 cm above SWL. The peak pressures at various heights above SWL did not decrease so quickly with increasing distance above SWL as those did in shallow water breaking waves, indicating p_{peak} = 70 to 100 gr per sq cm even at a distance of a wave-height H = 15.5 cm above SWL for the maximum pressure

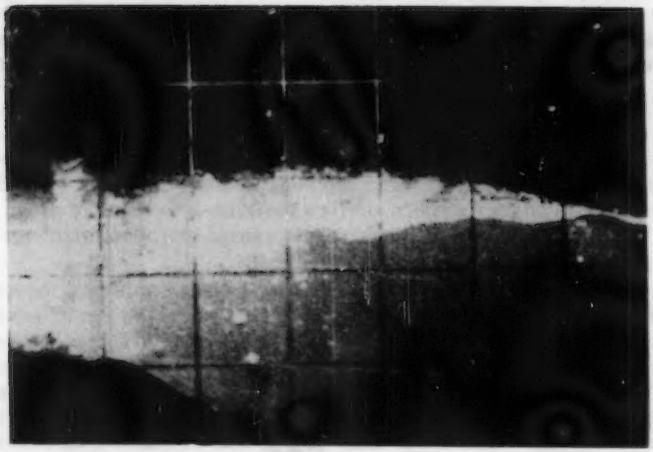

FIG. 7.—INSTANT WHEN WAVE PRESSURE BEGAN TO ACT.

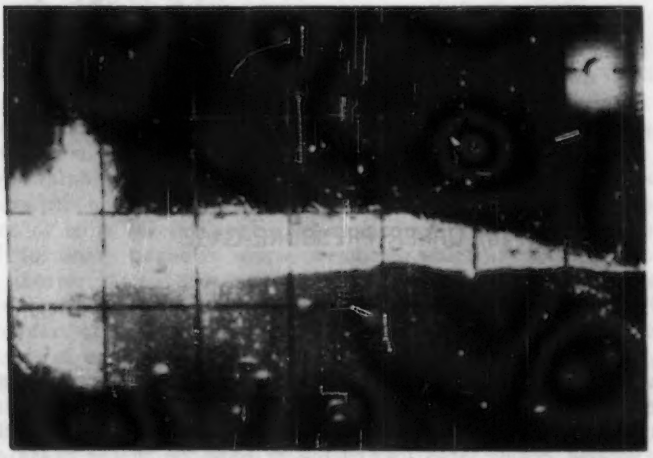

FIG. 8.—INSTANT WHEN PRESSURE INDICATED MAXIMUM VALUE.

on the wall, p_{max} = 150 gr per sq cm. The facts above mentioned show that the behavior of a breaking solitary wave which strikes against a breakwater is distinguishably different from that in a shallow-water breaking wave.

Velocity of Water Running up along a Vertical Wall and Height of Spray.— When the breaker of a shallow-water wave approaches a composite-type breakwater, water particles near the trough of the breaker obtain an upward component of velocity by the effect of the slope of a base-mound. Owing to

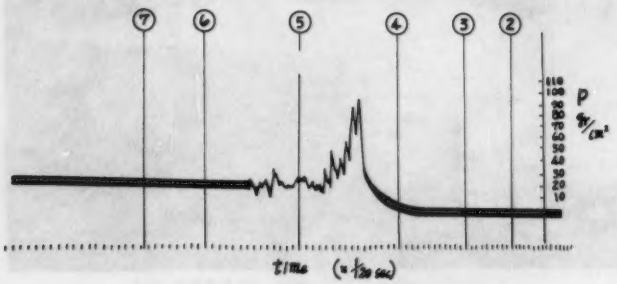

(*a*) LOWER PRESSURE-GAGE

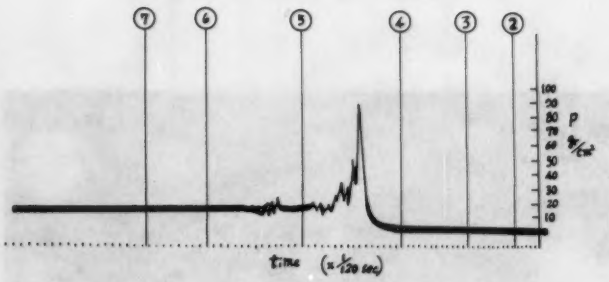

(*b*) UPPER PRESSURE-GAGE

FIG. 9.—PRESSURE-TIME CURVES OF THE BREAKER OF A SOLITARY WAVE SHOWN IN FIG. 3.

this, a submerged flow with opposite direction against a progressive wave cannot occur on the mound slope at an instant and just after the breaking wave strikes against the vertical wall. Therefore it is considered that nearly all of the water volume transported toward the breakwater by the breaking wave runs up with a thin layer of water along the vertical wall. The velocity of water running up along the wall reaches the maximum at the beginning of run-up. The maximum run-up velocity was measured by the use of the high speed movie camera and the oscillograph as $v_{max.} \doteqdot$ 4.1 to 4.3 m per sec, which

agreed well with the computed values by the equation of continuity, using 5 cm as the thickness of the running up water-layer.

Assuming the initial velocity of run-up as $v_{max.} = 4.2$ m per sec which is an average value of the measured velocities, the height of the run-up or the spray is obtained: $\frac{v^2_{max}}{2g} = 0.90$ m. The value compares favorably with the measured height of wave run-up.

Pressure-Time Curves of Breaking Waves.

Kinds of Waves Striking Against Breakwaters.—The configuration of waves observed when breaking against breakwaters changes in a wide range, depending on the types of breakwaters, the characteristics of waves, and the ratio of a water depth in front of a vertical wall to a wave height, h_1/H, and can be divided approximately into three categories as follows:

a. Perfect breaking wave. This is a typical type of breaking wave observed when waves break perfectly just before and strike against the vertical walls of a breakwater. This type of a breaking wave produces an instantaneous and severe shock-pressure on the vertical wall, accompanied by high spray which contains a comparatively small quantity of water.

b. Partial breaking wave. This type of a breaking wave is observed when a wave breaks at a short distance away from a vertical wall, when only a part of a wave-crest breaks in front of the wall, or when a wave with the appearance of a non-breaking wave plunges into the wall, as if it were a jet flow. This type includes all kinds of breaking waves from the perfect breaking wave previously defined to a clapotis.

c. Clapotis. This means a standing wave, which is a kind of non-breaking wave. The condition in which a standing wave is produced in front of the vertical wall of a breakwater was obtained for the steepness of a wave from the experiments, as shown in Fig. 15.

Pressure-Time Curves for Perfect Breaking Waves.—The typical shape of pressure-time curve in "the perfect breaking waves" is shown in Fig. 10 (a). In this type of pressure-time curve it is seen that the wave pressure reaches a peak value at a short interval of 1/30 to 1/60 sec after the beginning of pressure-action, and drops down at a much shorter duration of $\tau = 1/100$ to 1/500 sec which becomes shorter as the peak pressure becomes greater. It sometimes happens in the perfect breaking wave that the peak pressure reach two times or more the peak pressure measured in ordinary breaking waves. Such extraordinary intensive shock-pressures which are supposed to act at an interval shorter than approximately 1/200 sec, do not always occur even at the same conditions. As is seen from the comparison of Fig. 2 with Fig. 6, each wave pressure at various elevations of the vertical wall appears to have indicated its first and higher peak value at an instant when the main part of a breaking wave struck against the elevation on the wall. Then the pressure decreases rapidly as the wave runs up along the wall, and drops down to the trough of the pressure-curve at approximately 1/10 sec after the wave has reached the highest point of the run-up. As the spray (the run-up wave) descends quickly along the wall, the pressure increases again and reaches the second and lower peak value at an instant when the spray stopped to descend. After this the pressure decreases slowly to the initial value, as the spray

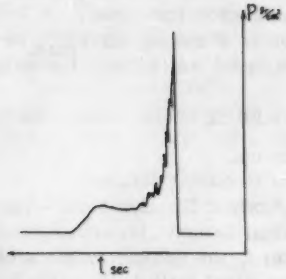

(a) PERFECT BREAKING WAVE

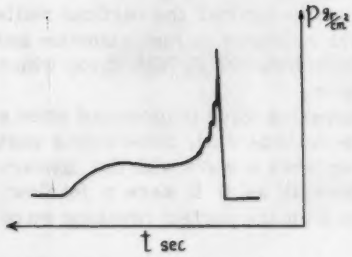

(b) PARTIAL BREAKING WAVE

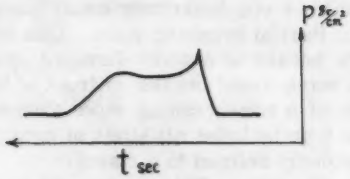

(c) PARTIAL BREAKING WAVE

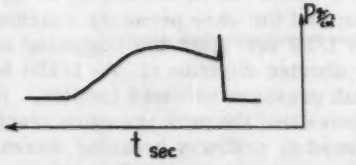

(d) PARTIAL BREAKING WAVE

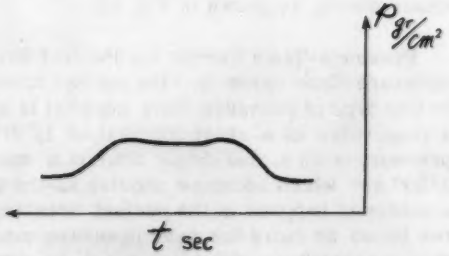

(e) PARTIAL BREAKING WAVE

FIG. 10.—PRESSURE-TIME CURVES

slowly descends to the still water level. As is known from the prior interpretation, the first higher peak pressure is due to a dynamic water pressure generated by the striking of the main part of the breaking wave against the vertical wall, and the second lower peak pressure should be attributed to the fall of the run-up wave. This consideration was proved by the fact that the intensity of the second peak pressure coincided well with a dynamic water pressure-intensity due to the fall of the run-up wave, $p = w_o \frac{v^2}{2g}$, in which v was the fall-velocity of the spray measured by the use of the high speed movie, g the acceleration of gravity, and w_o the unit weight of water.

Pressure-Time Curves for Partial Breaking Waves.—Though the partial breaking wave includes a wide range of breaking waves between the perfect breaking wave and a clapotis, pressure-time curves for the partial breaking waves can be divided approximately into four categories as shown in Figs. 10 (b), (c), (d) and (e).

Fig. 10 (b) shows the typical type of a pressure-time curve for a partial breaking wave most similar to a perfect breaking wave. The first higher peak pressure of this curve is smaller than that for a perfect breaking wave, and in general the time duration of its action is approximately 1/100 to 1/120 sec.

Fig. 10 (c) shows a pressure-time curve for a partial breaking wave not so severe as that corresponding to Fig. 10 (b).

Fig. 10 (d) shows a pressure-time curve recorded when a wave with long period and small steepness partially breaks in front of a vertical wall. The first and sharp peak pressure is attributable to the striking of the partially broken wave-crest against the wall, and the second and low round peak is considered to be due to the weak striking of the main part of the wave against the wall, because there was no appreciable wave run-up along the wall. Therefore the second peak pressure is slightly greater than the static water pressure there.

Fig. 10 (e) shows a pressure-time curve recorded when a wave with comparatively great steepness strikes with such appearance as a clapotis against a vertical wall, the depth in front of which is large as compared with the wave height. The first peak of the pressure-time curve is due to a horizontal dynamic water pressure exerted by the striking of the wave, and the second peak due to a vertical dynamic pressure generated by the fall of the run-up wave.

Vertical Distribution of Wave Pressures.

Vertical Distribution of Peak Pressures over a Wall.—Vertical distribution of peak pressures at various elevations on a vertical wall is affected by the shape of the breakwater and the behavior of the breaking wave. The types of the distribution curves are divided into three categories as follows:

a. A-type distribution. The peak pressures at locations above and below SWL are symmetrically distributed, according to

$$p_y = p_{max.} \left(1 - \frac{y}{H}\right)^2, \quad \ldots\ldots\ldots\ldots\ldots \quad (4)$$

in which p_y is the peak pressure-intensity at a distance of y above and below the location of the maximum pressure.

Figs. 11 (a) and (b) show some experimental data of the A-type distribution.

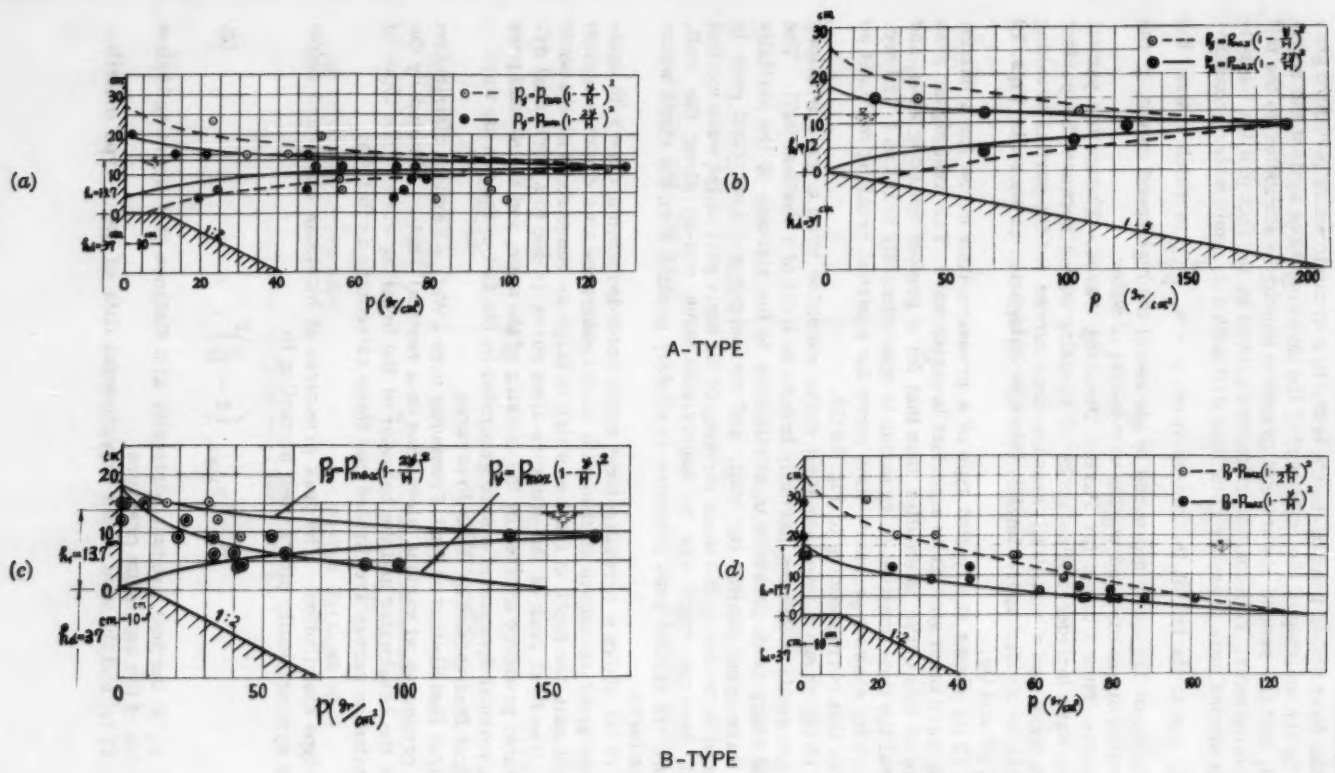

FIG. 11(a),(b),(c),(d).—VERTICAL DISTRIBUTIONS OF PEAK PRESSURES AND MAXIMUM SIMULTANEOUS PRESSURES.

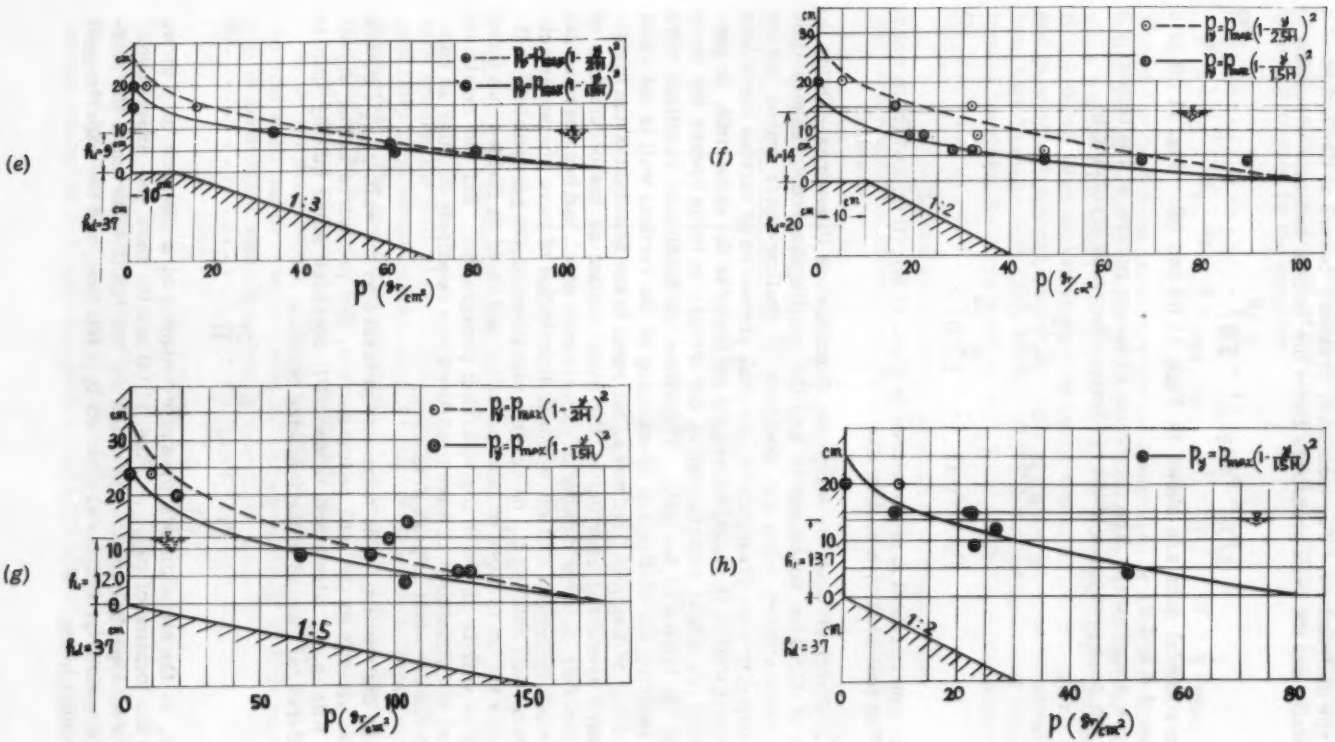

C-TYPE

FIG. 11(e),(f),(g),(h).—FIG. 11 CONTINUED.

b. B-type distribution. The maximum pressure occurs at the bottom of a vertical wall, and the peak pressures above the bottom decrease according to

$$p_y = p_{max.} \left(1 - \frac{y}{2H}\right)^2, \quad \ldots\ldots\ldots\ldots\ldots \quad (5)$$

Some experimental data are shown in Figs. 11 (c) and (d). Fig. 11 (d) is a mixed type of A and B.

c. C-type distribution. The maximum pressure occurs at the bottom of a wall, and the peak pressures above the bottom decrease according to

$$p_y = p_{max.} \left(1 - \frac{y}{2H}\right)^2, \quad \ldots\ldots\ldots\ldots\ldots \quad (6)$$

or

$$p_y = p_{max.} \left(1 - \frac{y}{2.5H}\right)^2, \quad \ldots\ldots\ldots\ldots\ldots \quad (7)$$

Several experimental data are shown in Figs. 11 (e), (f) (g) and (h) in which Eq. 6 or 7 is indicated by a broken line.

Vertical Distribution of the Maximum Simultaneous Pressures.—Owing to the films of the high speed movie and the oscillograms of pressure-time variation curves taken when the breakers of shallow-water waves struck against composite-type breakwaters, the peak pressures at various elevations of the vertical wall of the breakwaters did not occur at the same time. In general, there were slight retardations of occurrence in turns toward the wave crest from the bottom of the wall. Therefore the maximum resultant wave pressure inducing the sliding and overturning of the vertical wall is not equal to the resultant of the peak pressures, but equal to the resultant of the simultaneous wave pressures exerting at the same instant as the occurrence of $p_{max.}$ on the wall. A large number of experiments which had been carried out in this laboratory proved that the vertical distribution of wave pressures acting simultaneously with $p_{max.}$ on various elevations of the vertical wall indicated similar trends to those of peak pressure and could be divided into three categories as will be shown in the following paragraphs. But the maximum resultant of the simultaneous wave pressures was relatively smaller as compared with the resultant of peak pressures.

a. A-type distribution. The maximum pressure on the wall, $p_{max.}$, occurs at or in the vicinity of the still water surface, and pressures acting simultaneously with $p_{max.}$ above and below SWL decrease more quickly than in peak pressures, according to the following equation

$$p_y = p_{max.} \left(1 - \frac{2y}{H}\right)^2 \quad \ldots\ldots\ldots\ldots\ldots (8)$$

in which p_y is the simultaneous pressure-intensity at a distance of y above and below the location of $p_{max.}$. Figs. 11 (a) and (b) show the experimental examples of A-type distribution, in which the distribution curves of the maximum simultaneous pressures are shown by a full line, and the experimental data by double circle.

The resultant, P, of the maximum simultaneous wave pressures acting on the unit longitudinal length of a vertical wall is computed for the case of A-type distribution by the equation

$$P = 2\int_0^{H/2} p_y \cdot dy = 2\, p_{max.} \int_0^{H/2} \left(1 - \frac{2y}{H}\right)^2 \cdot dy = \frac{1}{3} p_{max.} H \quad \ldots (9)$$

Though the conditions necessary for the production of A-type pressure distribution are difficult to decide precisely, they seem to be defined as follows: when waves with short periods of $T \leqq 1.5$ sec and large steepnesses of $H/L \geqq 0.045$ have broken at shallow water depths ($h_1/H \leqq 1.0$) just in front of and have struck against the vertical wall of composite-type breakwaters which have high base-mounds ($S/L \geqq 0.27$) with a 1:2 front slope and the horizontal tops of considerably large width or with a 1:5 front slope, the wave crests attack against the wall at or in the vicinity of the still water surface, exerting generally large shock pressures and sometimes extraordinary severe shock-pressures. The maximum simultaneous pressures indicate the vertical distribution of the A-type curve.

TABLE 4.—SUMMARY OF A-TYPE DISTRIBUTION

Breakwater				T, in sec	h_1, in cm	h_1/h_o	h_1/H	H/L	Simultaneous Pressure Distribution
h_d, in cm	B, in cm	Front Slope 1:m	S/L						
37	10	1:2	$\geqq 0.34$	1.29 ~1.31	6.4 ~13.7	0.147 ~0.270	0.53 ~0.91	0.056 ~0.065	A-type
37	10	1:2	$\geqq 0.30$	1.42	19.7 ~21.7	0.348 ~0.369	1.0 ~1.1	0.071 ~0.073	A-type
37	0	1:5	$\geqq 0.74$	1.29	6.0 ~15.0	0.140 ~0.288	0.42 ~0.69	0.064 ~0.086	A-type
37	10	1:2	0.29	1.5	13.7 ~17.7	0.270 ~0.324	0.79 ~0.96	0.061 ~0.065	A, B Mixed type
37	10	1:2	$\geqq 0.31$	1.5	$\leqq 6.4$	0 ~0.147	0 ~0.53	0.045	A-type

Table 4 is a summary of the A-type distribution.

b. B-type distribution. The maximum pressure occurs at the bottom of a vertical wall, and pressures above the bottom decrease with increasing elevation in accordance with the following quardratic equation

$$p_y = p_{max.} \left(1 - \frac{y}{H}\right)^2, \quad \ldots (10)$$

in which p_y represents the pressure-intensity acting simultaneously with $p_{max.}$ at an elevation of y above the bottom of a vertical wall. The experimental examples of B-type distribution are shown in Figs. 11 (c) and (d).

The resultant, P, of the maximum simultaneous pressures on the unit longitudinal length of a vertical wall is obtained by

$$P = \int_0^H p_y \, dy = p_{max.} \int_0^H \left(1 - \frac{y}{H}\right)^2 dy = \frac{1}{3} p_{max.} H. \quad \ldots\ldots (11)$$

This is the same as Eq. 9.

From Figs. 11 (c) and (d), the B-type distribution appears to occur when waves with large steepnesses of $H/L \geqq 0.050$ and a short period of $T \doteqdot 1.3$ sec have broken at large depths of $h_1/H \doteqdot 1.0$ before reaching the vertical wall and plunged into the bottom of the wall, or have struck as a spilling breaker against the vertical wall of a breakwater which has a high base-mound ($S/L \geqq 0.27$) with considerably wide top, and when waves with moderate periods of $T \doteqdot 1.5$ to 1.6 sec have plunged into the bottom of the vertical wall at moderate depths of $h_1/H \doteqdot 0.6$ to 1.3. But it is difficult to decide precisely the conditions necessary for the production of the B-type distribution, and the B-type distribution is supposed to occur at a transition state from A-type distribution to C-type. The B-type distribution was observed only in a few cases.

c. C-type distribution. The maximum pressure, $p_{max.}$, in C-type distribution also occurs at the bottom of a vertical wall such as B-type distribution, but run-up along the wall is larger than that of B-type, according to

$$p_y = p_{max.} \left(1 - \frac{y}{1.5\,H}\right)^2, \quad \ldots\ldots\ldots\ldots (12)$$

The experimental examples of the C-type distribution are shown in Figs. 11 (e), (f), (g) and (h).

The resultant, P, of the maximum simultaneous wave pressures on the unit longitudinal length of a breakwater is obtained for the C-type distribution by the equation

$$P = \int_0^{1.5H} p_y \, dy = p_{max.} \int_0^{1.5H} \left(1 - \frac{y}{1.5\,H}\right)^2 dy = \frac{1}{2} p_{max.} H \quad \ldots (13)$$

In general the C-type distribution occurs when a wave with large steepness breaks as a spilling breaker at a large water depth of h_1 as compared with the height, h_d, of base-mound, and plunges into the bottom of the vertical wall of a breakwater. Therefore the run-up along the wall is larger than that of B-type.

The conditions in which the C-type distribution occurs are as follows:

(1) At a composite breakwater with the horizontal top of the base-mound When the front slope of the mound is 1:2 and S/L is smaller than 0.27, or the front slope is 1:3 and S/L is equal to or smaller than 0.50.

(2) At a composite breakwater without the horizontal top of the base-mound From all cases when the front slope of the mound is 1:2 to 1:3, and for most of the cases when the front slope of the mound is 1:5.

(3) At a composite breakwater with low base-mound ($h_d/L < 0.12$). For all cases when the front slope of the mound is 1:2, 1:3, and 1:5, no matter what the width B of the top of the mound may be.

(4) Vertical distribution of the maximum simultaneous pressures by breaking waves with a period of 1.9 sec. Since the steepnesses of the waves with a period of 1.9 sec and heights of H = 6.8 cm to 13.2 cm were as small as H/L = 0.019 to 0.033, these waves collapsed weakly in front of the vertical wall of a composite breakwater, the base-mound of which has a 1:2 front slope, a 10 cm-wide top, and a height of 37 cm, acting on the wall considerably smaller pressures than the shock pressures of other breaking waves with short periods of T < 1.9 sec. The vertical distribution of the maximum simultaneous pressures over the wall were also quite different such as the maximum pressure, $p_{max.}$, in each case when h_1 changed from 4.4 cm to 13.7 cm, occurred at the constant elevation of 6 cm above the top of the base-mound and pressures acting simultaneously with $p_{max.}$ decreased above $p_{max.}$ in

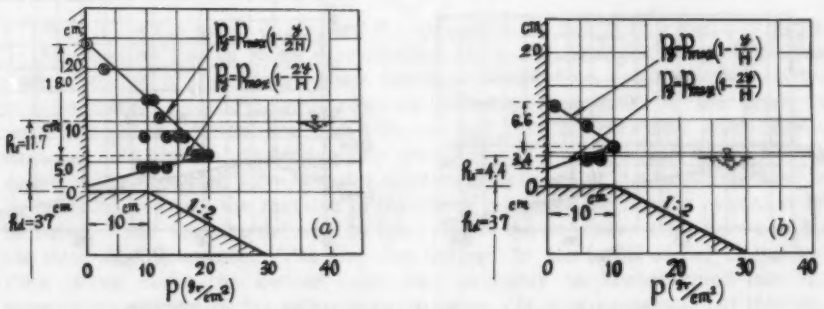

FIG. 12.—VERTICAL DISTRIBUTIONS OF MAXIMUM SIMULTANEOUS PRESSURES

accordance with the rectilinear Eq. 14 and below $p_{max.}$ with the rectilinear Eq. 15, as shown in Figs. 12 (a) and (b) for $h_1 \leqq 6.4$ cm,

$$p_y = p_{max.}\left(1 - \frac{y}{H}\right) \quad \ldots\ldots\ldots\ldots\ldots\ldots \quad (14a)$$

for $h_1 = 8.4 \sim 13.7$ cm

$$p_y = p_{max.}\left(1 - \frac{y}{2H}\right) \quad \ldots\ldots\ldots\ldots\ldots\ldots \quad (14b)$$

and for $h_1 = 4.4 \sim 20.0$ cm,

$$p_y = p_{max.}\left(1 - \frac{2y}{H}\right) \quad \ldots\ldots\ldots\ldots\ldots\ldots \quad (15)$$

When the depth, h_1, in front of the vertical wall reached 24 cm, $h_1/H = 1.82$, $H/L = 0.033$, the intensities and vertical distribution of the pressures became nearly the same as those of clapotis.

Vertical Distribution of the Peak Pressures of a Breaking Solitary Wave over a Wall.—When a solitary wave broke completely at the depths of $h_1 = 4.4$ cm and 6.4 cm just in front of the vertical wall of a composite breakwater which had a base-mound with a top of 20 cm width and a gentle front slope of 1:10, the peak pressures at various elevations of the wall distributed as shown in Figs. 13 (a) and (b). In Figs. 13 the vertical distributions of the peak pressures over the wall by a breaking solitary wave are considerably different from those by breaking shallow-water waves, such that the peak pressures did not decrease so quickly as in the breakers of shallow-water waves, indicating peak pressures as large as 60% to 90% of $p_{max.}$ even on an elevation of $y = 2H$ from the bottom of the wall, and producing run-ups as high as 3H.

Theoretical Considerations for the Shock Pressures of Breaking Waves.

Momentum Equation.—The most important reason for the occurrence of the high shock pressures of breaking waves is considered to be an instantaneous

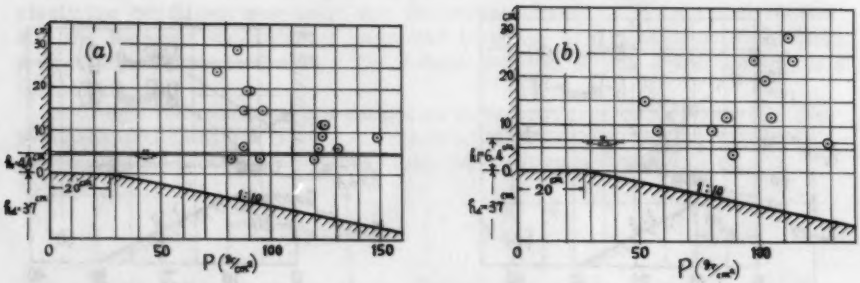

FIG. 13.—VERTICAL DISTRIBUTION OF PEAK PRESSURES OF A BREAKING SOLITARY WAVE

momentum-change due to the striking of breaking waves against a wall. That is, the high shock pressures are due to the fact that the momentum-transport of breaking-waves is not made so continuously as that of jet flows, but abruptly done, and the transported momentum is instantaneously converted into impulse by striking against a wall.

The time-integral of shock pressures during a period exerted by breaking waves on the unit longitudinal length of a vertical wall is

$$I = \int_0^{h_2} \int_0^{\tau} p \, dt \, dh , \quad \ldots\ldots\ldots\ldots\ldots (16)$$

in which h_2 is the height from the bottom of a wall to the wave-crest, and τ represents the duration of the shock pressures of breaking waves.

The volume of water transported by a breaking wave during a period on the unit traverse length of the wave-crest is expressed by Q, the momentum transported by the breaking wave during a period is $\rho Q u_b$, in which u_b is the horizontal water-particle velocity in the breaking wave and is assumed to be constant over all points in the wave. Since the horizontal water-particle velocity u_b at the instant of striking a wall has been proved by the experiments

to be equal to the wave celerity of the breaking wave, ω, Eq. 17 is obtained.

$$\rho\ Q\ u_b = \rho\ Q\ \omega \quad \ldots\ldots\ldots\ldots\ldots\ldots\ (17)$$

for the change of momentum when the breaking wave has struck the vertical wall. This change of momentum must be equal to the impulse of the shock pressure exerted by the breaking wave on the wall, therefore:

$$\rho\ Q\ \omega = \int_0^{h_2} \int_0^{\tau} p\ dt\ dh \quad \ldots\ldots\ldots\ldots\ldots\ (18)$$

If Q is assumed to be approximately equal to the volume of a solitary wave

$$Q = 4\ h_o^2 \sqrt{\frac{H}{3\ h_o}} \quad \ldots\ldots\ldots\ldots\ldots\ (19)$$

in which h_o is the water depth, and H represents the height of a solitary wave.

Interpreting Eq. 18 more specifically, since the first higher and steeper peak pressure of a pressure-time curve produced by a breaking wave is due to a horizontal hydrodynamic pressure caused by the strike of the breaking wave against a vertical wall, and the second, much lower and more gentle peak due to a vertical hydrodynamic pressure caused by the fall of the run-up water of the breaking wave, the net momentum-change of the breaking wave to be transformed into the impulse of the shock pressure during the impact must be equal to the impulse defined by the area of the pressure-time curve under the first peak pressure. The impulse defined by the area of the pressure-time curve under the second peak may probably be transformed into the momentum-change of the retrogressive wave. If it is assumed that this impulse of the second peak pressure is equal to the total momentum which the retrogressive wave has gained, Eq. 18 may be obtained correctly as the momentum transport of the breaking wave is in the reverse direction to the momentum of the retrogressive wave.

For the impulses which have been exerted by perfect as well as partial breaking waves on the vertical walls which were constructed on a 1:5 slope and located on the top of 10 cm width of a base-mound with a 1:2 front slope, the left side of Eq. 18 was calculated by use of Eq. 19, and the right side of Eq. 18 was numerically integrated from the oscillograms obtained by the experiments. Data for nine experimental waves are given in Table 5. From Table 5 the ratios of the impulses to the momentum changes for the six waves are seen to be smaller than one. This may be due to the fact that a part of the momentum is converted to turbulence and into the vertical motion of the spray.

Derivation of an Equation for Shock Pressure.—Expressing the mass transport per unit area of a breaking wave during a duration τ of the first peak shock pressure of a pressure-time curve by ρ l, Eq. 18 yields

$$\int_0^{\tau} p\ dt = \rho\ l\ \omega, \quad \ldots\ldots\ldots\ldots\ldots\ (20)$$

TABLE 5.—MOMENTUM

Characteristics of Wave			h_1, in cm	h_o, in cm	Q, in cu cm	ω, in cm per sec
H, in cm	L, in cm	T, in sec				
8.5	300	1.6	4.6	42.6	1880	187
11.7	200	1.2	5.6	42.6	2080	170
12.7	272	1.5	6.4	43.4	2350	179
12.8	271	1.5	8.4	45.4	2520	176
14.0	282	1.5	11.7	48.7	2930	187
14.3	315	1.6	17.7	54.7	3520	195
17.2	258	1.4	13.7	50.7	3460	187
16.3	308	1.6	19.7	56.7	3986	200
16.1	319	1.6	21.7	58.7	4135	207

in which l is an assumed length of a water column transported during τ. A value of 3 cm to 5 cm has been obtained for l from the experiments. Putting the left side of Eq. 20 approximately

$$\int_0^{\tau} p \, dt = k \, p_{peak} \, \tau \quad \ldots\ldots\ldots\ldots\ldots (21)$$

Eq. 20 yields

$$p_{peak} = \frac{\rho}{k} \frac{l \omega}{\tau} \quad \ldots\ldots\ldots\ldots\ldots (22)$$

for gravity unit

$$p_{peak} = \frac{w_o}{k g} \frac{l \omega}{\tau} \quad \ldots\ldots\ldots\ldots\ldots (23)$$

in which g is the acceleration of gravity, and w_o is equal to ρ g.

As previously mentioned, since the duration τ of the first peak pressure, p_{peak}, of the pressure-time curve of a breaking wave is very short (such as 1/100 sec to 1/500 sec) it may be assumed that the pressure-time curve of p_{peak} is approximately triangular, that is, k = 1/2. Hence from Eq. 23

$$p_{peak} = 2 \frac{w_o}{g} \frac{l \omega}{\tau} \quad \ldots\ldots\ldots\ldots\ldots (24)$$

This is the basic equation for the shock pressures of breaking waves, from which formulas for the maximum shock pressures of ordinary and extraordinary breaking waves have been derived and are presented here. If the shock pressures (the first peak pressures) were caused by a water-hammer phenomenon, the theoretical peak values should be of the order of 10 to 100 times the peak pressures obtained from the experiments, and the theoretical duration of the peak pressures should be of the order of 1/100 the duration observed in the experiments. Therefore it is correctly considered that there

$\rho Q \omega$, in gr cm per sec x 10^3	$\iint p\,dt\,dh$, in gr cm per sec x 10^3	$\frac{\iint p\,dt\,dh}{\rho Q \omega}$	Base-mound
351	334	0.95	B=0, 1:5
354	327	0.92	B=0, 1:5
421	406	0.96	B=10 cm , 1:2
443	443	1.00	B=10 cm , 1:2
548	595	1.08	B=10 cm , 1:2
686	907	1.32	B=10 cm , 1:2
647	626	0.97	B=10 cm , 1:2
797	598	0.75	B=10 cm , 1:2
855	723	0.85	B=10 cm , 1:2

does not exist any water-hammer phenomenon at an instant when breaking waves strike breakwaters, and only in this respect does the author agree with Bagnold's consideration.[4]

If it is assumed for comparatively weak partial breaking waves that horizontal water-particle velocities at the wave-crest are constantly equal to ω during the duration of the peak pressures, which are generally $\tau \doteqdot 1/80$ to 1/100 sec, the assumed length l can be written as

$$l = \tau \omega, \quad \ldots\ldots\ldots\ldots\ldots\ldots (25)$$

Hence Eq. 24 yields

$$p_{peak} = 2 \frac{w_o}{g} \omega^2. \quad \ldots\ldots\ldots\ldots\ldots\ldots (26)$$

This means that the peak pressure in a comparatively weak partial breaking wave is equal to 2 times the hydrodynamic pressure of a jet flow on a wall perpendicular to the jet. A comparative number of peak pressures corresponding to the p_{peak} of Eq. 26 were observed in the experiments of weak partial breaking waves.

Formula for the Maximum Shock Pressure.

Derivation of a Formula for the Maximum Shock Pressure.—Since the peak pressure in a pressure-time curve of a breaking wave at a point on a vertical wall is expressed analytically by Eq. 23, the maximum value of the peak pressures at various elevations on a vertical wall must also be expressed by the same equation as Eq. 23, in which l and τ cannot be obtained analytically except for a comparatively weak partial breaking wave, as previously mentioned. Therefore it is necessary that they be replaced with other factors easily measurable.

Main factors with which the value of $p_{max.}$ is affected are considered as follows:

a. Ratios of a depth h_1 in front of a vertical wall to a depth h_o over a part of horizontal bottom and a wave-height H therein, that is, h_1/h_o and h_1/H.

b. Width of the top of a base-mound, B, and its height h_d.
c. Wave-steepness H/L.

Since l and τ should be replaced with these various factors, from a dimension analysis

$$l = k_1 \quad h_1 \frac{h_1}{h_o} \quad \ldots\ldots\ldots\ldots\ldots\ldots (27a)$$

and

$$\tau = k_2 \quad \frac{L}{\omega} \quad \ldots\ldots\ldots\ldots\ldots\ldots (27b)$$

in which k_1 and k_2 are non-dimensional constants. Substituting Eq. 27 into Eq. 24 results in

$$p_{max.} = 2 \frac{w_o}{g} \frac{k_1}{k_2} h_1 \frac{h_1}{h_o} \frac{\omega^2}{L} \quad \ldots\ldots\ldots\ldots\ldots (28)$$

Equating ω approximately to the wave celerity of the breaker of a solitary wave,

$$\omega = \sqrt{2.28\ g\ H_b} \quad \ldots\ldots\ldots\ldots\ldots\ldots (29a)$$

For such waves of great steepness as $H/L \doteqdot 0.035$ to 0.070, the height H_b of the breaking waves is approximately equal to the height H of the non-breaking shallow water waves on a horizontal bottom basin, that is, $H_b \doteqdot H$, hence

$$\omega = \sqrt{2.28\ g\ H} \quad \ldots\ldots\ldots\ldots\ldots\ldots (29b)$$

Substituting Eq. 29b into Eq. 28,

$$p_{max.} = 4.56 \frac{k_1}{k_2} w_o\ h_1 \frac{h_1}{h_o} \frac{H}{L} \quad \ldots\ldots\ldots\ldots\ldots (30a)$$

If $4.56 \frac{k_1}{k_2} = K$, a dimensionless constant, Eq. 30a can be written as

$$p_{max.} = K\ w_o\ h_1 \frac{h_1}{h_o} \frac{H}{L} \quad \ldots\ldots\ldots\ldots\ldots (30b)$$

Eq. 30b is the basic equation for a practical use of computing the maximum shock pressures exerted by breaking waves on vertical walls, and in this equation the main factors defined in a, b and c are included.

Evaluation of the Constant of Eq. 30b by Experimental Data.—Eq. 30b was checked with a number of $p_{max.}$ obtained from some 2,000 experimental data of shock pressures exerted by breaking waves on composite-type breakwaters. These experiments include various shapes of composite-type breakwaters such as the heights of the base-mounds h_d = 20, 33.4, 36, 37, and 38 cm, the front slopes = 1:2, 1:3, and 1:5, the top widths B = 10 cm and 0, and

such characteristics of waves as heights $H \doteqdot 6$ to 24 cm, periods $T \doteqdot 1.2$ to 1.9 sec, and steepnesses $H/L \doteqdot 0.019$ to 0.083.

a. Formula for the maximum shock pressure of ordinary breaking waves. The relationship between the maximum pressure $p_{max.}$ and $h_1 \frac{h_1}{h_o} \frac{H}{L}$ of ordinary breaking waves, which include all of perfect and partial breaking waves except breaking waves acting extraordinary high shock pressures, are plotted in Fig. 14.

From Fig. 14 it is seen that the value of $p_{max.}$ increases linearly up to 130 gr per sq cm as the value of $h_1 \frac{h_1}{h_o} \frac{H}{L}$ increases in the region of $h_1 \frac{h_1}{h_o} \frac{H}{L} \leqq 0.22$ cm. But in the region of $h_1 \frac{h_1}{h_o} \frac{H}{L} > 0.22$ cm, $p_{max.}$ is nearly constant 100 to 130 gr per sq cm for increase of $h_1 \frac{h_1}{h_o} \frac{H}{L}$. This is considered to be due to the fact that as the depth h_1 in front of a vertical wall and the steepness H/L of a breaking wave increase up to a certain limiting value of $h_1 \frac{h_1}{h_o} \frac{H}{L}$, the breaking wave strikes more forcefully against the wall, but above the limit of $h_1 \frac{h_1}{h_o} \frac{H}{L}$ a wave has difficulty in breaking, resulting in no increase of the pressure. The limit of $h_1 \frac{h_1}{h_o} \frac{H}{L}$ may be 0.22 cm in the exment. As will be mentioned later, when h_1 increases and reaches $h_1/H \geqq 1.6$ to 2.0, a wave in front of a vertical wall transforms into a clapotis, the pressure of which approaches hydrostatic pressure.

In the region of $h_1 \frac{h_1}{h_o} \frac{H}{L} \leqq 0.22$ cm the maximum shock pressure of breaking waves, $p_{max.}$, in gr per sq cm

$$p_{max.} = 20 + 500\, w_o\, h_1 \frac{h_1}{h_o} \frac{H}{L} \quad \ldots\ldots\ldots\ldots (31)$$

The relationship between $p_{max.}$ and $h_1 \frac{h_1}{h_o} \frac{H}{L}$ mentioned previously, is applicable for all kinds of shock pressure with the simultaneous distribution of A, B and C-types exerted by ordinary breaking waves on composite-type breakwaters which have the front slopes 1:2, 1:3, and 1:5, the top-widths B = 10 cm and B = 0, and the heights h_d = 37 cm and 20 cm of the base-mounds. But it is not applicable for low pressures by very weak breaking waves.

b. Formula for the maximum shock pressures of extraordinary breaking waves. The maximum shock pressures of extraordinary breaking waves reached generally up to two times or more those of ordinary breaking waves. The relationship between $p_{max.}$ and $h_1 \frac{h_1}{h_o} \frac{H}{L}$ for extraordinary breaking waves is plotted in Fig. 14. According to Fig. 14, although the relationship does not have a good correlation, the average values of $p_{max.}$ are related to $h_1 \frac{h_1}{h_o} \frac{H}{L}$ by the following equation, obtained by least squares analysis over the whole pressures,

$$p_{max.} = 280 \left(0.040 + h_1 \frac{h_1}{h_o} \frac{H}{L}\right)^{1/3} \quad \ldots\ldots\ldots\ldots (32)$$

The upper limiting values of $p_{max.}$ are expressed by

$$p_{max.} = 300 \left(0.051 + h_1 \frac{h_1}{h_o} \frac{H}{L}\right)^{1/3} \quad \ldots\ldots\ldots\ldots (33)$$

The values of $p_{max.}$ in extraordinary breaking waves are not always constant for the same condition concerning wave characteristics as well as

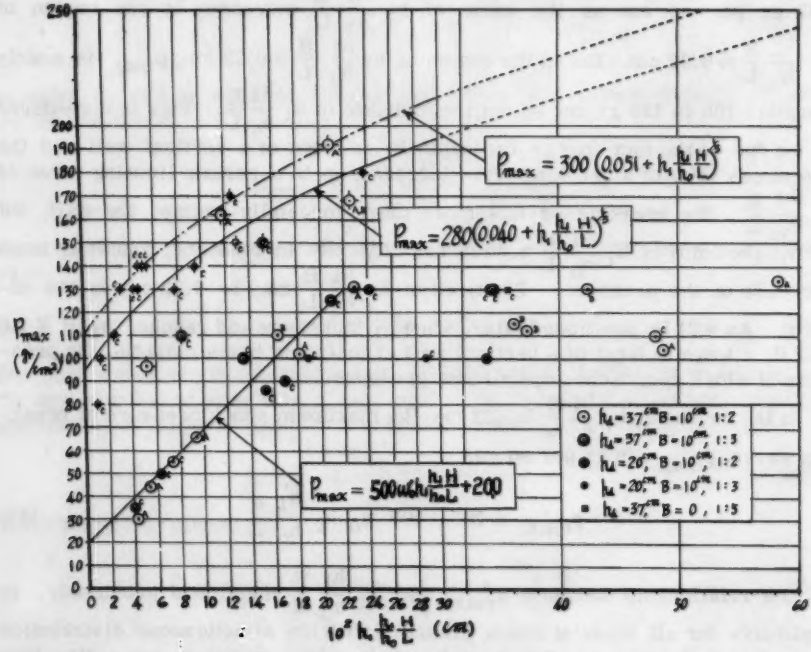
$p_{max} = 300\left(0.051 + h_1 \frac{h_1}{h_o} \frac{H}{L}\right)^{1/3}$
$p_{max} = 280(0.040 + h_1 \frac{h_1}{h_o} \frac{H}{L})^{1/3}$
$p_{max} = 500 \tanh \frac{h_1 H}{h_o L} + 200$
p_{max} (t/m^2)
$10^2 h_1 \frac{h_1}{h_o} \frac{H}{L}$ (cm)
$h_1 = 37^{cm}$ B = 10^{cm}, 1:2
$h_1 = 37^{cm}$ B = 10^{cm}, 1:3
$h_1 = 20^{cm}$ B = 10^{cm}, 1:2
$h_1 = 20^{cm}$ B = 10^{cm}, 1:3
$h_1 = 37^{cm}$ B = 0, 1:3

FIG. 14.—RELATIONSHIPS BETWEEN $p_{max.}$, AND $h_1 \frac{h_1}{h_o} \frac{H}{L}$

breakwater-types, and change to a comparatively large extent with a slight variation of boundary conditions. The scatter of the experimental data in Fig. 14 may be considered to be partly due to this fact.

Comparisons of Values Computed by Eqs. 31, 32, and 33, as well as Minikin's[6] and Hiroi's Formulas with Pressures Obtained by the Experiments.—As mentioned previously, since there exists no generally accepted shock-pressure formula established on the basis of a sufficient number of prototype or experimental data, Hiroi's and Minikin's formulas were selected as the representatives of shock-pressure formulas for the comparison of the computed values of pressure with the experimental values of shock pressure.

For Ordinary Breaking Waves.

a. Comparison of the maximum shock pressure intensity. For the maximum pressure intensity $p_{max.}$ and the resultant P of the shock pressures exerted simultaneously with $p_{max.}$ by ordinary breaking waves on unit longitudinal length of the vertical walls of composite breakwaters, the comparisons of computed values by Eq. 31, Hiroi's and Minikin's formulas with measured pressures by the experiments were made and tabulated in Tables 6

TABLE 6.—COMPARISONS FOR RESULTANT PRESSURES P PER UNIT LENGTH OF A WALL BETWEEN THE COMPUTED AND THE EXPERIMENTAL VALUES

Run No.	Resultant Pressure, P, in gr per cm				Percentage Deviation		
	Experimental value	Eq. 31	Hiroi's formula	Minikin's formula[a]	Eq. 31	Hiroi's formula	Minikin's formula[a]
1	185	193	312	237 (177)	+ 4	+ 69	+ 28 (- 4)
2	304	304	381	344 (262)	0	+ 25	+ 13 (- 14)
3	510	560	488	597 (480)	+ 10	- 4	+ 17 (- 6)
4	655	650	570	691 (560)	- 1	- 19	+ 6 (- 15)
5	780	780	750	1262 (1062)	0	- 4	+ 62 (+ 36)
6	120	164	295	192 (136)	+ 37	+ 146	+ 60 (+ 13)
7	230	234	350	273 (200)	+ 2	+ 53	+ 18 (- 13)
8	594	551	521	603 (475)	- 7	- 12	+ 2 (- 24)
9	690	710	776	1168 (963)	+ 3	+ 13	+ 70 (+ 40)
10	598	625	713	976 (783)	+ 5	+ 19	+ 63 (+ 31)
11	1045	925	760	1039 (832)	- 11	- 27	- 0.6 (- 20)
12	940	984	885	1239 (998)	+ 5	- 6	+ 32 (+ 6)
13	200	204	192	123 (91)	+ 2	- 4	- 39 (- 55)
14	451	504	304	292 (231)	+ 12	- 33	- 35 (- 49)
15	695	615	352	403 (325)	- 12	- 49	- 42 (- 53)
16	560	645	408	494 (400)	+ 15	- 27	- 12 (- 29)
17	105	120	144	67 (44)	+ 14	+ 37	- 36 (- 58)
18	378	441	286	238 (179)	+ 17	- 24	- 37 (- 53)
19	423	409	336	346 (269)	- 3	- 21	- 18 (- 36)
20	184	191	167	110 (74)	+ 4	- 9	- 40 (- 60)
21	465	530	270	287 (220)	+ 14	- 42	- 38 (- 53)
22	530	610	330	447 (360)	+ 15	- 38	- 16 (- 32)
23	1240	1010	844	1234 (1044)	- 19	- 32	- 0.5 (- 16)
24	250	206	428	164 (117)	- 18	+ 71	- 35 (- 53)
25	390	318	460	249 (186)	- 18	+ 18	- 36 (- 52)
26	486	459	502	379 (296)	- 6	+ 3	- 22 (- 39)
27	622	740	615	707 (576)	+ 19	- 1	+ 14 (- 7)
28	668	960	617	834 (685)	+ 44	- 8	+ 25 (+ 3)
29	850	1087	810	1346 (1134)	+ 28	- 5	+ 53 (+ 33)

[a]Figures in parenthesis are values substructed the static pressure from the total pressure.

and 7. In Table 6 Runs 1 to 23 are data for composite breakwaters with the top-width B = 10 cm of the base-mounds, and Runs 24 to 29 are data for weak breaking waves on composite breakwaters, the vertical walls of which are located on 1:2 slopes without the top-width. Therefore Runs 24 to 29 are originally exceptional for Eq. 31, but presented here only as a reference.

According to these comparisons, the values of $p_{max.}$ computed by Hiroi's formula are all too small to compare with the experimental values, but the

TABLE 7.—COMPARISONS OF COMPUTED VALUES BY EQ. 31, HIROI'S

h_d, in cm	B, in cm	1:m	h_1, in cm	T, in sec	H, in cm	H/L	h_1/H
37	10	1:2	13.7	1.5	17.3	0.061	0.79
20	10	1:2	9.0	1.3	6.3	0.028	1.43
20	10	1:3	9.0	1.33	7.6	0.034	1.18
37	10	1:3	9.0	1.5	13.0	0.047	0.69
37	10	1:3	12.0	1.5	15.0	0.052	0.80
37	10	1:3	15.0	1.5	16.2	0.054	0.93
37	0	1:5	9.0	1.21	16.2	0.074	0.56
37	0	1:5	12.0	1.21	17.1	0.081	0.70
37	0	1:5	8.0	1.65	11.6	0.035	0.69
37	0	1:5	12.0	1.65	14.4	0.043	0.83
37	0	1:5	6.0	1.29	14.3	0.064	0.42
37	0	1:5	9.0	1.29	15.6	0.067	0.58
37	0	1:5	12.0	1.29	17.0	0.071	0.71

values of $p_{max.}$ by Minikin's formula are comparatively similar to the experimental values, indicating the maximum deviation of approximately $\pm 60\%$, and especially smaller deviation for the cases of A-type distribution of the maximum simultaneous pressures.

b. Comparison of the resultant of the maximum simultaneous pressures. For the resultant P of the shock pressures exerted simultaneously with $p_{max.}$ on unit longitudinal length of a vertical wall, the comparisons of the computed values by the previously described three formulas with the experimental values are tabulated in Table 6.

In Table 6, P computed by Hiroi's formula are the values for composite breakwaters, the top of which are constructed 10 cm (this corresponds to 2.0 meters in prototype) high above the still water level. As is seen from Table 6, as far as the resultant pressure P concerns, the values computed by Hiroi's formula are comparatively similar to the experimental values in the nearly same order as the values by Minikin's formula, the deviation being in general within approximately $\pm 70\%$ except only one case of the maximum 146% deviation. This fact may be attributable to the reason that the method of calculation of P by Hiroi's formula was deviced from the experiences which had been obtained in Japan during some three decades for such composite breakwaters as the tops have been constructed at the elevations of 2m to 2.5m or less above the high water level of ordinary spring tide.

From these comparisons it was proved that both the values of $p_{max.}$ computed by Eq. 31 and of P by the use of Eqs. 9, 11, 13 and 31 agreed with the experimental results better than other two formulas, indicating approximately within $\pm 20\%$ of deviation except Runs 28 and 29 which were presented only for a reference.

For Extraordinary Breaking Waves.—For the much higher shock pressures of extraordinary breaking waves the comparisons of the computed values of $p_{max.}$ by Eq. 32 as well as by Hiroi's and Minikin's formulas with the experimental values are shown in Table 7.

As seen from Table 7, the values $p_{max.}$ computed by Hiroi's and Minikin's formulas are all too small to compare with the experimental values. The

AND MINIKIN'S FORMULAS WITH EXPERIMENTAL VALUES

Experimental Value $p_{max.}$, in gr per sq cm	$p_{max.}$ by Eq. 32, in gr per sq cm	$p_{max.}$ by Minikin's Formular, in gr per sq cm	p by Hiroi's Formular, in gr per sq cm	Simultaneous Pressure Distribution
169	179	108	26	A, B-type
130	137	34	10	C-type
140	144	41	11	C-type
110	139	52	20	C-type
150	162	80	23	C-type
150	181	107	24	C-type
150	155	82	24	C-type
180	182	124	26	C-type
140	125	34	17	C-type
170	154	66	22	C-type
97	126	45	21	A-type
162	151	74	23	A-type
192	176	109	26	A-type

values $p_{max.}$ computed by Eq. 32 give a better agreement with the experimental values, indicating the maximum deviation of 30% and for most cases small deviations of within $\pm 10\%$.

Application of Experimental Results to Prototype.

Scale Ratios of Model to Prototype.—Since all measurements of wave pressures and wave characteristics were carried out at the center longitudinal section of the 2-m width of the channel, and the lengths of the front slopes of the base-mounds of composite breakwaters were generally small compared with the wave-lengths used in the experiments of shallow-water waves, the energy loss of waves caused by frictional resistance at the bottom as well as both sides of the channel was small. Therefore Froude's law of similarity was applicable to these experiments with sufficient accuracy.

If the ratio of length l or height h in model to length or height in prototype is denoted by n, and subscripts p and m of symbols used herein refer to prototype and model respectively, it follows that

$$l_m = n\, l_p \quad \ldots\ldots\ldots\ldots\ldots\ldots \quad (34a)$$

and

$$h_m = n\, h_p \quad \ldots\ldots\ldots\ldots\ldots\ldots \quad (34b)$$

Denoting time and the intensity of pressure by t and p respectively, the following relationships according as Froude's law of similarity is obtained.

$$t_m = \sqrt{n}\, t_p \quad \ldots\ldots\ldots\ldots\ldots\ldots \quad (35a)$$

and

$$p_m = n\, p_p \quad \ldots\ldots\ldots\ldots\ldots\ldots \quad (35b)$$

The water-depth h_m, wave-height H_m, and wave-length L_m used in the experiments were approximately h_m = 20 to 70 cm, H_m = 10 to 25 cm, and L_m = 200 to 450 cm. Those generally used in prototype for the design of breakwaters are approximately h_p = 5 to 15 m, H_p = 2 to 6 m, and L_p = 40 to 90 m. These make the ratio of length in model to length in prototype approximately

$$n = 1/20 \quad \ldots\ldots\ldots\ldots\ldots\ldots \quad (36)$$

Hence the following values are obtained for the wave-period and the intensity of pressure in prototype.

$$T_p = \frac{1}{\sqrt{n}} T_m = 4.47\ T_m, \quad \ldots\ldots\ldots\ldots\ldots\ldots \quad (37)$$

and

$$p_p = n\ p_m = 20\ p_m \cdot \quad \ldots\ldots\ldots\ldots\ldots\ldots \quad (38)$$

Since

$$T_m = 1.2 \text{ to } 2.0 \text{ sec} \quad \ldots\ldots\ldots\ldots\ldots\ldots \quad (39a)$$

then

$$T_p = 5.4 \text{ to } 9.0 \text{ sec} \quad \ldots\ldots\ldots\ldots\ldots\ldots \quad (39b)$$

Since the maximum intensity of pressures observed in the experiments, $(p_{max.})_m$, was approximately 200 gr per sq cm, the maximum intensity of pressure in prototype corresponds to

$$(p_{max.})_p = 40 \quad \ldots\ldots\ldots\ldots\ldots\ldots \quad (40)$$

in tons per sq m. The values of wave-period and wave-pressure intensity in Eqs. 39 and 40 are considered to include almost the ranges of wave-period and wave-pressure used for the design of breakwaters, though a few prototype observations of $(p_{max.})_p = 60$ to 70 tons per sq m were reported hitherto.

Maximum Pressure Formula for Breakwaters in Prototype.

a. Maximum pressure formula for ordinary breaking waves. The formula for the maximum intensity of shock pressures in tons per sq m exerted by ordinary breaking waves on the vertical walls of composite-type breakwaters in prototype are obtained from Eq. 31 using Froude's modulus of similarity:

for the region of $h_1 \frac{h_1}{h_o} \frac{H}{L} \leqq 0.044$ m

$$p_{max.} = 4 + 500\ w_o\ h_1 \frac{h_1}{h_o} \frac{H}{L} \quad \ldots\ldots\ldots\ldots\ldots\ldots \quad (41)$$

for the region of $h_1 \frac{h_1}{h_o} \frac{H}{L} > 0.44$ m

$$p_{max.} = 20 \text{ to } 26 \quad \ldots\ldots\ldots\ldots\ldots\ldots \quad (42a)$$

as an average value

$$p_{max.} = 23 \quad \ldots\ldots\ldots\ldots\ldots\ldots \quad (42b)$$

Since the value of $h_1 \frac{h_1}{h_o} \frac{H}{L}$ will be greater than 0.044m in most of the conditions used for the design of composite breakwaters encountered with severe storms, the maximum intensity of shock pressures exerted by ordinary breaking waves, $p_{max.}$ may be assumed to be likely equal to 20 to 26 tons per sq m for those conditions without any calculation, and it may be appropriate to use $p_{max.}$ = 26 tons per sq m for breakwaters exposed to an open sea and $p_{max.}$ = 20 tons per sq m for breakwaters located in an inland sea or a bay.

b. Maximum pressure formula for extraordinary breaking waves. For the maximum intensity of much higher shock pressures exerted by extraordinary breaking waves on the vertical walls of composite breakwaters in prototype,

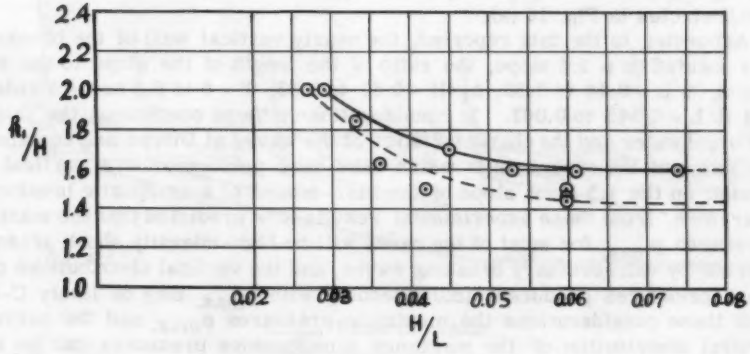

FIG. 15.—RELATIONSHIP BETWEEN H/L AND THE LIMITING VALUE OF h_1/H

the following formulas are obtained from Eqs. 32 and 33 using Froude's modulus of similarity: for average values between the upper and lower limits

$$p_{max.} = 96 \left(0.008 + h_1 \frac{h_1}{h_o} \frac{H}{L} \right)^{1/3} \quad \ldots\ldots\ldots\ldots (43)$$

for the upper limiting values

$$p_{max.} = 103 \left(0.01 + h_1 \frac{h_1}{h_o} \frac{H}{L} \right)^{1/3} \quad \ldots\ldots\ldots\ldots (44)$$

Limit Between a Breaking Wave and a Clapotis.—It has been well known that when the depth in front of a vertical wall increases up to twice or larger than the height of a progressive wave, a standing wave or a clapotis is produced seaward of the wall by superimposing the progressive wave on the reflected wave, producing a weak pressure near the hydrostatic pressure. From a number of the experiments in various shapes of composite breakwaters it was found that when the steepnesses of progressive waves were comparatively large, clapotis were produced in the seaward depths of a vertical wall which were smaller than twice the heights of progressive waves, that is, for such steep waves as $H/L \geqq 0.060$, in depths of $h_1/H \fallingdotseq 1.5$ to 1.6, and for waves of such low steepnesses as $H/L \leqq 0.030$, in depths of $h_1/H \geqq 2.0$.

The relationship between wave-steepness H/L and the limiting value of h_1/H in which a clapotis is produced is shown in Fig. 15.

Comparisons of Values Computed by the New Formulas with Observed Pressures at Dieppe.—It is most desirable to check the applicability of the new formulas for the design of breakwaters in prototype by the use of a number of observed data concerning shock pressures exerted by breaking waves during storms, but only very few data are available on the shock pressures of hurricane waves, as far as actual observations are concerned. Only the ten data of actual measurements observed in the harbor of Dieppe by French engineers[7] were used to check the new formulas.

Comparison of the Observed Data in 1937 with the Computed Values.—Pressures observed on the wall of the breakwater in the harbor of Dieppe during the storms of February 9 and 23 and March 1 in 1937 are shown by small circles in Fig. 16 (a).

According to the data reported, the nearly vertical wall of the breakwater was located on a 1:5 slope, the ratio of the length of the slope to the wavelength, S/L = 0.44 to 0.50, h_1/H = 0.61 to 0.83, T = 6 to 6.5 sec (calculated), and H/L = 0.045 to 0.063. In consideration of these conditions, the shape of the breakwater and the characteristics of the waves at Dieppe are contained in the range of the experiments which have been performed on a vertical wall located on the 1:5 front slope of the base-mound of a composite breakwater. Therefore, from those experimental results it is predicted that the maximum pressures $p_{max.}$ for most of the cases will be high-intensity shock pressures exerted by extraordinary breaking waves, and the vertical distributions of the shock pressures produced simultaneously with $p_{max.}$ may be likely C-type. With these considerations the maximum pressures $p_{max.}$ and the curves of vertical distribution of the maximum simultaneous pressures can be computed by the use of Eqs. 41 to 44 as well as Eqs. 8 to 13 from the characteristics of waves observed at the same times as the measurements of the pressures, as shown in Fig. 16 (a) by full lines.

As is seen from Figs. 16 (a), the computed values of $p_{max.}$ and P, as well as the predicted curves of the pressure-distributions give comparatively good agreement with the observed values for the case of (1), (2) and (5), but for the cases of (3) and (4), the computed values of $p_{max.}$ and P indicate deviations of minus 54% to 55% from the observed values. For such high-intensity shock pressures as these, Minikin's formula gives too small values to compare.

Comparison of Observed Data in 1935 with the Computed Values.—Since the recording of wave characteristics in December, 1935, were not always carried out at the same times as the measurements of pressures, the pressures and the vertical distributions were calculated by the use of Eqs. 41 to 44 as well as Eqs. 8 to 13 from the characteristics of the two representative waves, one of which was the wave observed at $12^h\ 15^m$ and was used for the waves on December 2 and the other was the wave observed at $12^h\ 45^m$ for the waves on December 16. The comparisons of the computed values of $p_{max.}$ and P, as well as the predicted curves with the observed data are shown in Fig. 16 (b). From Fig. 16 (b) it is seen that many of the computed values agree roughly with the observed values. Though the pressure-distribution in the cases of (9) and (10) appears to be A-type at the instants observed, it is sup-

---

[7] "Etat actual des études internationales sur les efforts dus aux lames," by Rouville, Besson, and Petry. Ponts et Chaussées, July, 1938.

posed from the experimental results such as shown in Fig. 11 (b) that the breaking waves were in a transient state from A-type to C-type distribution.

CONCLUSIONS

1. Applicability of the experimental results to prototype. In consideration of the following three facts, it may be correctly considered that the new Eqs.

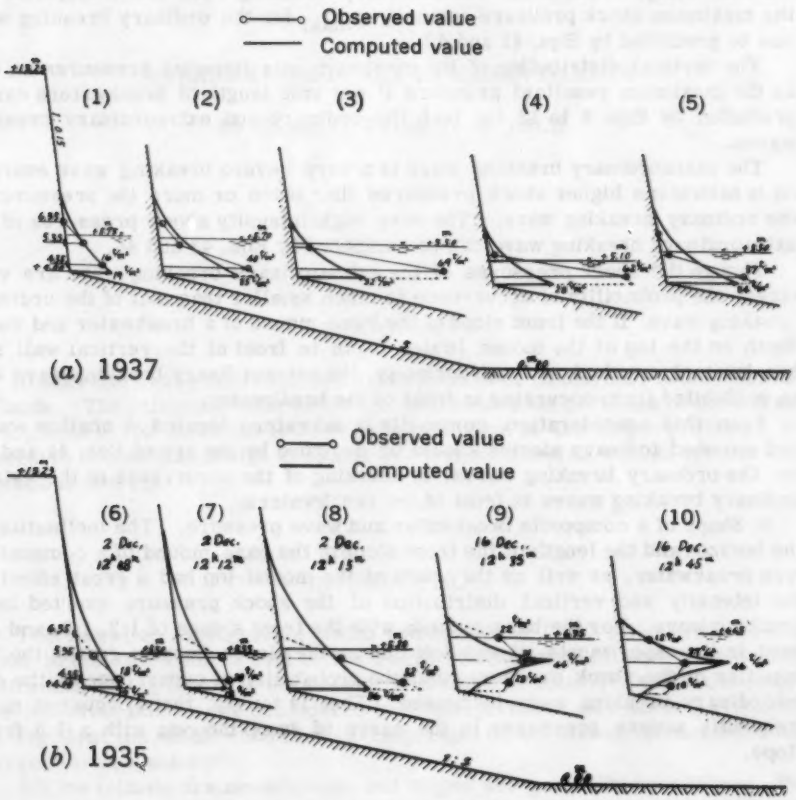

FIG. 16.—COMPARISON OF PREDICTED VALUES WITH OBSERVED PRESSURES.

8 to 13 as well as Eqs. 41 to 44 derived from the experimental data will be applicable for the design of actual breakwaters: (a) since the effect of the frictional resistance on the slope of the base-mound as well as on the bottom and both side-walls of the channel were small, the experimental results may be applicable to prototype conditions with sufficient accuracy by the use of Froude's law of similarity; (b) most of the experimental values of the resultant P of the maximum simultaneous pressures indicated deviations smaller than $\pm 70\%$ from the values computed by Hiroi's and Minikin's formulas derived empirically from the disastrous damages of actual breakwaters; and

(c) the seven values of P computed by the use of Eqs. 8 to 13 as well as Eqs. 41 to 44 agreed with the corresponding seven observed values of the ten pressure-measurements at Dieppe with plus or minus deviations smaller than 20%.

2. Ordinary and extraordinary breaking waves. Breaking wave striking severely against breakwaters can be divided into the two kinds of ordinary and extraordinary breaking waves.

The ordinary breaking wave includes various types of breaking waves over the wide range between the extraordinary breaking wave and a clapotis, and the maximum shock pressure-intensity $p_{max.}$ for the ordinary breaking wave can be predicted by Eqs. 41 and 42.

The vertical distribution of the maximum simultaneous pressures as well as the maximum resultant pressure P per unit length of breakwaters can be predicted by Eqs. 8 to 13 for both the ordinary and extraordinary breaking waves.

The extraordinary breaking wave is a very severe breaking wave exerting on breakwaters higher shock pressures than twice or more the pressures of the ordinary breaking wave. The very high-intensity shock pressures of the extraordinary breaking wave can be computed by Eqs. 43 and 44.

Though the shock pressures of the extraordinary breaking wave are very large, the probability of occurrence is much smaller than that of the ordinary breaking wave. If the front slope of the base-mound of a breakwater and water depth on the top of the mound (water depth in front of the vertical wall of a breakwater) are designed appropriately, the extraordinary breaking wave will be prohibited from occurring in front of the breakwater.

From this consideration, composite breakwaters located at shallow water and exposed to heavy storms should be designed by the use of Eqs. 41 and 42 for the ordinary breaking waves, by blocking of the occurrence of the extraordinary breaking waves in front of the breakwaters.

3. Shape of a composite breakwater and wave pressure. The inclination to the horizon and the length of the front slope of the base-mound of a composite-type breakwater, as well as the width of the mound-top had a great effect on the intensity and vertical distribution of the shock pressure exerted by a breaking wave. For the base-mounds with the front slopes of 1:2, 1:3, and 1:5 used in the experiments, it was felt that as the slopes became gentle, the intensities of the shock pressures and the probability of occurrence of the extraordinary breaking wave increased. That is to say, there occurred most frequently severe pressures in the cases of base-mounds with a 1:5 front slope.

ACKNOWLEDGMENTS

The author wishes to express his appreciation to S. Tamai and S. Konishi, assistants of this hydraulic laboratory, in carrying out the experiments and preparing the figures. The author is indebted to K. Takahashi who made the shock-pressure gauge used in the experiments, and also to Mr. Yamauchi, Director of the Technical Research Laboratory of Hitachi Shipbuilding Co. Ltd., T. Horiuchi and M. Uehara, engineers of the Technical Research Laboratory, who cooperated with great kindness in photographing the breaking waves by 16 mm high-speed movies.

Journal of the
WATERWAYS AND HARBORS DIVISION
Proceedings of the American Society of Civil Engineers

BREAKWATERS IN THE HAWAIIAN ISLANDS

By Robert Q. Palmer,[1] M. ASCE

SYNOPSIS

Breakwaters have been required to create most of the harbors in the Hawaiian Islands. The following brief description of conditions pertinent to harbor development in the Hawaiian Islands presents some of the unique problems inherent in breakwater design and some of the innovations as well as conventional solutions thereof.

INTRODUCTION

The Hawaiian Archipelago, which extends about 1,500 miles from east to west in the east central part of the Pacific Ocean, was created by a chain of volcanoes rising from the ocean floor at a depth of about 18,000 ft. Generally, the Hawaiian Islands are considered to be comprised of only the islands, shown in Fig. 1, at the eastern end of the archipelago. Of the islands shown, the seven largest are populated.

All the islands are mountainous and slopes are generally precipitous. Two peaks on the island of Hawaii rise to almost 14,000 ft above sea level. The sea continuously carries away most of the talus and end products of erosion from the base of the mountains on all but the southern shores, leaving generally bold coasts faced with cliffs.

Fringing coral reefs, that have formed along the shores of the geologically-older portions of the islands, provide the most economical sites for harbor

Note.—Discussion open until November 1, 1960. To extend the closing date one month, a written request must be filed with the Executive Secretary, ASCE. This paper is part of the copyrighted Journal of the Waterways and Harbors Division, Proceedings of the American Society of Civil Engineers, Vol. 86, No. WW 2, June, 1960.

[1] Chf., Planning and Reports Branch, Engrg. Div., U. S. Army Engr. Dist., Honolulu, Hawaii.

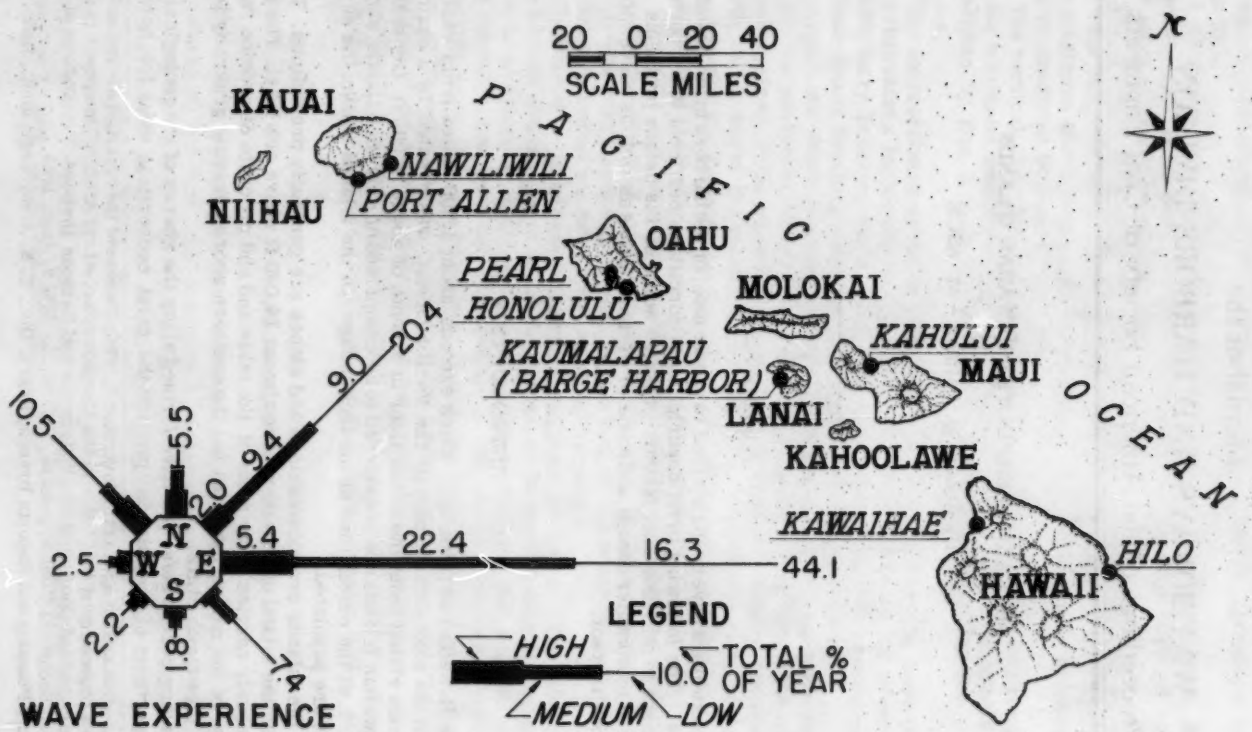

FIG. 1.—DEEP WATER HARBORED IN THE HAWAIIAN ISLANDS

development. Where streams discharge into the ocean over a coral reef, the fresh water deters the growth of coral. Thus, open channels to the sea remain when the reefs are formed. The size of these channels appears to be approximately proportional to the volume of stream flow. Although irregular and hazardous, most of the channels are navigable by small craft during fair weather.

Dredging is usually required to provide harbors for deep-draft vessels. Exceptions are Pearl Harbor, where relatively little dredging was required to open a channel through the bar into the three spacious lochs of the famous naval base, and the much smaller Honolulu Harbor, which was improved in 1905, to permit navigation by large sea-going vessels. Turning basins and connecting channels were dredged from time to time in Honolulu Harbor to serve the needs of increasing commerce. The natural sites at the locations of the five other deepwater commercial harbors developed by the Corps of Engineers, Dept. of the Army and shown in Fig. 1 were not as favorable, and none are landlocked. Dredging inland was precluded at most of the sites by solid basaltic rock formations.

The coasts of the islands are exposed to attack by waves generated in a vast expanse of ocean extending more than 2,000 miles in all directions. The prevailing tradewinds from the north and northeast generate swells which hammer persistently on the northern shores. A wave rose is shown in Fig. 1. About every two years during the winter months, intense extra-tropical storms spawn huge waves that attack the northern and eastern shores. Southerly storms, known locally as Kona storms, create smaller waves that attack the southern shores. Records show that hurricanes rarely occur in the locality. The record has been marred in recent years by Hurricane Nina which, in 1957, passed to the south of the islands, and Hurricane Dot which passed directly over the island of Kauai in 1959. Medium to large tsunamis occur every few years. The normal tidal range is approximately 2 ft and the extreme variation in tide is about 4 ft.

Although the islands are comprised largely of volcanic rock, this extrusive material is usually checked with seams and joints. The older formations are also deeply weathered. Stone of sufficient size and quality for breakwater construction is economically available for only a few harbor sites. Only three good quarries have been developed for the production of suitable breakwater stone. The basalt rock from these quarries has a specific gravity ranging from 2.6 to 3.0 and can be quarried to produce stones weighing as much as 12 tons each. Basalt is also crushed to yield coarse aggregate for concrete used in breakwater construction, while coral sand is normally used as fine aggregate.

Notation.—The letter symbols adopted for use in this paper are defined where they first appear, in the illustrations or in the text, and are arranged alphabetically, for the convenience of reference, in the Appendix.

BREAKWATER DESIGN PRIOR TO 1950

Breakwaters built in the Hawaiian Islands prior to 1950, are generally of the typical section shown in Fig. 2. The controlling factors of design were the type and capacity of available equipment, native materials, labor costs, and sea conditions. In accordance with the general practice of the era, designs were based largely on the opinions of experienced breakwater men. In these

breakwaters the crest is about 15 ft in width and varies in elevation from about 11 to 13 ft above mean lower low water, or only 9 to 11 ft above high tide. The seaward slope is about 1-on-1 $\frac{1}{2}$, and the landward slope varies from 1-on-1 to 1-on-1 $\frac{1}{2}$. Core stones range in weight from less than 100 lbs to about 500 lbs each, while cap stones weigh from 8 to 12 tons each. A single layer of cap stone extends to only 3 ft below mean lower low water. At greater depths, random placed stones weighing from 6 to 10 tons each are in evidence on the slopes.

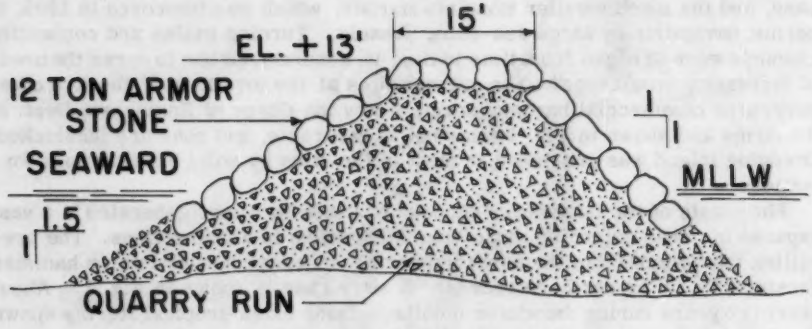

TYPICAL SECTION
BREAKWATER DESIGNED BEFORE 1950

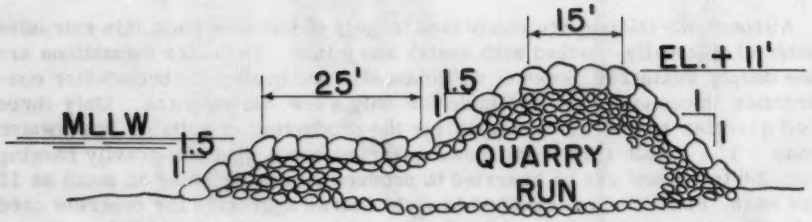

SECTION OF HILO BREAKWATER

FIG. 2.—TYPICAL BREAKWATER SECTIONS

A significant feature of the breakwaters is the fitting and keying of the stones in the armor layer. This greatly increased the stability of the structures. The workmanship was so superior that, in many cases where the core material subsided, the cover layer remained in place arching spans up to 20 ft. The outstanding example of this type of breakwater is at Port Allen. The armor stone, placed as dry masonry, is extremely well-fitted and keyed together. In this case, an underlayer of "B" stone was also used. The Port Allen breakwater is located on the southern shore of the island of Kauai where there is

less exposure to severe storms. However, the structure has successfully withstood attacks by waves that were estimated to be up to 20 ft in height. The major weaknesses of this type of construction are that displacement of a single keystone may result in failure of complete sections of the breakwater and that it is not practicable to extend keyed stonework more than a few feet below the water surface. Also, present-day labor costs virtually preclude such time-consuming work.

Another interesting feature of one of the older structures is the 25-ft wide berm of the Hilo breakwater. The berm is at about mean lower low water and extends around the end and along the seaward side of the structure for about 300 ft (Fig. 2). The head of the breakwater has successfully weathered several severe storms, one of which breached the structure about 2,700 ft from the seaward end. During preparation of the design analysis for repair, it was surmised that the berm possibly contributed to the stability of the head of the

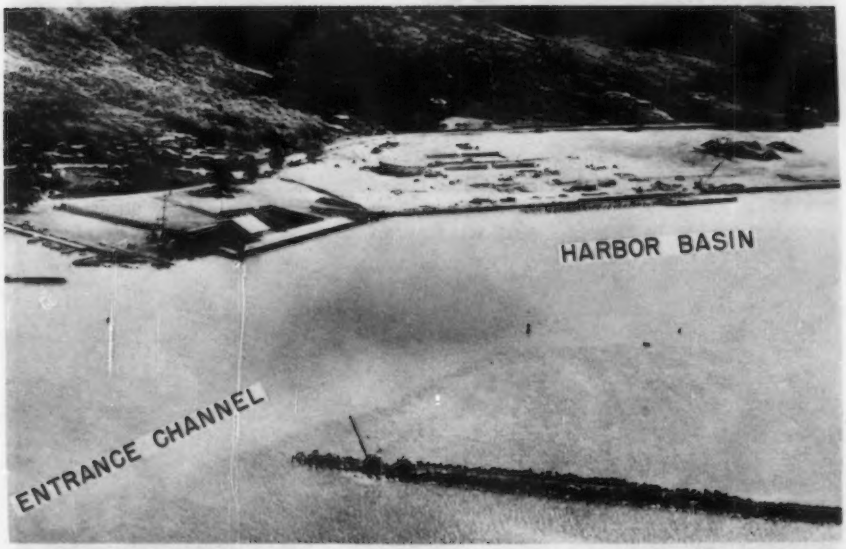

FIG. 3.—KAWAIHAE HARBOR BREAKWATER UNDER CONSTRUCTION

structure. Model studies of the Nawiliwili breakwater indicated that breaking waves tend to stabilize the section of a rubble-mound structure by the creation of a berm.

RECENT BREAKWATER DESIGN AND CONSTRUCTION

Since the only new federal breakwater to be constructed in the Hawaiian Islands since 1950, is at Kawaihae Harbor, this section will also deal with recent major repairs to existing breakwaters.

Kawaihae Harbor.—Kawaihae Harbor is located on the northwestern coast of the island of Hawaii. The rubble-mound breakwater was completed in 1959. Photographs of the structure during and after construction are shown in Figs. 3 and 4.

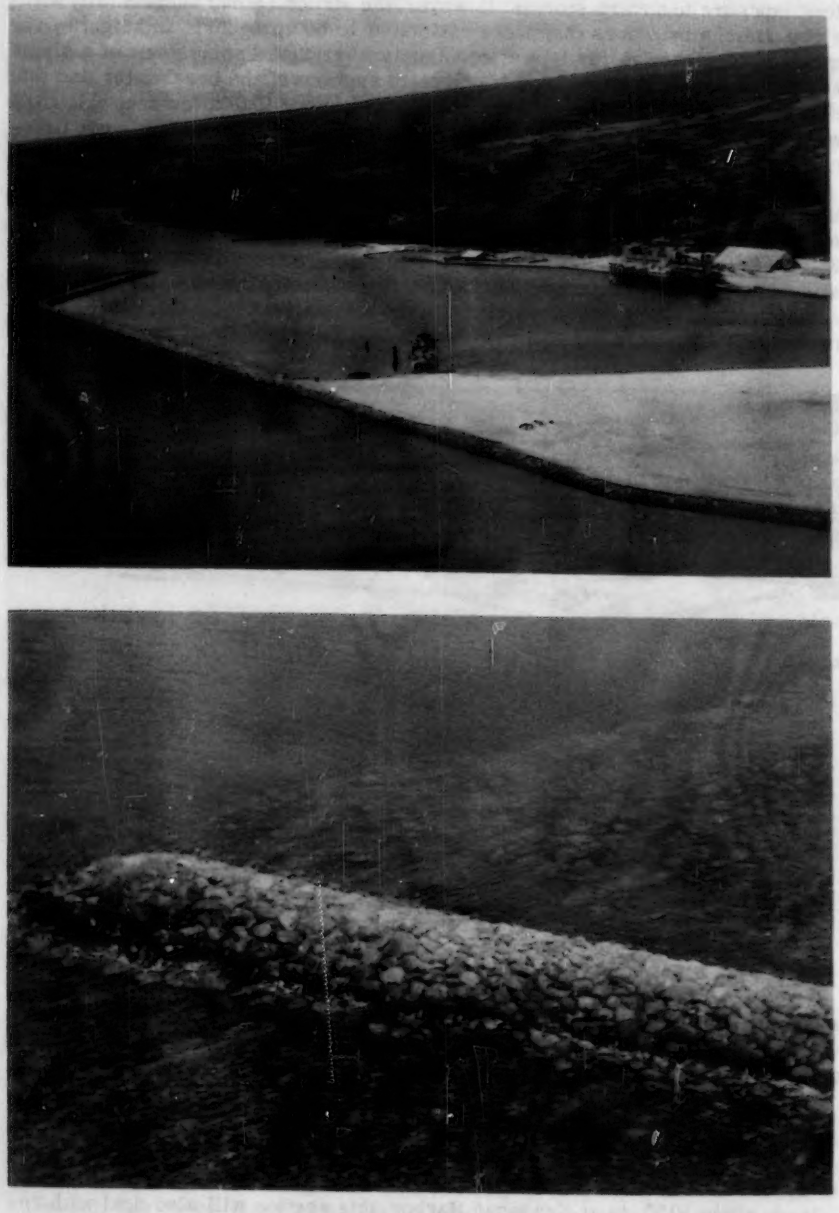

FIG. 4.—KAIWAIHAE HARBOR BREAKWATER

The harbor is located in a shallow bight on the leeward coast of the island where an extensive coral reef has grown. At the project site, the reef lay only a few feet below the surface; in fact, some coral heads were exposed at low tide. The seaward edge of the reef is about one-half mile from shore, 6 to 9 ft below the surface, and slopes abruptly into deep water. The texture of the reef is extremely rough, being characterized by thousands of coral heads, deep holes, grooves and caverns, which, in effect, approach the ultimate for an irregular surface. Advantage was taken of the protection afforded by the reef in siting the breakwater as far shoreward as possible from the seaward edge of the reef. For a minimum distance of 400 ft seaward of the structure, the maximum depth of water is about 9 ft at higher high tide.

Generally, waves break in a depth of water equal to about 1.3 times the wave height.[2] It was, therefore, indicated that waves greater than about 7 ft in height would break well seaward of the breakwater. However, on rare occasions exceptionally high tides have occurred. Included in the consideration of high tides were the possible effects of tsunamis, that, historically, have been triggered by earthquakes having epicenters along the Aleutians and the coasts of South America. The usual effect of tsunamis on coasts sheltered from the direct approach of the waves is a series of high and low tides occurring at intervals of about 10 to 20 min. In view thereof, a design wave height of 9 ft was selected.

Since the basin is located immediately behind the breakwater, overtopping would not be desirable. Therefore, the crest elevation was set at 1.2 times the design wave height, or 11 ft above normal high tide. The minimum weight of armor stone on a 1-on-2 slope was determined to be 3 tons by the Iribarren formula as modified by Hudson. Actually, a large quantity of stones weighing 5 tons and more was used in the armor layer because the quarry operation produced an excess of oversized stones. The remainder of the section was proportioned to meet gradation requirements and to make economical use of stone sizes produced at a nearby quarry. The section is shown in Fig. 5. The design of the head of the breakwater indicated a crest width of 20 ft and an armor layer composed of stones weighing about 12 tons each on a slope of 1-on-2 (Fig. 5).

In the past 25 yr the most severe storm affecting Kawaihae Harbor occurred in January, 1959. The deepwater waves, that were generated from the south and southwest, were estimated to be about 18 ft in height. In August, 1959 Hurricane Dot, passing south of the island of Hawaii, created 15-ft waves off the seaward edge of the reef. In both storms, the waves broke on the edge of the reef, as expected. No damage was sustained by the breakwater during either storm, although the structure was still under construction when the January storm occurred.

Kahului Harbor.—Kahului Harbor is located on the northern coast of the island of Maui. A small cove behind the reef, where 19th century whalers anchored, was developed into a deepwater port by dredging and by the construction of the east and west rubble-mound breakwaters that were 2,850 ft and 2,396 ft in length, respectively. The breakwaters were completed in 1931. Major repair of the structures at, and near, the heads was accomplished in 1957. A record of damages and cost of repairs for the past 12 yr is shown in Table 1.

---

[2] "The Interpretation of Crossed Orthogonal in Wave Refraction Phenomenon," by Willard J. Pierson, Jr., Technical Memorandum No. 21, Beach Erosion Bd., Office of the Chf. of Engr., Dept. of the Army, 1951.

Prior to design for the reconstruction in 1957, hind-casts of two major storms were made to determine the characteristics of deepwater storm waves. The following results were obtained:

Storm of January 1947	Storm of March 1954
H_o = 26 feet	H_o = 27 feet
T = 16.6 seconds	T = 18 seconds
L_o = 1,410 feet	L_o = 1,660 feet
Direction - north	Direction - north-northeast

in which H_o is the deepwater wave height, T is the wave period, and L_o is the deepwater wave length.

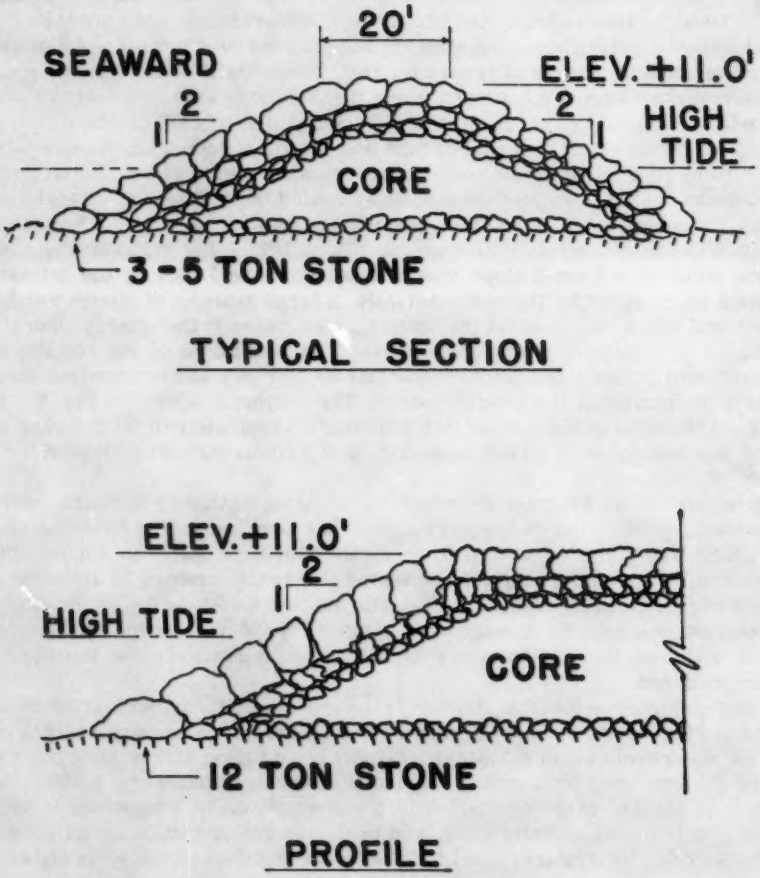

FIG. 5.—SECTIONS OF KAWAIHAE BREAKWATER

Wave refraction analyses showed that a submerged knoll of coral about 9,000 ft offshore caused convergence of the orthogonals on the ends of the breakwaters (Fig. 6). Convergence was such that the maximum refraction coefficient, $K = \sqrt{2}$, was indicated.[2] Application of this coefficient to the aforementioned data in estimating the height of waves approaching the heads of the breakwaters resulted in an increase in height to about 40 ft. Based on the breaking depth to wave height relation previously mentioned, waves of this height would break about 1,000 ft seaward of the structures in water about 52 ft deep.

In view of these findings, it was concluded that the controlling depth at a safe distance seaward of the breakwaters would be the limiting factor in determining the design wave height at the structures. The most applicable criterion available for determination of this safe distance was presented by Melville S. Priest.[3] It is assumed that a breaking wave will have full effective force for a maximum distance of 0.4 L shoreward of its point of breaking, in which L is the wave length at the point of breaking. At the breaking depth of 52 ft, 0.4 L was found to be 254 ft, which is only one-fourth of the actual distance

TABLE 1.—KAHULUI BREAKWATER DAMAGES AND COST OF REPAIRS

Date of Storm	Damaged Area	Cost
January 1947	Seaward Ends of Both Breakwaters, Center and Near Root of East Breakwater	$ 500,000
January 1952	Seaward Ends of Both Breakwaters	80,000
March 1954	Seaward Ends of Both Breakwaters	1,300,000
November 1958	Breach in Stone Portion East Breakwater and End of East Breakwater	Not Yet Repaired

from the point of breaking to the breakwaters. Consequently, the height of the design wave was based on that breaking wave at a distance of 0.4 L seaward of the structures. This height at a breaking depth of 44 ft was determined to be about 34 ft.

The breakwaters were repaired using 33-ton tetrapods in the armor layer. Two layers of components were placed on the slopes around the heads of the breakwaters. The seaward slope and the end slope (along the breakwater center line) were set at 1-on-3 with a transition to a 1-on-2 landward slope.

Subsequently, model studies undertaken in March, 1958, (at the U. S. Army Engineer Waterways Experiment Station, Vicksburg, Miss.) of a breakwater at another harbor, revealed a serious weakness in the design of the ends of the Kahului breakwaters. The "before" and "after" photographs, Fig. 7, depict the results of the model study of a design similar to the one used at Kahului. The "before" photograph shows two layers of tetrapods assimilating 21.7-ton units on an end slope of 1-on-2. The "after" photograph indicates the results of attacks (about 10 waves) by the equivalent of 30-foot high breakers, in 16 sec wave periods.

The dire prediction of the model study proved all too accurate. The severe storm of November 22, 1958, caused substantial damage to the east breakwater. The upper aerial photograph, in Fig. 8 shows waves attacking the Kahului break-

[3] "Wave Behavior Over a Fringing Coral Reef," by Melville S. Priest, The Military Engineer, July-August, 1955.

waters during this storm. The picture was taken about 12 hr after the peak of the storm, when it had abated to some extent. Note the 70-ft breach in the old stone portion of the east breakwater. The breach later widened to about 150 ft. Also, note that the wave completely obscures the end of the west breakwater (to the left). It was estimated that at the peak of the storm the breaker heights were 25 ft. About thirty 33-ton tetrapods were rolled away from the inboard quadrant of the end of the west breakwater where the slope was transitioned from 1-on-3 to 1-on-2 (see lower photograph in Fig. 8). Some of them rolled as far as 100 ft on a more or less level grade. Of the units on the seaward slope of the breakwater, three were broken.

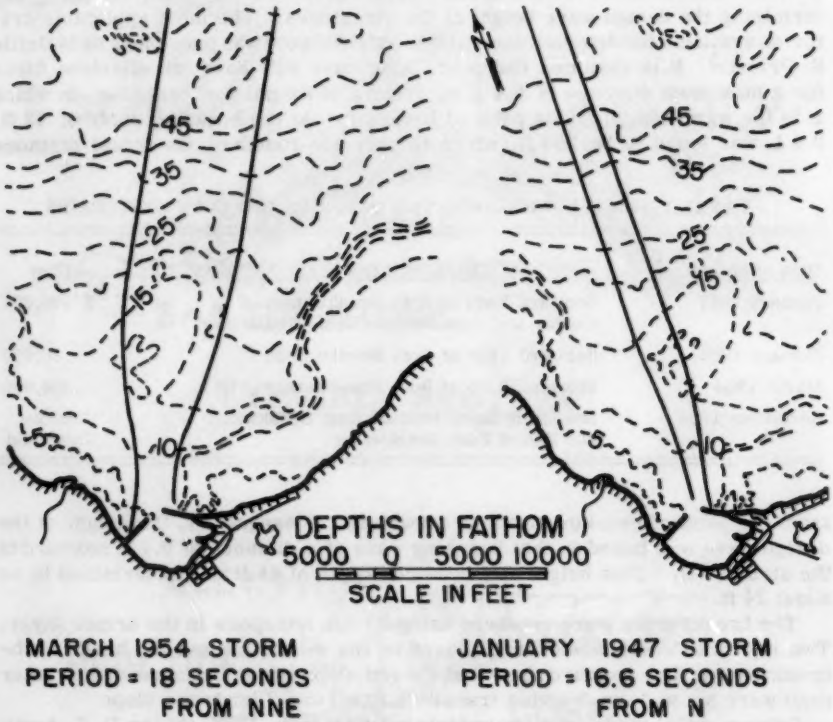

FIG. 6.—KAHULUI HARBOR WAVE REFRACTION DIAGRAMS

A review of the design for the repair work of 1957, indicated that more consideration should have been given to the following statement made by Mr. M. H. Marty, Chief Engineer, Establissements Neyrpic, Grenoble, France, at a conference in December, 1955:

> "Tetrapods generally are not used at the seaward end slope (of the breakwater). However, when used, the weight of the tetrapods should be increased over that of the tetrapods used on the side slopes."

Stopgap repairs of the damage caused by the 1958 storm were made in 1959. Complete reconstruction of the breakwater is contemplated when funds become available.

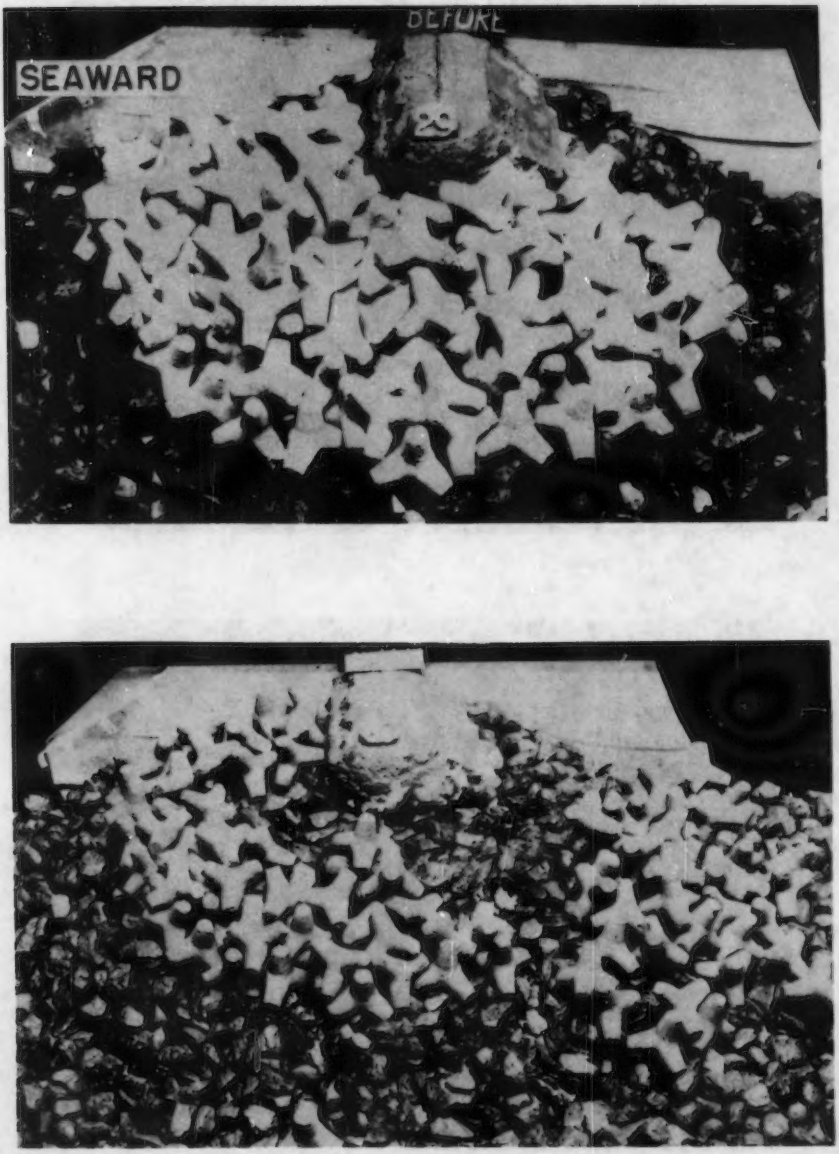

FIG. 7.—EFFECT OF WAVE ATTACK ON MODEL

FIG. 8.—STORM DAMAGE OF KAHULUI BREAKWATER

Nawiliwili Harbor.—Nawiliwili Harbor is located on the southeastern coast of the island of Kauai. The harbor was developed at the mouth of Huleia River by dredging and by construction of an approximately 2000-ft long rubble-mound breakwater, that was completed in 1930.

Although the Kahului and Hilo breakwaters were damaged by the storm of January, 1947, no damage was sustained by the Nawiliwili breakwater because the waves were from due north, a direction that is not a critical exposure for Nawiliwili Bay. However, waves generated by the storm of March, 1954 caused failure of the end of the structure and damage to the adjoining seaward slope. The storm of September, 1957, and Hurricane Nina further damaged the breakwater. In all, approximately 105 ft of the seaward end was knocked down and about 600 ft of the adjacent seaward slope severely damaged.

Preparatory to planning the repairs, that were completed in February, 1959, a study was conducted on the waves generated by the extra-tropical storm of March, 1954. A hindcast was made to determine the characteristics of the waves in deep water. These estimated characteristics were:

Storm of March 1954

H_o = 32 feet
T = 15 seconds
L_o = 1150 feet
Direction - northeast

A wave refraction analysis showed that orthogonals representing the phenomenon converged on the head of the breakwater. Convergence was such that the maximum refraction coefficient, $K = \sqrt{2}$, was indicated.[2] Use of the aforementioned data in estimating the height of waves approaching the head of the structure resulted in an increase in wave height to about 34 ft. However, it was determined that waves of this magnitude would break in water about 44 ft deep, a depth that was at a distance greater than 0.4 L seaward of the breakwater. This condition was similar to that encountered in the Kahului refraction analyses. Therefore, the maximum breaking wave affecting the structure was determined by the controlling depth at a distance (seaward of the breakwater) equal to the maximum distance of full effective force. This controlling depth below high tide level at a distance of 0.4 L, or 184 ft, was found to be 31 ft. By application of the equation for breaking depth, the design wave height was then computed to be 24 ft.

With the results obtained, designs were developed for repair of the breakwater using; 1) all stone, 2) stone and tetrapods; and 3) stone and tribars.

The three designs were checked by model studies at the Corps' Waterways Experiment Station in March, 1958. These model tests were conducted for the following reasons: 1) the complex hydrographic configurations seaward of the breakwater site, and 2) the lack of design criteria pertinent to (a) heads of breakwaters, (b) breaking waves attacking rubble-mound structures, (c) severe overtopping ($h = 0.4\ H_b$, in which H_b is the breaking wave height) (the usual criterion is h = H above design water surface), and (d) tribar, a recently developed breakwater component.

The section and the model studies of the all-stone design will be discussed separately from those of the designs using precast concrete components, in view of the fact that the tests on the all-stone models differed somewhat from those on the models having tetrapods or tribars in the armor layer.

The design section of the all-stone plan consisted of a broad-crested mound having an 80-ft crest width and a seaward slope at the angle of repose (1-on-1.4±). This design reflected the anticipation that wave action would reduce the slope to at least 1-on-4 by causing stones to roll down the slope, thereby reducing the crest width to about 15 ft (Fig. 9). Still water level was +2 ft of mean lower low water. This concept was not applied to the end slope (along the longitudinal axis) at the head because it was feared that the stones would roll into the entrance channel (see plan view in Fig. 9). The model having the equivalent of 10-ton stones in the armor layer of the breakwater was constructed with hydrographic conditions assimilating the ocean floor seaward of the prototype.

The first test definitely showed that the controlling depth seaward of a breakwater limits the magnitude of breaking waves that can attack the structure. In this case, the height of the breakers approaching the breakwater was less than the design wave height of 24 ft. In fact, most of them were about 21 ft in height. Some stones rolled down the seaward slope, but did not reduce it to 1-on-4.

It was desired to determine the approximate factor of safety of the design by subjecting the model to attack by waves greater than design magnitude. Therefore, modifications were made to the hydrography seaward of the breakwater to increase the controlling depth by about 50% in order to permit proportionally larger broken waves (up to 36 ft high) to attack the structure. Contrary to the anticipated effect that the stones would be rolled down the slope, a high percentage was taken over the crest by wave action. After an equivalent of about 30-prototype-hr, sufficient stones had rolled onto the crest to increase its elevation from 13 ft to 22 ft (Fig. 10) and very few were carried completely over the breakwater.

The design was subsequently modified to include a change in the crest elevation to 18 ft above design water surface with the seaward slope remaining at the angle of repose. Because the wave energy is proportional to the square of the wave height, it was assumed that this modified design provided a safety factor of 2.25, as a result of the 50% increase in design wave height.

The model of the head of the breakwater included a facsimile of the mound of stone lying around the end of the structure and below the water surface. In the prototype, the mound had been formed over a period of years by the dislodging of stones from the original structure and repair work. The end slope of the breakwater model was set at the angle of repose.

It was observed during the test that waves passing over the mound of stones were refracted from the channel toward the end of the breakwater. It was further noted that waves shunted or spilled off the seaward slope of the end of the structure converged with the aforementioned refracted waves. This action, coupled with the breaking waves transforming into waves of translation, created a high velocity jet across the end of the breakwater. As expected, stones were rolled down the slope by wave action. Results of the test were not considered conclusive because of the width restrictions of the test tank. It was not possible to assimilate all conditions in the prototype.

The designs using the two types of precast concrete components were similar and were subjected to a series of duplicate model tests. The armor layer of sections tested included tribars in a single layer, a double layer, and a combination of single and double layers. Since tetrapods are not suitable for use in a single layer, only double layers of this component were used in the tests.

In sections back from the head the original designs indicated the following cover layer compositions on a 1-on-1 $\frac{1}{2}$ seaward slope; 1) 21.8-ton tetrapods

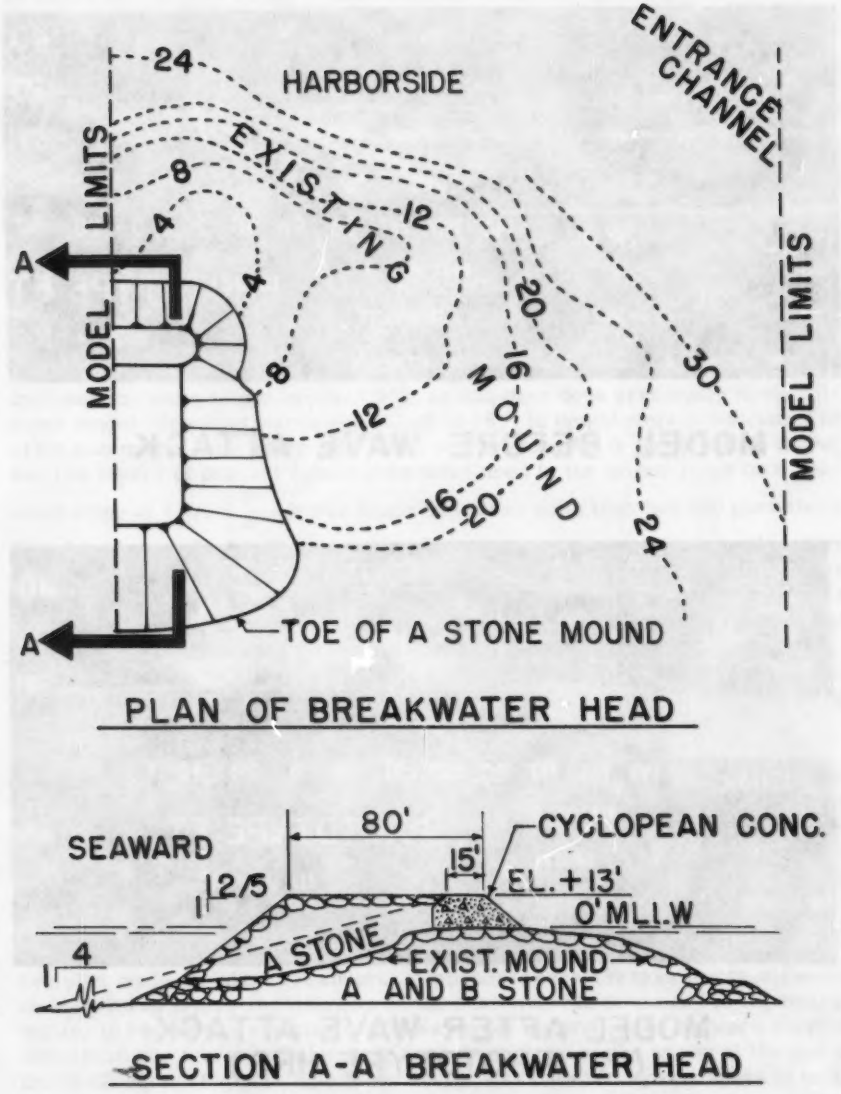

FIG. 9.—PLAN AND SECTION OF BREAKWATER HEAD

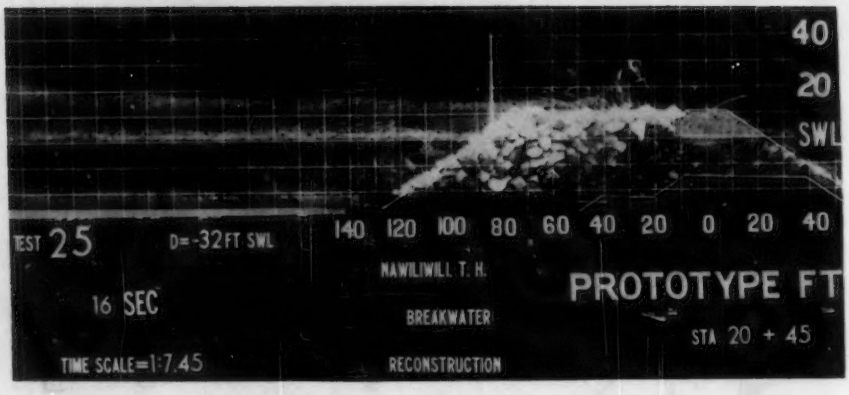

MODEL BEFORE WAVE ATTACK

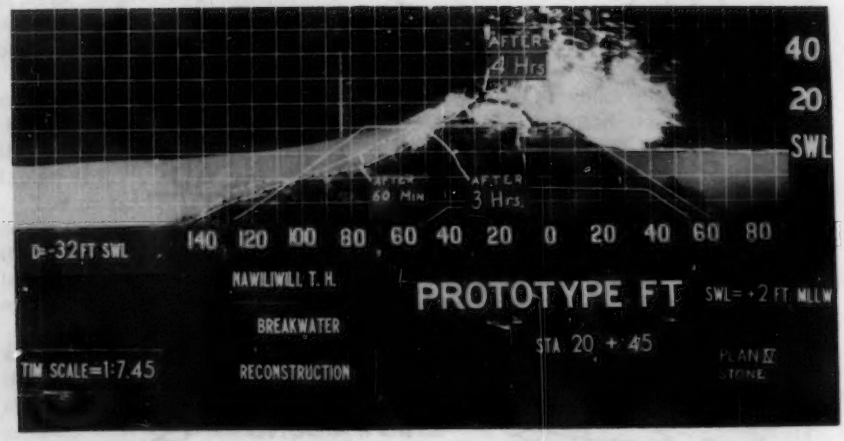

MODEL AFTER WAVE ATTACK
(30 PROTOTYPE HRS)

FIG. 10.—WAVE ATTACK ON MODEL

in two layers, and 2) 17.8-ton tribars in a combination of two layers below the water surface and a single layer above sea level (Fig. 11). Plans for reconstruction of the head of the breakwater were identical in that they were designed for two layers of precast components on a slope of 1-on-1 $\frac{1}{2}$ (see note in Fig. 11).

As in the case of the first test on the all-stone design, the models for the first series of tests on tetrapods and tribars were constructed with hydrographic features assimilating the conditions in the prototype. The section of the breakwater in each model corresponded to a typical section near the seaward end, but did not include the head. The breaker heights approximating the design wave height of 24 ft further substantiated the fact that controlling depth limits the magnitude of waves. No damage was sustained by the test sections, and, therefore, no weaknesses were revealed.

It was considered imperative, however, that all weaknesses due to varied conditions be exposed and that the final selected sections provide an adequate factor of safety.

Modifications were made to the hydrography seaward of the breakwater to increase the wave height by about 50%, as had been done previously to the all-stone model. Breaking waves equivalent to 36 ft in height were produced. The crest was only 0.3 H_b above still water level, where H_b is the breaking height, and two layers of precast components were used in the armor layer on a seaward slope of 1-on-1 $\frac{1}{2}$. It was found that those units that had any part above the elevation of the breakwater crest were rolled over the structure by wave action. This occurred with both tetrapods and tribars. In another case, where a single layer of tribars was used, the top row or two of units were carried over the crest. In all cases, concrete stops placed on the seaward edge of the crest successfully prevented the failure.

As previously indicated, the plans denoting precast components in the reconstruction of the head were identical, each having an armor layer consisting of two layers of units at a slope of 1-on-1 $\frac{1}{2}$.

When subjected to attack by breaking waves of design magnitude, failure of both sections occurred. As in the case of the test on the stone design of the head, it was observed during the conduct of these tests that a high velocity jet across the end of the breakwater was created by the convergence of the refracted waves and the shunted waves, and by the breaking waves transforming into waves of translation.

Consequently, two modified designs were made and both proved successful against attack by breaking waves ranging in height from 24 ft to about 36 ft. One plan made use of a wave absorbing mound of precast breakwater components at least three layers in thickness on the seaward side of the end of the breakwater, to reduce the shunting of the waves off the end of the seaward slope of the structure, thereby diminishing the convergence of the waves at the end of the breakwater (Fig. 12). The other design was featured by two layers of units placed on a 1-on-4 end slope (along the longitudinal axis) and a 1-on-3 back slope (Fig. 13). The plan with the wave absorbing mound was selected for use because of slightly greater stability. Furthermore, the mound would be within reach of land-based construction equipment. Thus, more contractors would be able to bid.

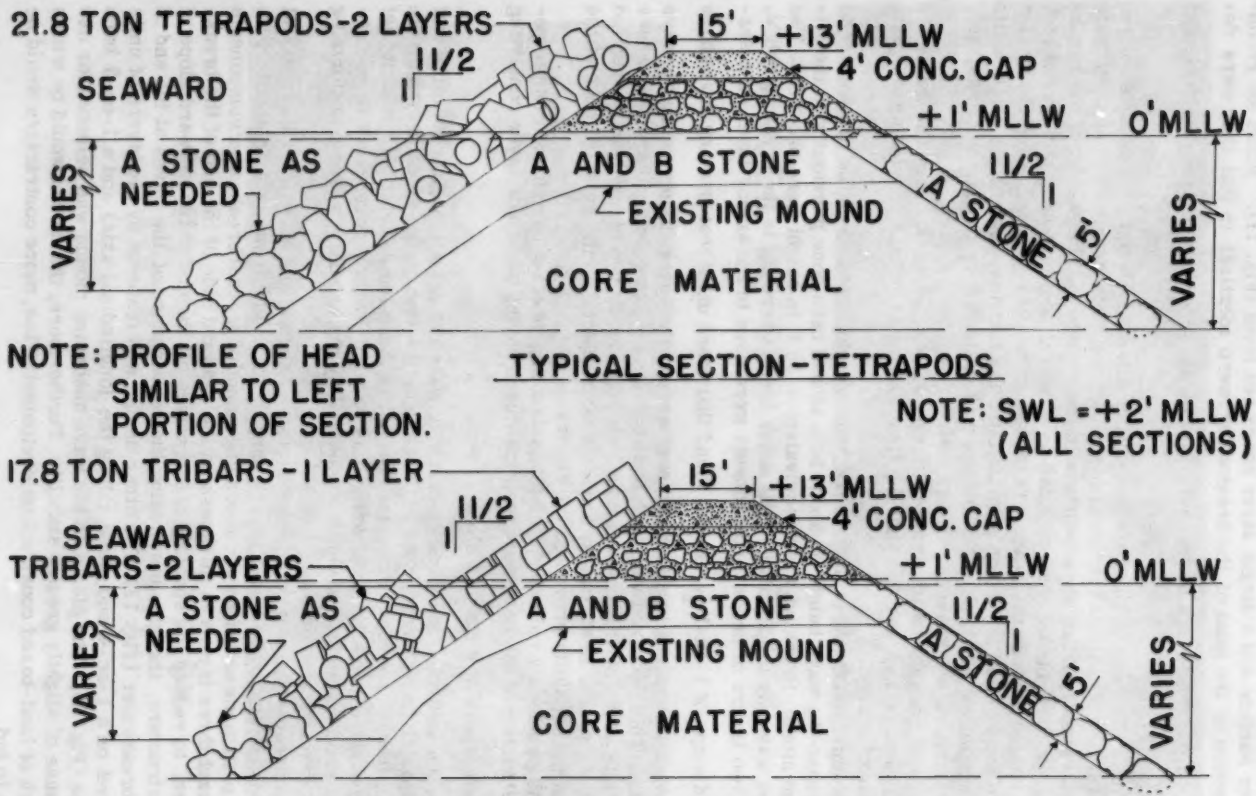

FIG. 11.—TYPICAL SECTIONS OF TETRAPODS AND TRIBARS

FIG. 12.—SUCCESSFUL HEAD DESIGN WITH WAVE ABSORBING MOUND

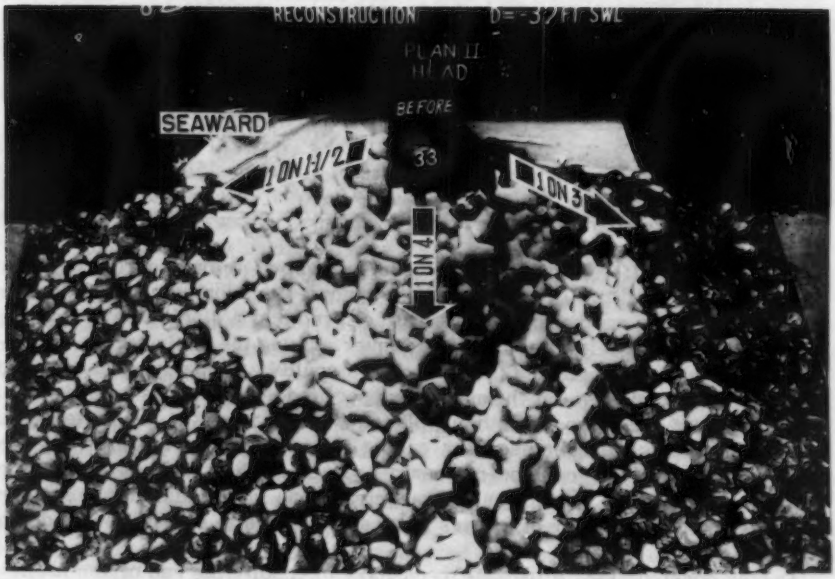

FIG. 13.—SUCCESSFUL HEAD DESIGN WITH FLAT END SLOPE

Since the models of the modified designs for repair of the breakwater, using precast components successfully, withstood attacks by broken waves equivalent to 36 ft, a height 50% greater than the design wave height, it was assumed that a safety factor of about 2.25 was being provided.

The three different plans for the repair of the Nawiliwili breakwater having been revised according to results of the model studies, bidders were given the option of bidding on any of the three proposals.

With regard to the all-stone design, major disadvantages existed. On Kauai no quarries are capable of producing suitable breakwater stone because the island is geologically the oldest of the major islands and rock outcrops are consonantly deeply weathered. Also, since relatively flat seaward slopes are required to stabilize an all-stone section, the volume of prime stone to armor the slope, as well as the total volume of breakwater stone, is increased. Therefore, it was doubtful that this plan would be competitive with either of the two plans using precast concrete components. This was borne out by the fact that no bids were received on the stone scheme.

The successful bidder submitted bids on the plans using tetrapods and tribars, with the bid on the latter being lower. The other bid received was on the tribar plan only. A comparison of the low bid and the Government estimate on the tribar and tetrapod plans is given in Table 2.

TABLE 2.—COMPARISON OF COST OF BID ITEMS ON TETRAPODS AND TRIBARS

	Bid Price		Government Estimate (Without Profit)	
Items	Tetrapods	Tribars	Tetrapods	Tribars
Forms	$ 30,800	$ 16,000	$ 28,000	$ 14,545
Cement	124,704	80,520	114,312	73,710
Casting	294,030	179,950	259,200	159,890
Placing	133,650	89,680	121,500	97,350
Total	$583,184	$366,150	$523,012	$345,595
Difference		217,034		177,417
Saving		37%		34%

Although model tests proved that a single layer of tribars nested together is more stable than two layers placed at random, the adopted plan showed the latter below water surface because it was believed that a single layer could not be properly placed below sea level. However, during the early stages of construction it was demonstrated that the tribars could be properly placed (nested together) in a single layer at the maximum specified depth on the seaward slope. Observation of the components being placed was enhanced by the white Hunts compound, which had been used for curing the concrete. Furthermore, the tops of the legs of the components could be seen as the trough of each wave passed over the units. As a result, the contract was modified by change order to substitute a single layer of tribars for the two layers to the full design depth of armor cover.

During construction, it became necessary to modify the end of the breakwater by the addition of components to provide a flatter end slope and to "toe-in" the back slope where stone had been removed to provide flotation for construction equipment.

The 17.8-ton tribars were placed by a floating crane operating on the seaward side of the breakwater. Difficulty in placing was encountered even during what was considered "working weather" because swell conditions often caused the end of the boom to rise and fall from 5 ft to 10 ft. The components could not simply be released at the bottom of the downward motion of the boom, since it was specified that the tribars in the single layer were to be placed in contact. Maneuvering of the components, in order to place them in accordance with the specifications, caused the tribars to collide, often with considerable force. Consequently, 13 of the 351 unreinforced units were broken during placement. However, experience in placing greatly reduced the breakage rate. The last 247 units were reinforced and none were broken. It was originally estimated that 590 tribars would be required for the project. Actually, 598 were cast and placed. "As built" drawings of the Nawiliwili breakwater are shown in Fig. 14.

A comparison of the loss by breakage to the cost of reinforcing to prevent breakage showed that for 18-ton tribars reinforcing is not economically justified. However, since the stress in the bars, or spoke members, increases as the square of the linear dimensions of the component, that is, the diameter of the bar, it is probable that tribars weighing more than 20 tons should be reinforced. In general, since concrete breakwater components are exposed to salt water, reinforcing or other imbedded steel (lifting eyes and so forth) is not desirable due to the poor durability of reinforced concrete under these conditions, especially in tropical climates. However, when reinforcing is necessary, a minimum 4-in. cover of dense concrete over all steel should be required.

During the first week in August, 1959, Hurricane Dot, moving in a westerly direction south of the island of Hawaii, turned northerly and passed directly over Nawiliwili Harbor. Weather planes flew into the storm, and fairly accurate data with respect to wind velocity and barometric pressures were obtained. Unfortunately, the anemometer for recording instantaneous wind velocity at the United States Weather Bureau Station, at Lihue Airport, about two miles north of the harbor, was inoperative during the peak of the storm.

The day before the hurricane reached Kauai, an engineer from the Corps of Engineer, Honolulu District, and two Army Signal Corps photographers were dispatched to that island to obtain data. The inspection party occupied an observation point on a cliff located across the channel and about 1,500 ft from the head of the breakwater. Wind-driven rain and spray hampered observation of the waves breaking on the breakwater after 2:00 p.m. on August 6, 1959, which was about six hr before the height of the storm. Wave heights could not be accurately obtained from the photographs shown on Fig. 15 due to the unavailability of a reference object for use as a scale. However, the consensus of different trial approximations, and observations by the engineer on the scene indicated breaker heights of about 22 ft at the time the photographs were taken.

Two trials of hindcasts were made to estimate the height of the waves generated by the hurricane, and wave refraction analyses were conducted to estimate the magnitude of the waves at the breakwater site during the peak of the storm. The first trial indicated the following deepwater characteristics of the waves; H_o = 35 ft, T - 12.5 sec, L_o = 800 ft, and the direction as south-southeast. The ensuing refraction analysis suggested an increase in the wave height to about 50 ft at the breakwater. This height appeared unreasonable in comparison with the previously estimated height. The second hindcast study in which conservative values for wind velocity and duration were used rendered the following deepwater characteristics; H_o = 27 ft, T = 11.5 sec, L_o = 680 ft and the direction as southeast.

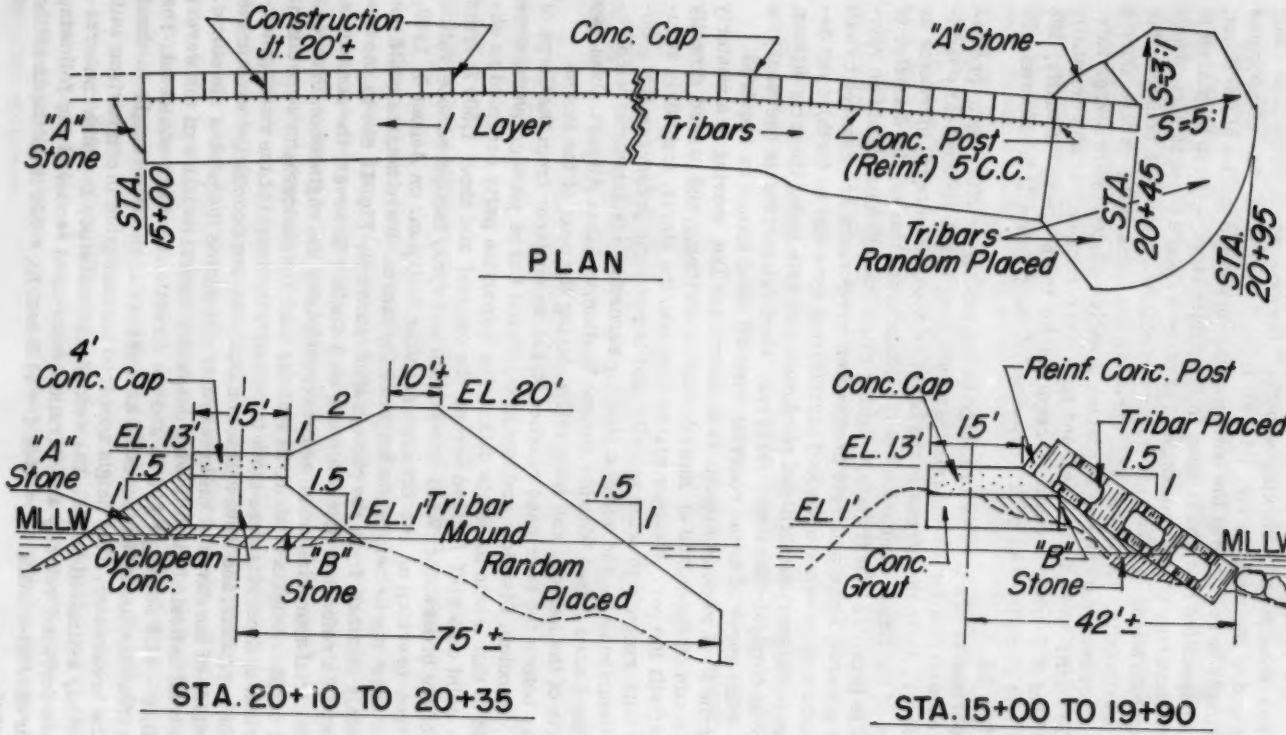

FIG. 14.—NAWILIWILI BREAKWATER

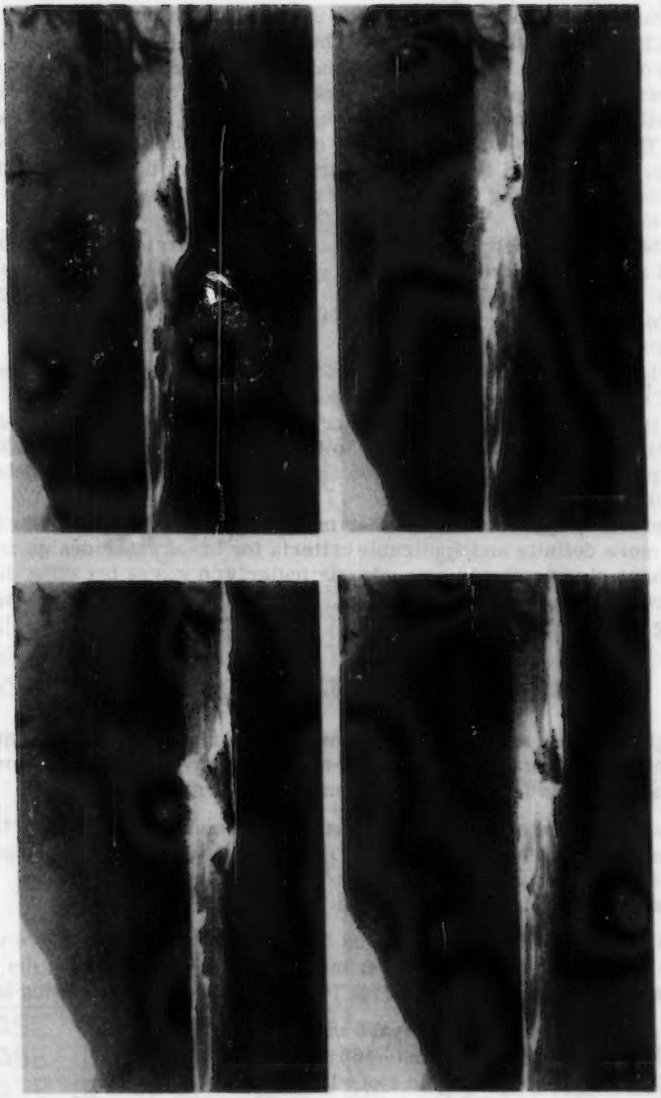

FIG. 15.—ATTACK OF HURRICAN DOT WAVES ON NAWILIWILI BREAKWATER

A refraction analysis indicated a refraction coefficient, K = 0.92. The wave height was then computed to be about 25 ft at the breakwater. In view of the more conservative estimate, it appeared that the structure was subjected to attack by waves of design magnitude, 24 ft, for several hours' duration.

The breakwater sustained very minor damage during that hurricane. One reinforced concrete post was broken off by a tribar that had been swept from the top row of units over the crest. A probable explanation for the displacement of the tribar is that a part of the component extended about 2.5 ft above the plane (parallel to the seaward slope) through the tops of the other tribars down the slope. There was no evidence that any other units had moved upslope at all. Conversely, it was noted that a few tribars moved down the slope, the maximum distance moved being 9-in. The only other damage consisted of two components being broken.

The stability of the Nawiliwili breakwater, during Hurricane Dot, cannot be considered a conclusive test of the breakwater or its armor components. It is anticipated that more severe wave action will result should the structure be subjected to attack by long period waves, that are usually generated by extra-tropical storms to the northeast.

As previously mentioned, the factor of safety of the Nawiliwili breakwater design was estimated to be 2.25, based on results of the model studies. Since one of the tribars was carried over the breakwater crest by waves generated during Hurricane Dot, doubt exists as to the actual safety factor provided in the prototype. However, no conclusive criteria is available for the determination of this actual factor of safety.

It is, therefore, apparent that further model studies should be conducted in order that more definite and applicable criteria for breakwater design may be derived. These studies should be made particularly on waves breaking directly on breakwaters, heads of breakwaters, and structures to withstand severe overtopping.

COMPARISON OF ARMOR LAYER COMPONENTS

The purpose of this section is to present a comparison of the three types of armor layer components used in rubble-mound breakwater construction and repair in the Hawaiian Islands. These components are:

1. Stone, the natural material traditionally used in rubble-mound structures;
2. Tetrapods, a patented shape and the first scientific breakwater component developed in a hydraulic laboratory; and
3. Tribars, patented and model tested.

Comparisons were made on structures having crest elevations (above water surface) of 15 ft in the first case, 16 ft in the second, and 18.5 ft in the third case. These comparisons, shown in Fig. 16, were done on the following basis:

1. Cost of core stone per cubic yard in all cases—$7.00,
2. Weight of stone per cubic foot—165 lbs,
3. Weight of concrete per cubic foot—150 lbs,
4. Specific gravity of sea water—1.03,
5. Maximum weight of available stone—12 tons,
6. Maximum capacity of available land-based crane—12 tons, at 80-foot radius,

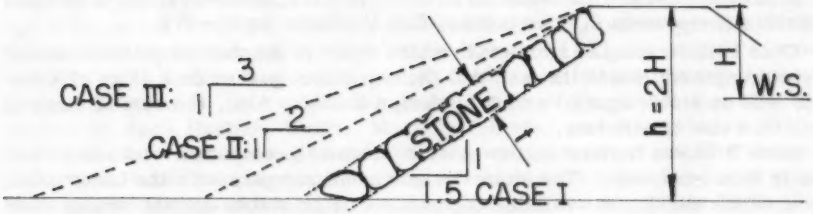

SECTION ··· STONE

CASE I: H= 15', W=12 Ton, t=5.5', $ 730/LF
CASE II: H= 16', W=12 Ton, t=5.5', $ 970/LF
CASE III: H=18.5', W=12 Ton, t=5.5', $1550/LF

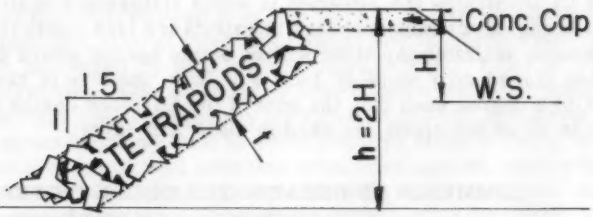

SECTION ··· TETRAPOD

CASE I: H= 15', W=6.3 Ton, t=10', $ 930/LF
CASE II: H= 16', W=8.5 Ton, t=11', $1060/LF
CASE III: H=18.5', W=12.7 Ton, t=12', $1290/LF

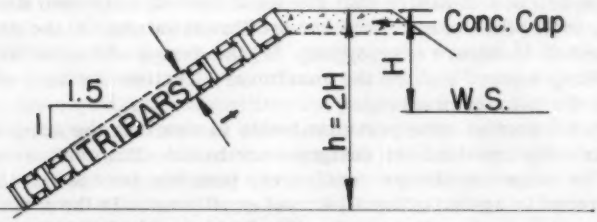

SECTION ··· TRIBAR

CASE I: H= 15', W=2.2 Ton, t=3.5', $ 740/LF
CASE II: H= 16', W=3.0 Ton, t=3.9', $ 840/LF
CASE III: H=18.5', W=4.4 Ton, t=4.2', $1110/LF

FIG. 16.—COMPARATIVE COST AND DESIGN OF BREAKWATER SECTIONS

7. Costs: Concrete per cubic yard (in place)—$33.00, and Stone (a) Armor stone per ton—$11.00 (b) Other per ton—$7.00, and

8. Per cent voids: in Stone (a) Armor—30% (b) Other—30% and in Precast concrete components (a) Two layers—50% (b) Single layer—47%.

Case I illustrates the situation in which stone is the most economical armor layer component due to the fact that the cap stone, placed on a slope of 1-on-1.5, will be stable against attack by design waves. Also, the cost of stone is less than that of concrete.

Case II shows tribars as the most economical component and stone less costly than tetrapods. The stone design cannot compete with the tribar plan, because the maximum available cap stone will be stable against design wave attack only when placed on a slope no steeper than 1-on-2. This reduced seaward slope increases the size of the section and, consequently, the cost for the additional armor and core stones. The cost, however, is not increased so that it exceeds the cost of tetrapods. Tribars are generally more economical than tetrapods because they are more stable and can be used in either a one- or two-layer armor cover having higher porosity.[4]

Case III illustrates the situation in which tribars are again the most economical breakwater components and tetrapods are less costly than stone. Since the maximum available cap stone will be stable against attack by design waves only when placed on a slope of 1-on-3 or less, the size of the section is increased to a degree such that the cost of the all-stone design exceeds that of the plan in which tetrapods are used in the armor layer.

COMMENTS ON BREAKWATER DESIGN CRITERIA

The review of designs and the results from consultation pertaining to about ten breakwaters in the Pacific, and damages sustained by these structures during storms have caused questioning of the accuracy of design coefficients and wave analyses. Doubt also exists as to the applicability of certain criteria to unique field conditions. No well-established procedures are available to meet certain specific design requirements.

Experience indicates that the most needed additional design criteria pertains to; (1) the design of the heads of breakwaters, (2) the design of structures subjected to severe overtopping, (3) the design of berms for stability against breaking waves, and (4) the maximum effective distance of breaking waves from the point of breaking.

Model studies have proved valuable in checking the adequacy of designs and the criteria on which the designs were based. However, even in these studies results were not always conclusive, possibly because of the difficulties encountered in assimilating all actual conditions. In the tests on the Nawiliwili breakwater designs for repair, as valuable as they were, appeared to be unreliable to some extent. Notwithstanding this, model studies have been the source of much design data.

At the Waterways Experiment Station, the following formula was developed for determination of the weight of breakwater components:

$$W = \frac{\gamma_c \ H^3}{K_1 \left(\gamma_c/\gamma_\omega - 1\right)^3 \cot \alpha} ,$$

4 "Design of Tribar and Tetrapod Cover Layers for Rubble-mound Breakwaters," by Robert Y. Hudson and R. A. Jackson, Miscellaneous Paper No. 2-296, U. S. Army Engr. Waterways Experiment Sta., January, 1959.

in which W is the weight of breakwater component, γ_c is weight per cubic foot of breakwater component, γ_w refers to the weight per cubic foot of water at site, α is the angle of seaward slope of breakwater with horizontal (Good for cot α between 1.5 and 3), H is design wave height, K_1 for stone = 3.2 (safety factor of 1), K_1 for tetrapods = 8.4 (safety factor of 1), K_1 for tribars (random 2 layers) = 12 (safety factor of 1), and K_1 for tribars (single layer nested) = 27 (safety factor of 1). During the design for repair of the rubble-mound breakwaters at Apra Harbor, Guam, Mariana Islands, and Kaumalapau Harbor, Lanai, Hawaii, the existing seaward slopes were compared with the theoretical stable slopes computed by the above-mentioned formula. The latter slopes were superimposed on the cross sections of the breakwaters (see Figs. 17(a), Guam, and (b), Kaumalapau. The comparisons show reasonably good correlation in view of possible appreciable error in the estimated wave heights and considerable variation in the weight of stones in the armor layer.

CONCLUSION

Breakwaters have been required to create most of the harbors in the Hawaiian Islands because the natural sites are usually not landlocked and dredging inland has been precluded by basaltic rock formations. Prior to 1950, the rubble-mound structures were featured by keyed stonework in the armor layer. Kawaihae Harbor has the only recently constructed federal breakwater. The rubble-mound structure, completed in 1959, employs stone in the armor layer because an extensive coral reef provides protection against severe wave action. The Kahului breakwaters, repaired in 1957, with tetrapods, sustained substantial damage during the severe storm of November 22, 1958. In 1959, the Nawiliwili breakwater was repaired, the design for which was model tested and subsequently modified. The tribar-armored structure sustained very minor damage during Hurricane Dot, in August, 1959.

The design of breakwaters has undergone significant changes from the period prior to 1950 to the present. A scientific approach has replaced the practice of "doing the best with what was available." Practical techniques have been developed for conducting wave hindcasts and refraction and diffraction analyses. Considerable design criteria have been established and model tests have become accepted as an invaluable means of checking the adequacy of designs and verifying theoretical design criteria. Precast concrete breakwater components have been developed, and competitive bid prices and field tests indicate that they provide an economical armor cover against design waves of significant height. However, stone should not be regarded as uneconomical when its cost is lower than that of concrete and when labor costs are low, since indications are that all-stone structures may be stabilized by using flatter slopes, berms, and keyed placement.

In the design of rubble-mound breakwaters, problems not susceptible to solution by application of criteria heretofore established are often encountered. Although the designer is provided with fairly reliable techniques for determining the breakwater cross section, he is still confronted with questions pertaining to this and other aspects of design. What is the maximum effective distance of a breaking wave? How does the force decrease as the broken wave proceeds shoreward? How should a structure be designed to withstand severe overtopping? What is to be considered in the design for waves breaking directly on

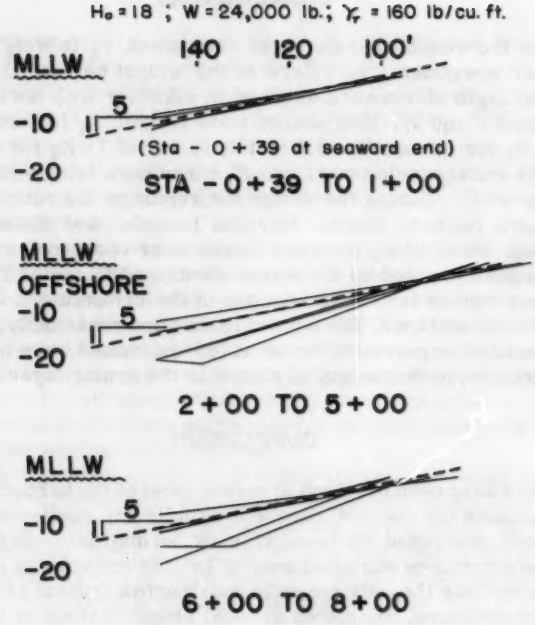

(a)

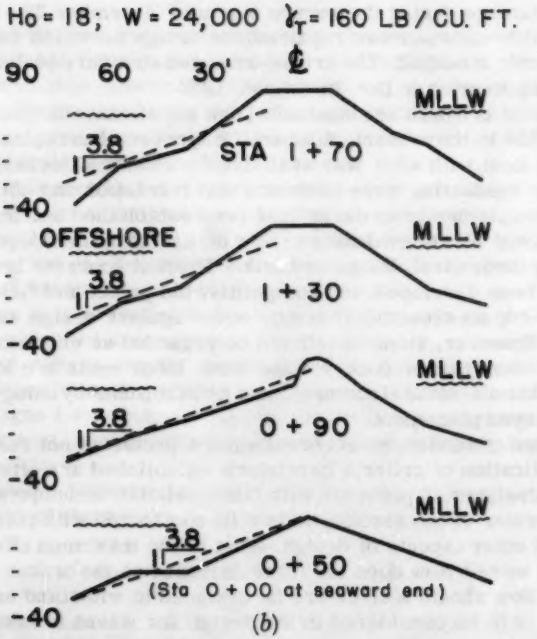

(b)

FIG. 17(a),(b).—THEORETICAL STABLE SLOPES COMPARED TO PROTOTYPE SLOPES STABILIZED UNDER WAVE ATTACK.

breakwaters? How should the head of a breakwater be designed? Having limited criteria and, in some cases, none pertaining to the uncertainties, the designer over-designs in an attempt to insure an adequate structure.

In the case of the repair of the Nawiliwili breakwater, an experienced engineer offered repeated reminders throughout the design, model tests, and construction that "You can't build it too strong."

Economical breakwaters will be built "strong enough" when criteria for all aspects of design are developed, in order that the desired factor of safety can be assured for each element of the structure.

APPENDIX. NOTATION

Following are definitions of the letter symbols used in the paper:

- h = height of overtopping;
- H = design wave height;
- H_b = breaking wave height;
- H_o = deepwater wave height;
- K = refraction coefficient;
- K_1 = shape coefficient;
- L = wave length at a point along the direction of travel of the wave;
- L_o = deepwater wave length;
- T = deepwater wave period; and
- W = weight of breakwater component.

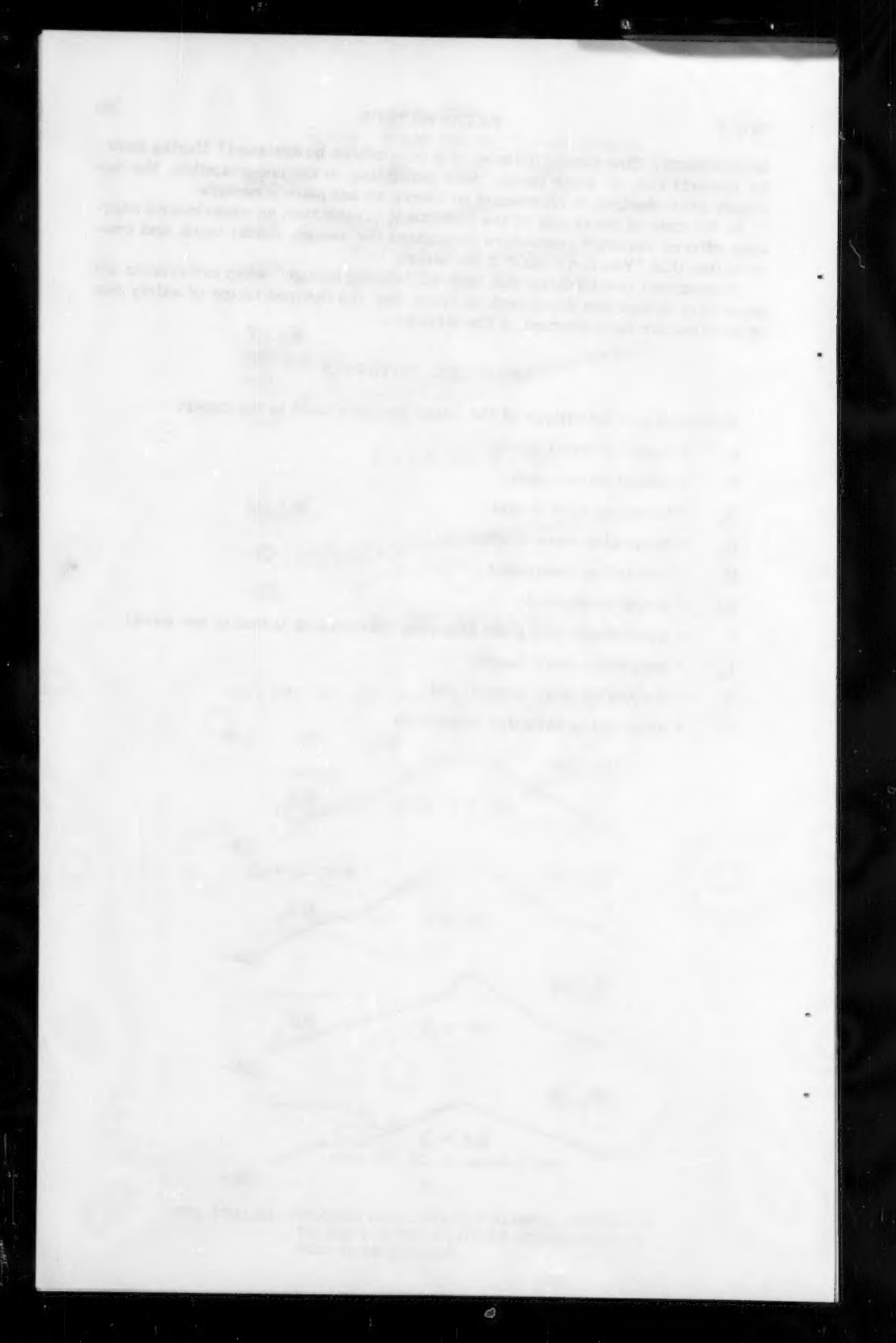

Journal of the
WATERWAYS AND HARBORS DIVISION
Proceedings of the American Society of Civil Engineers

PREDICTION OF MAXIMUM PRACTICAL BERTH OCCUPANCY

By Thomas J. Fratar,[1] F. ASCE, Alvin S. Goodman,[2] M. ASCE, and Austin E. Brant, Jr.,[3] A. M. ASCE

SYNOPSIS

Studies of observed berth occupancy patterns at commercial marine terminals have been made for many United States ports. Based on the close agreement between these observed patterns and theoretical frequency distribution functions, a method for predicting maximum berth occupancy has been developed.

TYPES OF MARINE TERMINALS STUDIED

Marine terminals may be divided into two groups, based on type of operations: commercial terminals, which are operated more or less on a public basis for the use of several shippers or consignees and which handle the vessels of several shipping companies; and proprietary terminals, which are operated on a private basis for the use of a single shipper or consignee or which handle the vessels of a single shipping company or of several companies which coordinate their vessel schedules.

The occupancy of a proprietary terminal is controlled by the terminal operator, which may be a shipper, consignee, or shipping company, who can adjust vessel arrivals and departures to attain as high a berth occupancy as re-

Note.—Discussion open until November 1, 1960. To extend the closing date one month, a written request must be filed with the Executive Secretary, ASCE. This paper is part of the copyrighted Journal of the Waterways and Harbors Division, Proceedings of the American Society of Civil Engineers, Vol. 86, No. WW 2, June, 1960.

[1] Partner, Tippetts-Abbett-McCarthy-Stratton, Engrs. and Archt's., New York, N. Y.
[2] Proj. Engr., Tippetts-Abbett-McCarthy-Stratton, Engrs. and Archt's., New York, N. Y.
[3] Proj. Engr., Tippetts-Abbett-McCarthy-Stratton, Engrs. and Archt's., New York, N. Y.

quired by commerce demands. The occupancy of a commercial terminal, however, is determined largely by ship arrivals and departures over which the terminal operator has little or no control. Moreover, vessel arrivals and departures are influenced and often disrupted by one or more of a multitude of unpredictable factors such as weather, ice conditions, operating difficulties, loading and unloading problems, fluctuations in trade, holidays, labor strikes, and the like. Thus, while ship schedules might indicate a potentially high berth occupancy at a commercial terminal, the actual berth occupancy will often be entirely different.

INFLUENCE OF BERTH OCCUPANCY ON THE CAPACITY OF COMMERCIAL MARINE TERMINALS

Operations at a commercial marine terminal may be divided into three distinct and independent functions:

1. The movement of cargo into or out of rail cars, trucks or barges;
2. The transit storage of cargo at the terminal; and
3. The movement of cargo into or out of vessels.

The practical operating capacity of a terminal is the volume of cargo which can be handled through the terminal with reasonable efficiency and only infrequent congestion, and may be limited by any one of the terminal's three operating functions.

At many United States ports, the factor determining the practical operating capacity of a commercial marine terminal is the capacity for moving cargo into or out of vessels berthed at the terminal.

This capacity is basically the product of two components; the cargo handling rate (expressed in tons per day of occupancy per berth) which can reasonably be attained and the number of days in a year that the berths at the terminal can be occupied under the prevailing operating conditions without undue congestion. This latter component of terminal capacity is the subject of this paper.

The maximum practical occupancy of a group of berths at a commercial terminal is largely limited by the ability of the group to meet the demands imposed by the pattern of ship arrivals and departures. In a hypothetical case, where a terminal contains a very large number of berths and the level of business is also very high, it can be expected that each berth will be reoccupied very quickly each time it is vacated. The occupancy per berth under these conditions would be very high. At the other extreme, where a terminal has only one or two berths, ship arrivals cannot be matched nearly as well with ship departures. Since the use which can be made of each berth is greater at terminals having a large number of berths, the operating capacity of a terminal increases at a greater rate than the proportional increase in the number of berths.

OBSERVED BERTH OCCUPANCY PATTERNS

Two sources of data were used for the analyses presented herein; first, data on berth occupancy at general cargo marine terminals collected in the

course of port development studies at Houston, Texas,[4] Portland, Oregon,[5] and Baltimore, Maryland; [6] and second, a study of the arrivals and departures of general cargo vessels during a six-month period at the ports of Boston, New York, Philadelphia, Baltimore, and Hampton Roads prepared by the Baltimore Association of Commerce.[7] The Baltimore Association of Commerce data were analyzed to determine the number of vessels in each port on each day of the period studied. No analyses were made for the port of New York because of the special conditions of terminal operation at that port, where many of the larger shipping companies operate terminals for the exclusive use of their own vessels. No analyses were made for the port of Baltimore since more detailed data were available elsewhere.[6]

A typical berth occupancy pattern derived from these data is given in Fig. 1, which shows the number of general cargo vessels in Philadelphia, Pa., on each day of July, 1955. During the period July through December, 1955, the number of general cargo vessels in Philadelphia ranged from 2 to 25. The randomness of berth occupancy is apparent.

The pattern of occupancy of commercial general cargo berths at a port can be more clearly shown by a frequency distribution curve. Fig. 2 shows the frequency distribution of the number of general cargo vessels in the port of Boston, Mass., during the period July through December, 1955. For example, on 4 days in this 184-day period, no vessels were in Boston; on 10 days, 1 vessel was in port; on 20 days, 2 vessels were in port; and so forth.

Similar studies at other United States ports indicate that the patterns of berth occupancy for commercial terminals are essentially random in that the following conditions are met:

1. The probability of a number of vessels in a port on a given day is not influenced by the number of vessels in the port on any other day; and
2. Each vessel arrives and departs independently of the movements of other vessels.

These conditions represent fairly well the operations at commercial general cargo terminals at the ports studied. When these conditions are met, the berth occupancy patterns can be represented by a theoretical probability distribution function.

STATISTICAL ANALYSIS OF BERTH OCCUPANCY PATTERNS

To determine the probability distribution functions that most nearly fit the observed data, a detailed statistical analysis was made.[8] It was found that only two of the theoretical probability distribution functions would meet the condi-

4 "Master Plan Survey for Port of Houston," prepared for Bd. for Commrs., Harris County, Houston Ship Channel Navigation Dist., Tippetts-Abbett-McCarthy-Stratton, 1953.

5 "Portland Harbor Development Survey," prepared for the Comm. of Pub. Docks, Portland, Oreg., Tippetts-Abbett-McCarthy-Stratton, 1959.

6 "The Port of Baltimore," prepared for the Maryland Legislative Council Port Committee, Tippetts-Abbett-McCarthy-Stratton, 1954.

7 "Service Provided at the Ports of Boston, New York, Philadelphia, Baltimore and Hampton Roads by Vessels Carrying General Cargo in Foreign Trade which Entered or Cleared During the Period July - December, 1955," submitted before the Interstate Commerce Comm., Investigation and Suspension Docket No. 6615, W. S. Hamill, Baltimore Assn. of Commerce, 1957.

8 "Probability and Its Engineering Uses," by Thornton C. Fry, D. Van Nostrand Co., New York, 1928.

tions of asymmetry and flatness imposed by the observed berth occupancy patterns. These two theoretical functions, the Poisson Law and the Binomial Law, were then examined further to determine which one had a higher level of agreement with the observed data. It was found that the Poisson Law, which can be derived directly from the conditions of randomness stated above, is more suitable than the Binomial Law to represent the occupancy of berths at commercial marine terminals. Using a different method of derivation, moreover, the

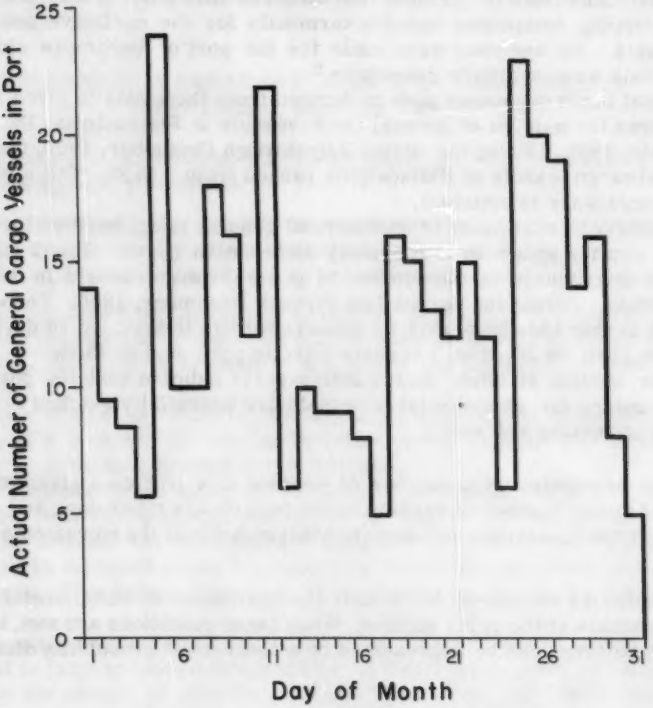

FIG. 1.—BERTH OCCUPANCY PATTERN

Poisson Law can be shown to be a limiting case of the Binomial Law.

The Poisson Law is

$$P_n = \frac{(\bar{n})^n e^{-\bar{n}}}{n!} \quad \ldots\ldots\ldots\ldots\ldots\ldots (1)$$

in which P_n is the probability of n berths being occupied at a terminal (or n vessels being in a port) on a given day, n represents the number of berths occupied (or the number of vessels in port), the Napierian-logarithm base e is 2.71828. . . , n! represents n factorial = n (n-1) (n-2) . . . (3) (2) (1), and $\bar{n}$ is the average number of berths occupied (or average number of vessels in port). The Poisson Law has two important properties: first, the summation for a given value of $\bar{n}$ of the values of P_n as n varies from 0 to infinity is unity; and second, the summation for a given value of $\bar{n}$ of the products of n and

P_n as n varies from 0 to infinity is $\bar{n}$. These properties are expressed as:

$$\sum_{n=0}^{\infty} P_n = 1 \quad \ldots\ldots\ldots\ldots\ldots\ldots (2)$$

and

$$(\bar{n}) = \sum_{n=0}^{\infty} (n)\ (P_n) \ldots\ldots\ldots\ldots\ldots\ldots (3)$$

For a study covering a given period of time, the frequency (expressed in number of days) of occurrence of each n-value is the product of the corresponding P_n-value and the total number of days in the period. Mathematically,

$$F_n = N(P_n) \ldots\ldots\ldots\ldots\ldots\ldots (4)$$

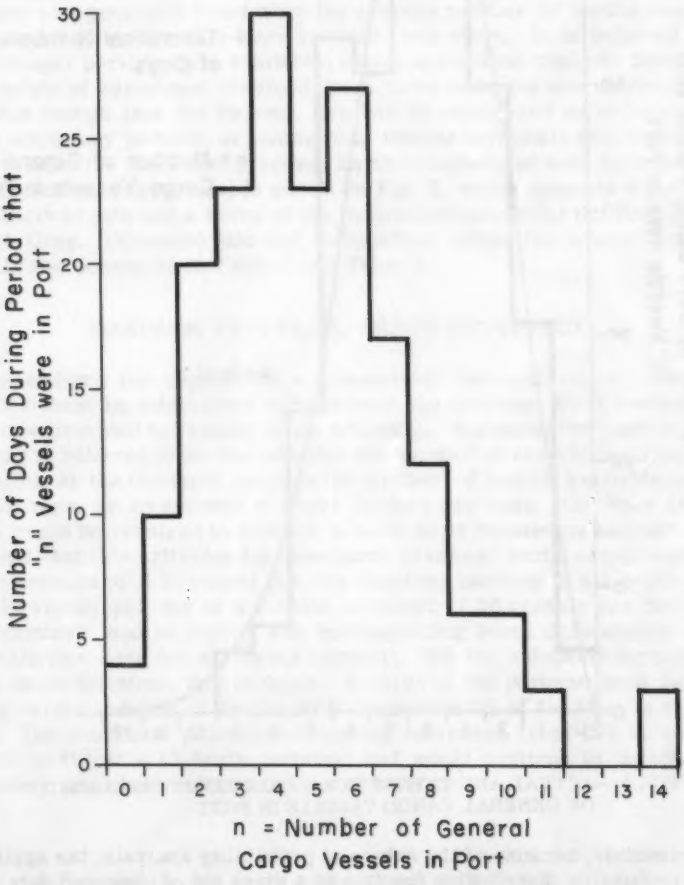
Number of Days During Period that "n" Vessels were in Port
30
25
20
15
10
5
0
0 1 2 3 4 5 6 7 8 9 10 11 12 13 14
n = Number of General Cargo Vessels in Port

FIG. 2.—FREQUENCY DISTRIBUTION CURVE

in which N is the total number of days in the period, and F_n is the theoretical number of days in the period that n berths are occupied at a terminal (or n vessels are in a port), as determined from the Poisson Law.

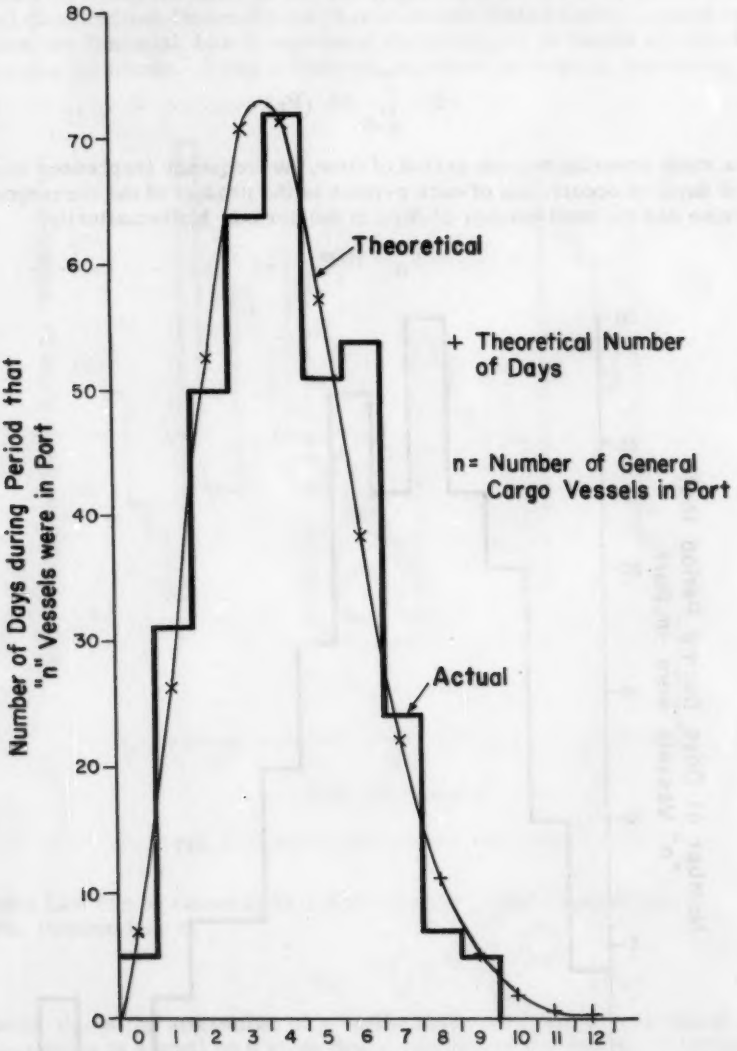

FIG. 3.—ACTUAL AND THEORETICAL FREQUENCY DISTRIBUITON OF GENERAL CARGO VESSELS IN PORT

Unfortunately, because of the nature of probability analysis, the applicability of a probability distribution function to a given set of observed data cannot definitely be determined. The probability that the observed data could result

from the Poisson Law ("goodness of fit") can be determined, however, by use of the chi-square test. The value of chi-square is determined as

$$\chi^2 = \sum_{n=0}^{\infty} \frac{(F_n - f_n)^2}{F_n} \quad \ldots\ldots\ldots\ldots\ldots\ldots (5)$$

in which f_n is the actual number of days in the period that n berths are occupied at a terminal (or n vessels are in a port), as determined from the observed data. The goodness of fit between the calculated values and the observed data is determined by the use of tables such as have been given elsewhere.[8]

The goodness of fit between the observed data and the theoretical values obtained by using the Poisson Law ranges from about 65% (considered to be excellent agreement) to less than 1% (considered to be poor agreement). Poor agreement was generally found when the average number of berths was large and the period for which data were available was short. It is believed that if data for longer periods were available, better agreement would be found.

The levels of agreement obtained from these analyses are believed to be reasonable enough that the Poisson Law can be considered as representative of berth occupancy patterns at commercial marine terminals and, thus, can be used to predict the maximum practical berth occupancy of such terminals. An illustration of this agreement is shown on Fig. 3, which presents a histogram of the observed data and a curve of the theoretical values for the year 1957, at Portland, Oreg. Observed data and theorectical values for several ports and terminals are compared in Table 1 and Table 2.

MAXIMUM PRACTICAL BERTH OCCUPANCY

In determining the capacity of a commercial marine terminal, a level of congestion must be established to represent the practical limit beyond which the service provided to vessels is not adequate. A reasonable limit for berth occupancy is believed to be that at which the number of vessels desiring to occupy berths at the terminal exceeds the number of berths available on about 5% of the time, or an average of about 18 days per year. On these 18 days, vessels would be required to wait for a berth to be vacated by another vessel. It is found that this criterion for maximum practical berth occupancy is met when an average of 0.35 vessel per day requires berthing at a 1-berth terminal; 0.82 vessel per day at a 2-berth terminal; 1.36 vessels per day at a 3-berth terminal; and so forth. The corresponding berth occupancies are 29% of the calendar days for a 1-berth terminal, 38% for a 2-berth terminal, 43% for a 3-berth terminal, and so forth. A curve of the percentage of berth occupancy versus number of berths with congestion 5% of the time is shown on Fig. 4. The maximum practical occupancy increases from 29% at a 1-berth terminal to 66% at a 15-berth terminal and would continue to increase (at a diminishing rate) for greater numbers of berths.

TABLE 1.--COMPARISON OF ACTUAL AND THEORETICAL NUMBER OF VESSELS AT COMMERCIAL GENERAL CARGO TERMINAL

(n) Number of General Cargo Vessels at Terminal on a Given Day (1)	Number of Days During Period n Vessels at Terminal (f_n) Actual (2)	(f_n) Theoretical From Poisson Law (3)	Average Number of Vessels at Terminal (4)	Value of chi-square (5)	Goodness of Fit (6)
(a) Portland, Oregon: January-December 1957					
0	5	6.6			
1	31	26.3			
2	50	52.9			
3	64	71.0			
4	74	71.3			
5	51	57.3			
6	54	38.4	4.02	11.97	16%
7	24	22.1			
8	7	11.1			
9	5	5.0			
10	0	2.0			
11	0	0.7			
12	0	0.3			
TOTALS	365	365.0			
(b) Houston, Texas: January-December 1952					
0	3	5.2			
1	26	22.2			
2	45	47.2			
3	56	66.8			
4	78	71.0			
5	71	60.3			
6	36	42.7	4.25	9.27	32%
7	27	25.9			
8	17	13.8			
9	6	6.5			
10	1	2.8			
11	0	1.1			
12	0	0.5			
TOTALS	366	366.0			
(c) Baltimore, Maryland: January, March, April, June, July, and September 1959					
0	7	3.9			
1	13	15.0			
2	27	28.9			
3	39	37.0			
4	32	35.6			
5	23	27.4			
6	24	17.6	3.85	3.97	65%
7	11	9.7			
8	5	4.7			
9	2	2.0			
10	0	0.8			
11	0	0.3			
12	0	0.1			
TOTALS	183	183.0			
(d) Baltimore, Maryland: January-September 1952					
0	13	19.2			
1	44	50.7			
2	74	67.2			
3	57	59.4			
4	60	39.3	2.65	29.03	Less than 1%
5	23	20.8			
6	0	9.2			
7	0	3.5			
8	0	1.2			
9	0	0.5			
TOTALS	271	271.0			
(e) Baltimore, Maryland: January, March, April, June, July, and September 1959					
0	21	18.2			
1	47	42.0			
2	44	48.4			
3	35	37.3			
4	15	21.5	2.31	8.83	12%
5	10	10.0			
6	5	3.8			
7	6	1.3			
8	0	0.4			
9	0	0.1			
TOTALS	183	183.0			

TABLE 2.—COMPARISON OF ACTUAL AND THEORETICAL NUMBER OF GENERAL CARGO VESSELS IN PORT

(n) Number of General Cargo Vessels in Port on a Given Day (1)	Number of Days During Period n Vessels in Port (f_n) Actual (2)	(f_n) Theoretical From Poisson Law (3)	Average Number of Vessels in Port (4)	Value of chi-square (5)	Goodness of Fit (6)
(a) Boston, Massachusetts: July-December 1955					
0	4	1.3			
1	10	6.2			
2	20	15.5			
3	23	25.8			
4	30	32.3			
5	23	32.3			
6	27	26.9			
7	17	19.2	5.00	17.03	3%
8	12	12.0			
9	6	6.7			
10	6	3.3			
11	3	1.5			
12	0	0.6			
13	0	0.3			
14	3	0.1			
TOTALS	184	184.0			
(b) Philadelphia, Pennsylvania: July-December 1955					
0	0	0			
1	0	0.1			
2	2	0.3			
3	1	0.8			
4	3	2.0			
5	8	4.1			
6	10	7.2			
7	4	11.1			
8	14	15.1			
9	17	18.5			
10	14	20.5			
11	9	21.0			
12	19	19.8	12.25	72.07	Less than 1%
13	13	17.3			
14	16	14.1			
15	10	10.8			
16	10	7.8			
17	7	5.3			
18	6	3.4			
19	6	2.1			
20	3	1.2			
21	1	0.7			
22	6	0.4			
23	3	0.2			
24	1	0.1			
25	1	0.1			
TOTALS	184	184.0			
(c) Hampton Roads, Virginia: July-December 1955					
0	1	0			
1	7	0			
2	3	0.2			
3	2	0.7			
4	2	1.8			
5	8	4.1			
6	7	7.5			
7	9	11.8			
8	17	16.2			
9	9	19.5			
10	20	21.9			
11	17	22.0			
12	12	20.2			
13	14	17.1	11.03	68.55	Less than 1%
14	16	13.5			
15	9	9.9			
16	7	6.5			
17	7	4.4			
18	6	2.7			
19	3	1.6			
20	2	0.9			
21	4	0.5			
22	1	0.2			
23	0	0.1			
24	0	0			
25	0	0			
26	0	0			
27	1	0			
TOTALS	184	184.0			

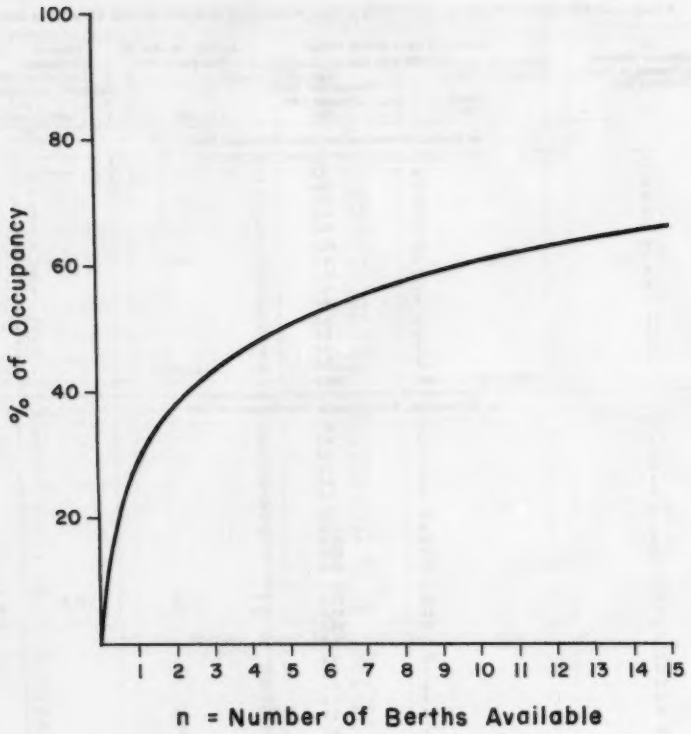

FIG. 4.—PERCENTAGE OF OCCUPANCY WHICH CAN BE ATTAINED WITH FROM 1 TO 15 BERTHS

CONCLUSION

The Poisson Law of Random Distribution appears to agree reasonably well with observed data on berth occupancy at commercial marine terminals. Moreover, this law is the basis for the solution of many problems of the quantity of equipment needed to perform a given service when the demands for that service are random. Because of the generally good agreement between observed data and the theoretical values given by the law, it is believed that it is reasonable to use the Poisson Law to determine maximum practical berth occupancies at commercial marine terminals. In so using the law, the criterion of congestion which has been set forth herein is that the number of vessels desiring to occupy berths at the terminal is greater than the number of berths available for about 5% of the time, or that the terminal is congested on only about 18 days per year. With this criterion, it is found that the maximum practical berth occupancy at a commercial marine terminal ranges from 29% for a 1-berth terminal to 66% at a 15-berth terminal.

Journal of the
WATERWAYS AND HARBORS DIVISION
Proceedings of the American Society of Civil Engineers

NAVIGATION MODEL STUDIES OF NEW OHIO RIVER LOCKS[a]

By Eugene P. Fortson, Jr.,[1] F. ASCE, and George B. Fenwick,[2] F. ASCE

SYNOPSIS

The major program of modernizing navigation facilities on the Ohio River and its tributaries involves replacement of the obsolete and inadequate system of low-lift, movable-wicket dams and small locks with a smaller number of relatively high, gated dams, including greatly expanded locking facilities suitable for handling modern tows. This paper describes the successful utilization of hydraulic models to investigate navigation conditions that will be encountered at the new locks and dams. Several model studies have been and are being used to develop optimum locations and arrangements of the locks and dams and appurtenant structures, as well as methods of operation of the dam gates, that will insure the elimination of hazardous or difficult navigation conditions for tows entering or leaving the locks.

INTRODUCTION

Modernization Program.—Canalization of the Ohio River at the present time is accomplished by means of 46 locks and dams, all but two of which were completed in 1929 or earlier. 41 of these dams are of the movable-wicket type with lifts averaging only about 7 ft, and each includes one lock chamber 110 ft by 600 ft in size.

Note.—Discussion open until November 1, 1960. To extend the closing date one month, a written request must be filed with the Executive Secretary, ASCE. This paper is part of the copyrighted Journal of the Waterways and Harbors Division, Proceedings of the American Society of Civil Engineers, Vol. 86, No. WW 2, June, 1960.

[a] Presented at the October 1958 ASCE Convention, in New York, N. Y.

[1] Chf., Hydr. Div., U. S. Army Engr. Waterways Experiment Sta., Vicksburg, Miss.
[2] Chf., Rivers and Harbors Branch, U. S. Army Engr. Waterways Experiment Sta., Vicksburg, Miss.

J. W. Bruce, D. W. Keller and J. A. Neill have presented[3] descriptions of the physical deterioration and obsolescence of the existing structures and the vastly increased demands of river traffic that make the modernization and replacement of existing navigation facilities on the Ohio River system, as well as the general requirements and criteria that establish the characteristics of the replacement facilities a necessity.

In order to provide modern facilities suitable for the efficient passage of current traffic as well as that which can reasonably be anticipated, a major program of replacement and modernization has been undertaken, and the replacement structures are now in various stages of construction or planning by the various districts of the Corps of Engineers, Dept. of the Army, under the supervision of the Ohio River Division. The old movable-wicket dams, with sills at river-bed elevation to permit open-river navigation at high stages, are being replaced by a smaller number of relatively high, gated dams (Fig. 1). The new dams will create deeper and longer pools—some more than 100 miles in length—and each will have a main lock with clear dimensions of 110-ft by 1200-ft and a 110-ft by 600-ft auxiliary lock.

Design for Navigability.—River travel will be speeded by the longer pools, requiring fewer lockages, and by the longer locks that will largely eliminate the present necessity for double or triple lockages to pass individual tows of optimum length. However, the new type structures also produce certain navigation and hydraulic design problems not encountered with the old movable-wicket dams. The maximum length of tow passing through the locks will be doubled. Also, since the gated dams will not permit open-river navigation during high flows as did the wicket dams, these longer tows will have to use the locks at much higher flows when current velocities in the approaches to the locks will be several times greater than those encountered heretofore.

Tows approaching a lock can be affected by adverse currents (Fig. 2) to such an extent as to cause or contribute to accidents or delays. The currents within the approaches to the lock or locks are controlled to a large extent by the configuration and alignment of the channel upstream and downstream therefrom, and are affected by the sudden contraction, then expansion, of the channel produced by the obstruction of the locks and guard walls.

The effect of such a contraction on currents in the upper approach is to produce an outdraft or cross-current that affects the movement of a down-bound tow at a time when its rudder power is reduced because of reduced speed with respect to the river currents. The intensity of cross-currents of this type is dependent upon the position of the locks with respect to the bankline, the total width of the locks and guard wall, the velocity and alignment of the river currents upstream of the locks, the width of the river channel, and the general elevation of the adjacent overbank area. The sudden expansion of the channel at the downstream end of the lower lock guard wall causes an eddy to form in the lower approach.

Currents in the eddy that affect navigation are those toward the bank at the lower end of the eddy, the upstream currents along the bank, and the outdraft or river-ward cross-currents at the upstream end of the eddy. An up-bound tow approaching the locks with little or no rudder control because of the reduced speed and upstream currents is at the mercy of the currents, which vary in position and intensity. Other currents which might affect navigation are

---

[3] "Modern Facilities for Ohio River Navigation," by James W. Bruce, Dwight W. Keller and James A. Neill, Proceedings, ASCE, Vol. 83, No. WW 2, May, 1957.

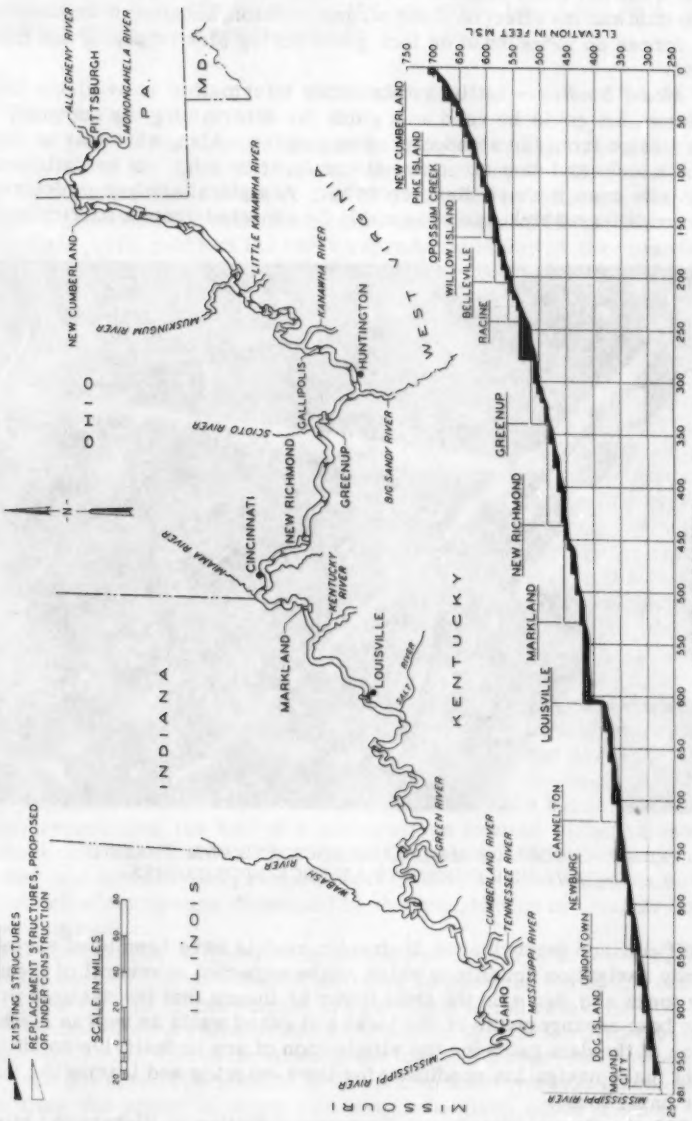

FIG. 1.—PLAN FOR REPLACEMENT OR MODERNIZATION OF NAVIAGTION STRUCTURES

those resulting from lock filling and emptying, operation of hydroplants, flow from tributary streams, and so forth. Some of the other problems in hydraulics with which a design must contend are accumulation of debris and ice, swell head at the dam and its effect on flood stages, erosion, shoaling in the approach channels, forces on gates, head on lock gates during lock emptying and filling, surges, etc.

Use of Model Studies.—Little authoritative information is available in assembled form that could be used as a guide for determining the adequacy of a particular design from the standpoint of navigation. Also, what may be satisfactory for a locks and dam structure at one location might not be satisfactory at another site even a short distance away. Analytical studies to determine hydraulic conditions which can reasonably be expected from a particular de-

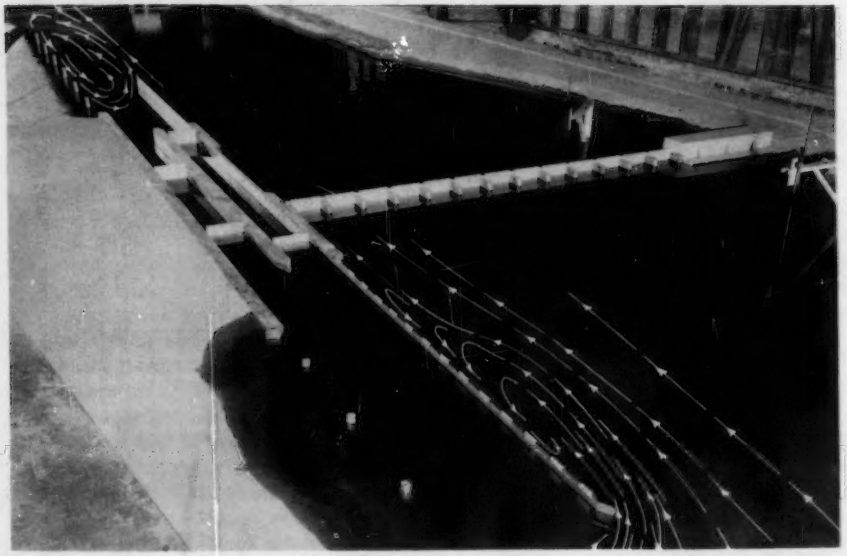

FIG. 2.—MODEL OF MARKLAND LOCK AND DAM SHOWING ADVERSE CURRENTS AT LOCK APPROACHES

sign are difficult and inconclusive. Hydraulic models have been used successfully to study navigation conditions which can be expected at several of the proposed new locks and dams on the Ohio River to insure that the designs would provide the best arrangements of the locks and guard walls as well as methods of operation of the dam gates for the elimination of any undesirable conditions which might make navigation conditions for tows entering and leaving the locks difficult or hazardous.

Since 1952 the Corps' Waterways Experiment Station at Vicksburg, Miss., has conducted several model studies of proposed modern locks and dam structures for the Ohio River and tributaries at the request of the Louisville, Huntington, and Pittsburgh districts of the Corps of Engineers. Studies have been completed on Greenup, Markland, New Richmond, and Louisville Locks and

Dams (formerly known as Locks and Dam No. 41). Studies are underway on the Pike Island, Maxwell Locks and Dam, and Locks and Dam No. 4; the latter two structures are on the Monongahela River, a tributary of the Ohio. All of the structures are to be new except for the Louisville Locks and Dam, and Locks and Dam 4 which will require considerable revision.

THE MODELS

Description.—The models used for study on navigation problems of these projects are of the fixed-bed type illustrated in Fig. 3. The models are built to an undistorted linear scale of 1 to 120, model to prototype, to insure the accurate reproduction of velocities, cross-currents, and eddies that would affect navigation. The reach of the river reproduced in any of these models is that required to reproduce accurately the currents within the upstream and downstream approaches to the locks. The reach varies from about 3 miles to about 6 miles, depending upon the alignment of the channel in the vicinity of the location of the proposed structure, and whether the location is fixed or alternate sites are considered.

The locks and dam structures are fabricated in the model shop of wood specially treated to prevent expansion, or sheet metal, or of a combination of wood and sheet metal. Since structural details of the dam gates play no part in the navigation studies, except in controlling flow over the dam and maintaining the upper pool elevation, they are simulated with sheet metal slide-type gates for economy. Similar type gates are also used to simulate the lock miter gates. In the design of models of this type, provisions are made for the installation of alternate plans being considered and for probable changes in the design and arrangement of the lock walls, in the composition of dam, and in dredging insofar as possible. Structural models used to study details of the locks and dam structures such as the effectiveness of the stilling basin, stability of gates, etc., are constructed to scales of 1 to 25 or larger.

Model Appurtenances.—Operation of the navigation models requires special appurtenances in addition to the usual equipment for providing and controlling water supply, water-surface elevations, tailwater, and so forth. One of the most important and most used special apparatuses in the remote-controlled self-propelled towboat and tow. The towboat shown in Fig. 4 is constructed to scale, reproducing the hull of a modern-type towboat including twin screws, rudders, and Kort nozzles. The towboat is powered by batteries placed within the tow, and is operated by remote control utilizing a 4-channel radio transmitter and receiver system developed by the modification of commercially available equipment.

The towboat can be operated in forward and reverse at one-fourth, one-half and full speed. An indicator is provided to show the set of the rudder at all times and various colored lights are provided to indicate direction and speed of the propellers. A rheostat and an ammeter are also provided to permit the adjustment of the maximum speed of the towboat to represent towboats of various push powers. The towboat is calibrated under various loads, and a curve indicating the speed in miles per hour in a given depth of water is plotted against meter readings for each load. The towboat and tow are used in the models to determine the effects of currents on a tow and the difficulties encountered in approaching and leaving the locks and in negotiating bends or special reaches of the river. Among other equipment used are floats submerged

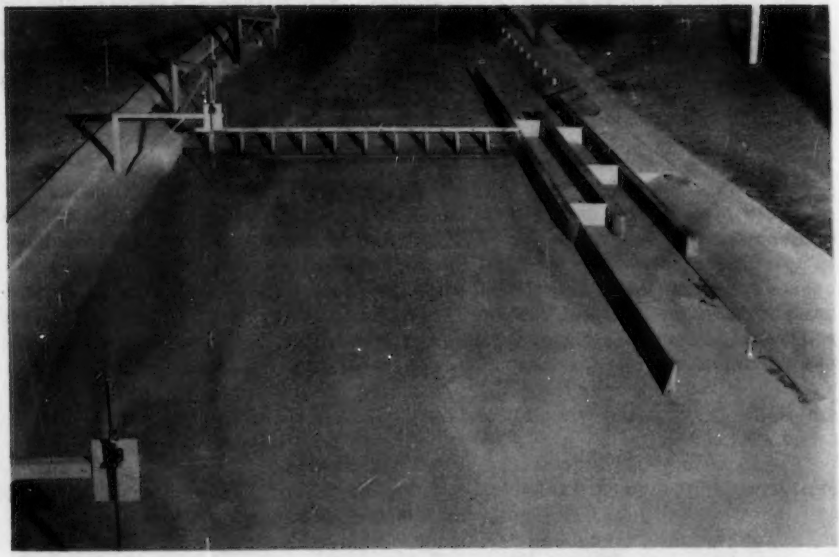

FIG. 3.—MODEL OF GREENUP LOCKS AND DAM—TYPICAL OF MODELS USED TO STUDY OHIO RIVER NAVIGATION STRUCTURES

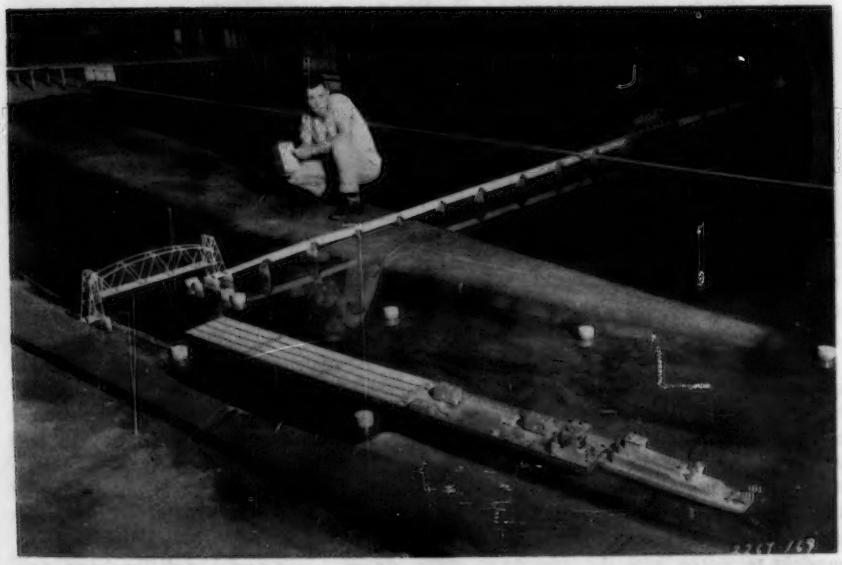

FIG. 4.—MODEL TOWBOAT AND TOW USED TO DETERMINE NAVIGATION CONDITIONS IN LOCK APPROACHES

to various depths, miniature current meters, movie and still cameras, special lighting equipment for obtaining progressive multiple exposures to show tow movements, force and displacement gages, Brush recorders, and universal amplifiers.

Testing Procedure.—The first step in the testing procedure of a navigation model of this type is to reproduce a series of selected representative river flows with the river in its natural state, that is, prior to construction of the proposed structure to be tested. Comparison of the results thus obtained with corresponding data obtained in the prototype insures that the model is accurately reproducing flow lines, current directions, and velocities of the prototype. The proposed locks and dam structure is then installed in the model and tested.

Testing of the structure involves the reproduction of several representative flows, including controlled and uncontrolled river flows. Studies are made of directions and strengths of significant currents in both approaches to the locks by plotting the paths and timing the travels of floats submerged to the depth of a loaded barge, and by measuring spot velocities in critical areas with a miniature current meter. Also, the effects of currents on tows are studied by observing the behavior of the model tow while drifting into the upper lock approach, while approaching and leaving the locks under power, and while navigating restricted areas.

Fig. 5 illustrates a photographic method of recording the maneuvering of a tow through a restricted reach in the upper approach to the Louisville Locks and Dam. Tests are also conducted on the navigation models to determine the effects of the proposed structures on high flood stages by measuring water-surface profiles before and after installation of the structures. Different structures also require investigation of special features such as effects of powerhouse operation, surges, and tributary inflow on navigation conditions.

Greenup Locks and Dam.—The results of a model study of one project have been useful in the design of other structures. The first of the series of studies of modern locks and dams for the Ohio River was that of the Greenup project. Two alternate plans for this structure (Fig. 6) were first considered, one with the main lock and long guide wall on the landside and one with the main lock and a long guard wall on the riverside. The study readily demonstrated that the latter alternate was preferable, and this arrangement has been incorporated in subsequent designs. With the main lock and long guide wall on the landside (Fig. 7), it was found that tows would have to approach the guide wall sufficiently close to attach mooring lines, and a slight misjudgment of currents by the pilot would place the tow in danger of hitting the end of the wall or of being moved too far river-ward to attach mooring lines. Tows attempting to avoid these hazards by driving ahead at an angle, toward the guide wall, to attach mooring lines, would be in danger of having their sterns moved river-ward by the cross-currents and breaking up against the end of the guard wall.

With the main lock on the landside, the eddy in the lower approach would extend upstream to the lower end of the guide wall, and the river-ward currents of the eddy at that point would move the head of an upbound tow away from the wall. Here again, a misjudgment of the currents in the eddy could cause the head of the tow to strike the end of the guide wall, or else to pass too far from the wall to permit the placing of mooring lines to snub the tow into alignment. The pilot could pass the end of the guide wall at a safe distance, drive the head of the two into the wall to attach lines, and then work the stern of the two into alignment with the wall. However, considerable time could be lost in making this maneuver against the currents.

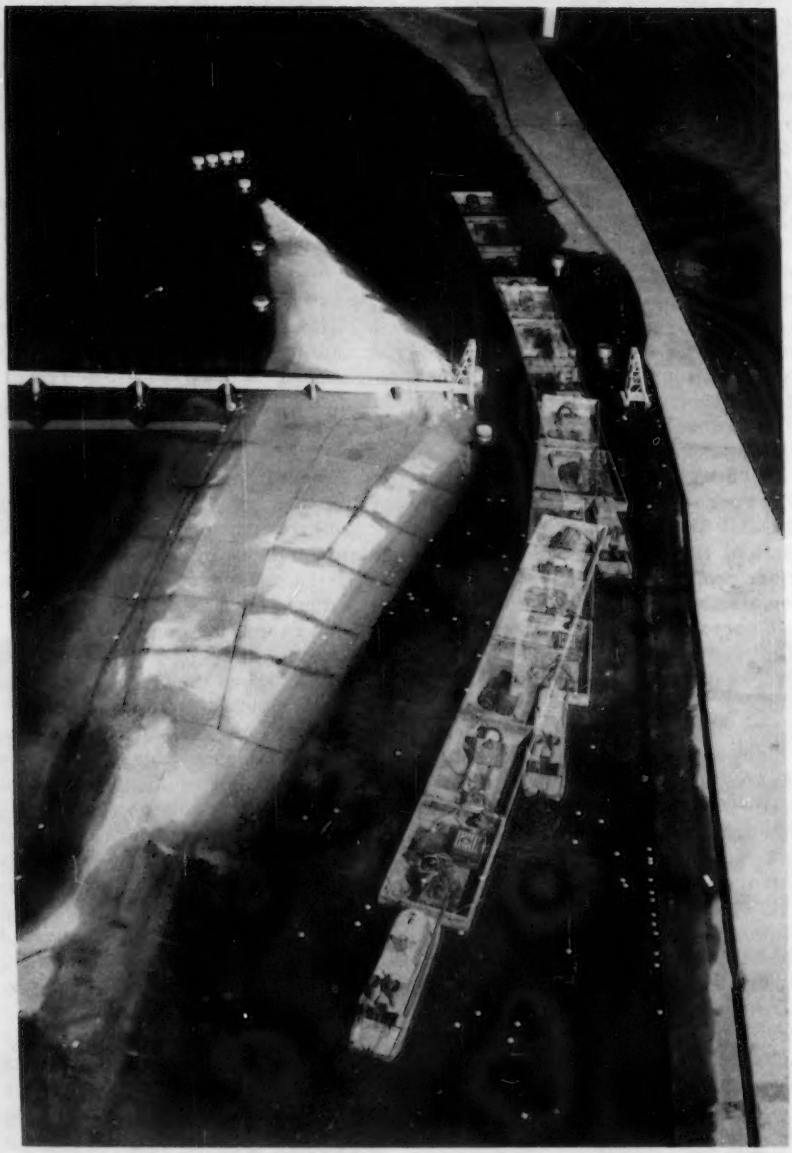

FIG. 5.—A SERIES OF INSTANTANEOUS EXPOSURES IS USED TO RECORD PHOTOGRAPHICALLY TOW MANEUVERS IN CRITICAL REACHES

With the main lock and a long guard wall located on the riverward side of the auxiliary lock, tows would enter relatively slack water before beginning to line up to enter the locks from either upstream or downstream. Even under this condition, however, the model tests indicated that ports through the upper guard wall would be required to reduce the hazardous riverward crosscurrents in the upper approach immediately above the end of this wall. Fig. 8 shows navigation conditions in the upper approach with and without ports through the guard wall, and the manner in which these conditions affect a downbound tow.

The Greenup Locks and Dam model study also demonstrated that the locks and walls could be moved riverward 100 ft to reduce the volume and cost of required dredging. In addition, the study demonstrated that the length of the intermediate wall could be reduced, and that discharge from the locks emptying system would not affect navigation in the lower approach during low flows with the main lock located on the riverside, even without special stilling arrangements.

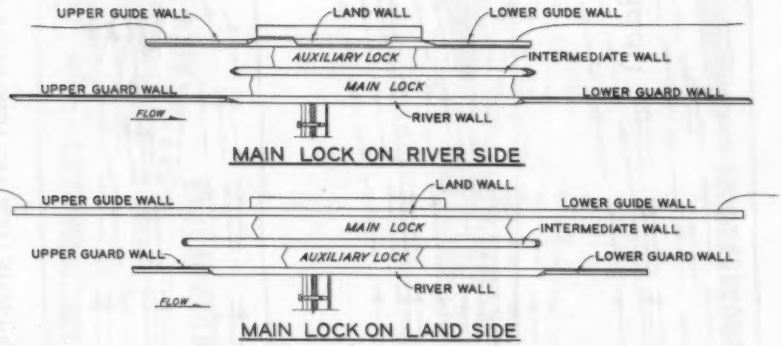

FIG. 6.—ALTERNATE LOCK ARRANGEMENTS, GREENUP LOCKS

Markland Locks and Dam.—The Markland Locks and Dam are to be located just downstream of a bend with the locks on the outside of the curve. Because of this position, flow will be concentrated on the lock side of the river and velocities in the approaches will tend to be higher than those encountered at the Greenup Locks. The results of tests of this structure indicated that ports would be required in the upper guard wall to reduce the intensity of the crosscurrents and that removal of a prominence and other irregularities along the left bank, above the guide wall, would be required to improve the alignment of currents in that vicinity and facilitate the proper aligning of tows prior to their entering the upper lock approach.

The study also indicated that dredging of the right bank opposite the lock would reduce the concentration of flow along the left bank above the guard wall, thus reducing velocities and improving the alignment of currents in the approach. Development on the model of a modified alignment for the dredge cut resulted in a reduction in the amount of dredging without affecting the results. The model also indicated that with this dredging the number of dam gates could be reduced from 13 to 12 without affecting navigation conditions.

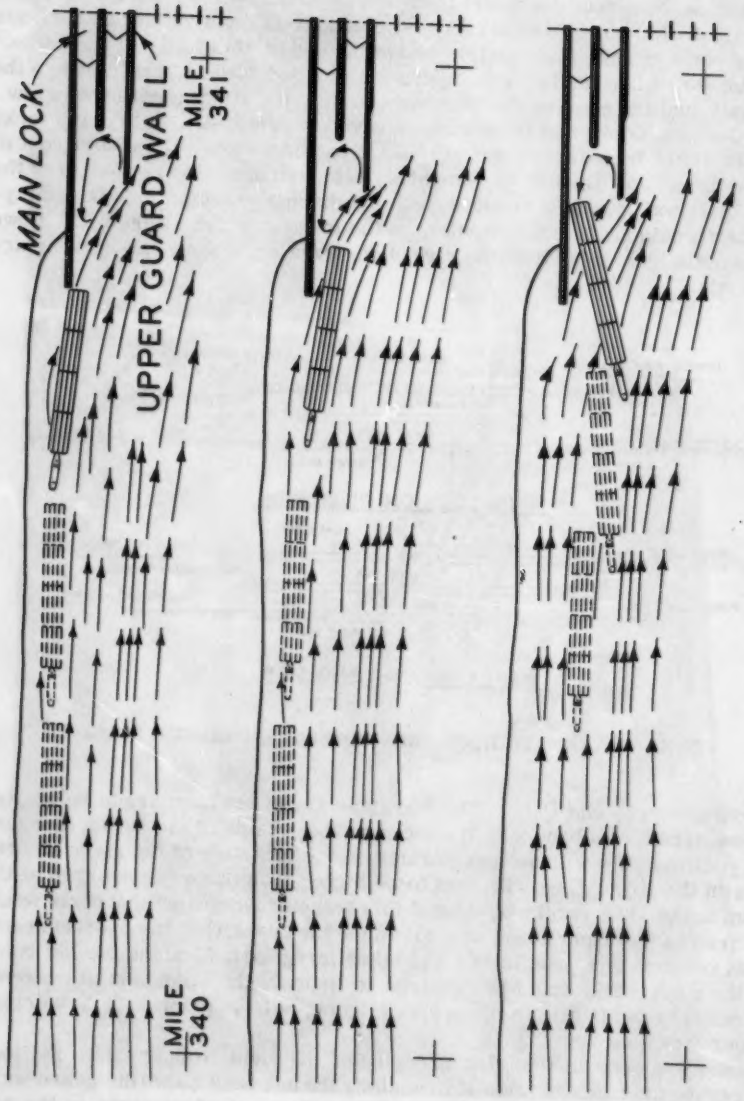

FIG. 7.—EFFECTS OF CURRENTS ON TOW WITH MAIN LOCK AND LONG GUIDE WALL ON LANDSIDE, GREENUP LOCKS

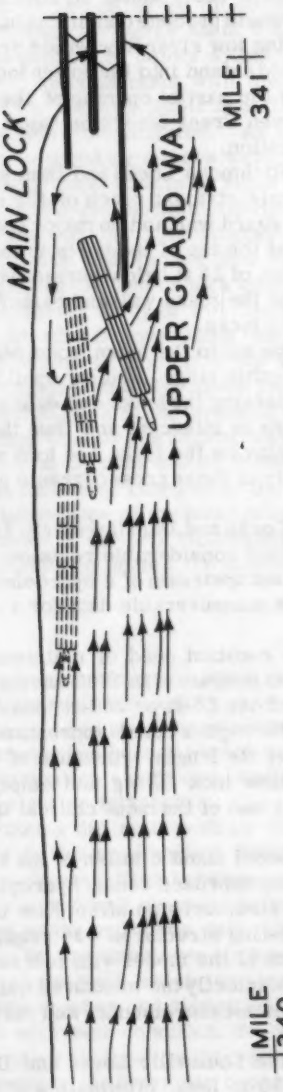

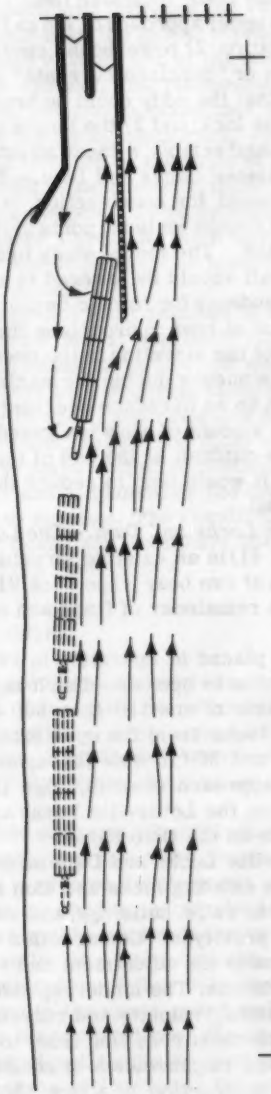

FIG. 8.—EFFECTS OF PORTS IN UPPER GUARD WALL, GREENUP LOCKS

Tests were also conducted to determine the effectiveness of an ice and debris chute in the upper guard wall and the effects of powerhouse operation and the Steven Creek diversion canal discharges on navigation conditions. The results of these tests indicated that: 1) the debris chute would be effective in clearing the upper approach of ice and drift but would produce conditions hazardous to navigation; 2) powerhouse operation during low river flow would produce a large eddy or "backlash currents" which would extend into the lower lock approach but that the eddy could be broken up by the partial opening of the third gate from the lock; and 3) the length of the Steven Creek diversion canal could be reduced appreciably without affecting navigation.

New Richmond Locks and Dam.—The New Richmond Locks and Dam structure is proposed for construction in a relatively straight reach of the river. The original design included ports in the upper guard wall and no major changes were indicated. The model study indicated that the top of the ports in the upper guard wall should be lowered to an elevation of 15 ft below normal pool to reduce the tendency for tows to be pinned against the guard wall and to facilitate the movement of tows approaching the auxiliary locks.

Because of the elevation of the overbank adjacent to the locks, considerable overbank flow occurs during the maximum navigable stage. Placing spoil along the overbank so as to reduce overbank flow bypassing the locks and dam would increase the amount of flow the guard wall tends to intercept and thus the intensity of the outdraft at the end of the wall. Moving the locks and lock walls landward 50 ft would tend to reduce the intensity of these crosscurrents at the end of the wall.

Louisville Locks and Dam.—The Louisville Locks and Dam (formerly Locks and Dam No. 41) is an existing structure requiring considerable revision. The dam consists of two bear traps each 91 ft long just upstream of a hydroelectric plant, and the remainder of fixed and of old type maneuverable dam for a total of 8700 ft.

The dam, placed in operation in 1927, is in constant need of maintenance and is dangerous to operate. The locks placed in operation in 1930 have a 37-ft lift and consist of one 110-ft by 600-ft lock and one 56-ft by 360-ft lock. Entrance to the locks from the upstream side is through a canal approximately 2 miles long and 200 ft wide throughout most of its length. Because of this long narrow approach channel, high lift, and slow lock filling and emptying characteristics, the Louisville Locks and Dam is one of the most critical traffic bottlenecks on the Ohio River.

The Louisville Locks and Dam model reproduced about 6 miles of the Ohio River with the existing locks and dam structures, approach canal, hydroplant, bridges, levees, walls, buildings, and such other structures as affect flow conditions in the prototype. Construction of the existing structures was required to provide a basis for adjustment and verification of the model with measured prototype conditions. The model reproduced satisfactorily the measured water-surface elevations, velocity and current direction measurements, and surges in the approach canal resulting from lock filling.

The proposed improvement of conditions at the Louisville Locks and Dam involved the construction of a new 1200-ft by 110-ft lock, elimination of the restricted approach channel, and revision of the existing dam. A large number of alternate plans and modifications were tested before a satisfactory solution was reached.

The design of the approach channel was dictated to a large extent by surge conditions that could affect navigation conditions within the channel and oper-

ation of the lock gates. The existing 600-ft lock is filled in about 18 min. This filling operation produces a surge varying from about 1 ft (low to high) to about 3 ft depending upon the number and timing of lock filling operations. The 1200-ft lock will be filled within about 9 min which will increase the rate of filling and tendency for surge about 4 times. In this case the model was used to study surges at critical points within the approach channel and at the powerhouse.

Also, in connection with the approach channel, the placement of a large quantity of dredge spoil and its effect on navigation conditions and on flood stages were investigated. As far as the dam was concerned, several plans including gated structures were tested and rejected on the basis of model indications of their effects on flood stages, high velocities in critical areas, and, in one instance, the indication that six of the proposed 14 gates would pass little or no flow during flood stages. In the lower approach, tests were conducted to eliminate undesirable flow conditions and to reduce the head on the lower lock gate at the end of lock emptying operations.

The model study of the Louisville Locks and Dam resulted in the development of satisfactory plans which included a 500-ft approach channel with a surge basin, the moving of one lock-filling intake so as to draw water from the surge basin, a ported lower lock guard wall with dredging along sand Island, the establishing of the grade and location of spoil, and revisions to the dam.

Other studies are in progress (as of October, 1958). The study of Pike Island Locks and Dam is one of these. Several plans and modifications have been tested including changes in the locations and alignment of the locks and dam and the position of the locks with respect to the dam. The results of these tests and tests of the two Monongahela River Locks and Dam have not progressed sufficiently to permit the drawing of definite conclusions.

CONCLUSIONS

The value of model investigations of navigation projects on the Ohio River has been well demonstrated. As a result of these investigations certain design features have been more or less standardized. Also, considerable general knowledge has been gained on certain other design features, methods of evaluating navigation conditions, and the type of structures desired by or acceptable to navigation interests.

Placing the main lock on the riverside of the auxiliary lock and including ports in the upper guard wall where locks and dams are located in the open river channel, have become accepted as a general requirement. Ports in the upper guard wall not only improve navigation conditions but also tend to reduce scour at the end of the wall. They further tend to minimize the swell-head produced by the structures through reduction in the size of the eddy on the river-side of the wall, which improves the distribution of flow over the dam.

The number and size of ports required in the upper guard wall vary somewhat with each condition, depending to a large extent upon the amount of river flow the wall tends to intercept and the hydraulic efficiency of the ports used. Increasing the hydraulic capacity of the ports will increase the ease with which a tow can be made to drift into the upper lock approach. On the other hand, increasing the capacity of ports will also increase 1) the tendency for ice and drift to be trapped in the upper lock approach, 2) the difficulty of tows approaching the guide wall for entrance into the auxiliary lock, 3) the tendency for tows to be pinned against the guard wall, and 4) the danger of tows hitting the upper

lock gate because of the increase in the speed of approach while drifting. Lowering the top elevation of the ports will tend to reduce the tendency for tows to be pinned against the guard wall and the difficulty of tows entering the auxiliary lock.

Because of the nature of stream flow, the configuration and alignment of a river channel is never exactly the same in any two reaches. For this reason, design features found satisfactory for a lock and dam structure in one locality cannot always be applied to another location. Observation of a model of a project in operation often brings to light certain undesirable design features or certain problems that will require special treatment which cannot be determined from an analysis of prototype conditions or which may not have been recognized as a design consideration. Each of the model studies of Ohio River locks and dams conducted at the Waterways Experiment Station has resulted in major changes or modifications in the original design except in the case of the New Richmond Locks and Dam where only minor revisions were indicated as desirable.

The amount of savings in initial and future costs attributable to these model studies is difficult to evaluate. The studies have resulted in a decrease in the number of dam gates required, in decreasing dredging volumes, and in the elimination of certain structures found to be ineffective or not required. Of still greater significance have been the design modifications that will greatly improve the navigability of the ultimate structures in the river through the elimination of navigation hazards, some of which would probably have otherwise required modification of the structures after their construction in the river.

The models have also proven to be a valuable tool for demonstrating the functioning of the proposed locks and dams to navigation interests who will be vitally concerned with navigating the Ohio and its tributaries. These demonstrations, arranged by the Ohio River Division and the Districts concerned, have produced two substantial benefits: 1) experienced navigation people have contributed valuable suggestions for improving the navigability of the proposed structures; and 2) navigation interests have been satisfied in advance as to the adequacy of the structures to meet their needs.

Journal of the
WATERWAYS AND HARBORS DIVISION
Proceedings of the American Society of Civil Engineers

ANALYSIS OF LOAD DISTRIBUTION IN THE PILES OF PIERS

By M. A. Gouda[1]

SYNOPSIS

Determination of the forces in piles of piers or a group of piles under the action of vertical, horizontal, and bending moment forces is outlined. By use of simplified assumptions and pile displacement, a method is developed for the analysis of load distribution on piles.

In a symmetrical pile group, forces are directly calculated, while in an unsymmetrical group the system is first treated as a symmetrical group and then by successive approximations (similar to moment-distribution methods) the forces are determined. A more exact solution for the problem is arrived at by considering the elastic deformation of piles together with the deck.

INTRODUCTION

Piers are mainly subjected to vertical forces due to loads from freight, cranes, vehicles, and the weight of the structure itself, as well as horizontal forces due to inward blows from ships berthing or to outward pull on mooring ropes. These forces, in some cases, will be the most serious factor affecting the design and the choice of a pile system. When the acting loads are not great, especially the horizontal force, vertical piles only are used.

On the other hand, when the horizontal force is of great intensity, the use of batter piles becomes necessary to provide sufficient lateral resistance and

Note.—Discussion open until November 1, 1960. To extend the closing date one month, a written request must be filed with the Executive Secretary, ASCE. This paper is part of the copyrighted Journal of the Waterways and Harbors Division, Proceedings of the American Society of Civil Engineers, Vol. 86, No. WW 2, June, 1960.

[1] Asst. Prof., Struct. Engrg. Dept., Alexandria Univ., Alexandria, U.A.R.

to increase the rigidity of the pier. Batter piles may be used alone or in combination with vertical piles.

PIERS WITH VERTICAL PILES ONLY

In the analysis of the load distribution on a group of vertical piles in a pier, the following assumptions are considered:

1. The deck of the pier (which may be considered as a pile cap) is rigid relative to the piles.
2. All piles are of the same cross section.
3. No settlement of the support of the piles occurs.
4. Points of support of the piles are at the same level.
5. Horizontal displacement of the top of each pile in relation to the point of embedment is the same for all piles.

In this type of pier the horizontal force is transferred to the ground by shear which produces bending moments on the pile. Hence the acting horizontal force must be small since the piles offer relatively little resistance to bending. For this reason, effective fenders as well as fender piles must be provided to absorb the shock and thus diminish the horizontal force causing the deflection.

Fig. 1 represents a pier on n vertical piles which is subjected to a vertical force V and horizontal force H. The loads on the piles are determined by a simple statical analysis.

If the group of piles in the pier is unsymmetrical and x is the distance of each pile from the centroid of the pile group and e is the eccentricity of the vertical force V from the axis of the centroid, the pier as a whole will be subjected to a moment V e - H h (e to right of centroid).

The axial load (P_x) on any pile is

$$P_x = \frac{V}{n} + \frac{x(V\,e - H\,h)}{\sum_1^h x^2} \quad \ldots\ldots\ldots\ldots\ldots (1)$$

According to assumption 5, the horizontal force H is resisted equally by each pile and the shearing force on any pile will be

$$Q_x = \frac{H}{h} \quad \ldots\ldots\ldots\ldots\ldots\ldots\ldots (2)$$

Assuming fixity at the top or datum level of pile, the bending moment will be

$$M_x = \frac{H\,h}{2\,n} \quad \ldots\ldots\ldots\ldots\ldots\ldots\ldots (3)$$

Example 1.—Given a symmetrical pier with three vertical piles subjected to vertical and horizontal forces (Fig. 2):

Apply Eqs. 1, 2, and 3 to the pier:

Since V is symmetrical, e = 0 and

$$P_1 = \frac{150}{3} - 7.5\left(\frac{100}{2\,(7.5)^2}\right)$$

$$= -\,50 - 6.67 = -\,56.67 \text{ tons}$$

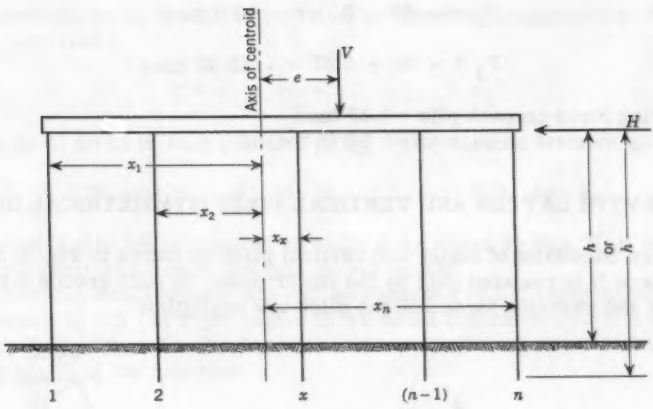

FIG. 1

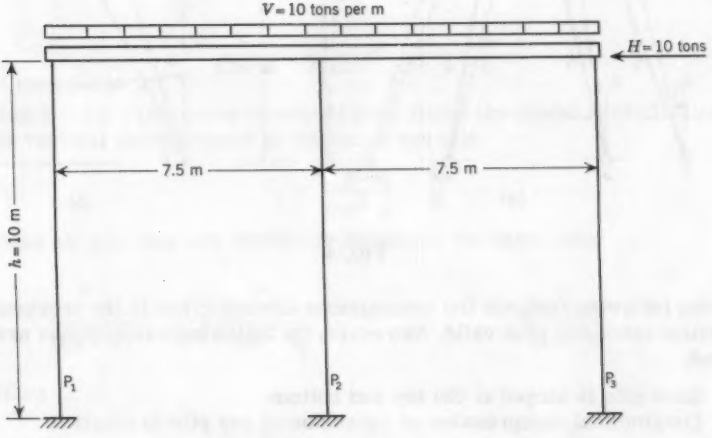

FIG. 2

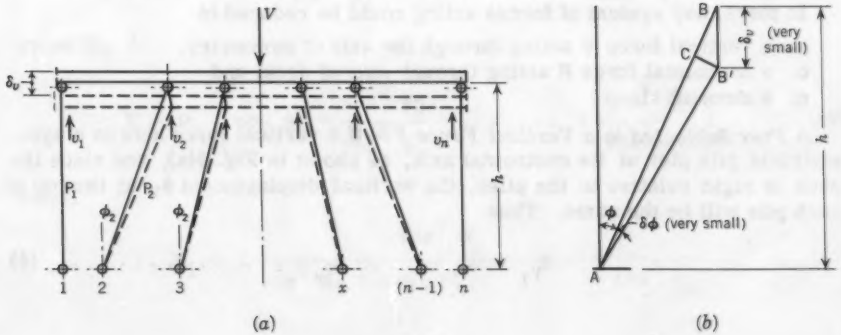

(a) (b)

FIG. 3

$$P_2 = - 50 - 0 = - 50.0 \text{ tons}$$

and

$$P_3 = - 50 + 6.67 = - 43.33 \text{ tons}$$

Shearing force on each pile = 3.33 tons
Bending moment on each pile = 16.65 ton-m

PIERS WITH BATTER AND VERTICAL PILES (SYMMETRICAL GROUP)

In piers consisting of batter and vertical piles as shown in Fig. 4, the horizontal force H is resisted only by the batter piles. In such groups the bending moments and shearing forces on the piles are negligible.

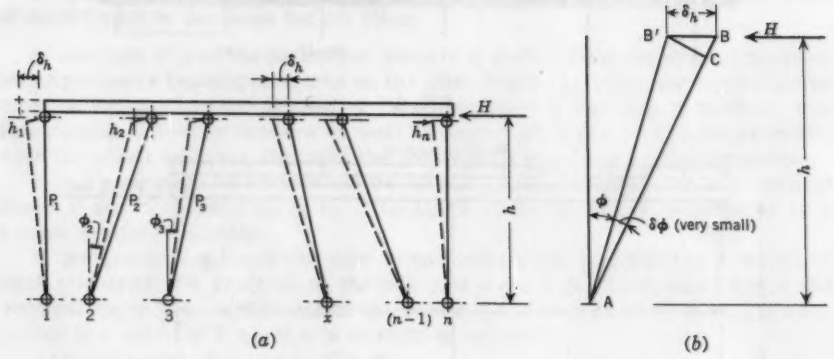

FIG. 4

In the following analysis the assumptions already given in the previous case of vertical piles are still valid. Moreover, the following assumptions are considered:

1. Each pile is hinged at the top and bottom.
2. Longitudinal compression or extension of any pile is elastic.

Fig. 3(a) shows a pier of a symmetrical group of n piles inclined at ϕ_1, ϕ_2, etc., each having the same dimensions, elastic constant, and height h.

In piers, any system of forces acting could be reduced to

a. a vertical force V acting through the axis of symmetry;
b. a horizontal force H acting through axis of deck; and
c. a moment M.

A Pier Subjected to a Vertical Force V.—If a vertical force acts on a symmetrical pile pier at its centroidal axis, as shown in Fig. 3(a), and since the deck is rigid relative to the piles, the vertical displacement δ_V at the top of each pile will be the same. Thus

$$\delta_{V_1} = \delta_{V_2} = \ldots . \delta_{V_n} \ldots \ldots \ldots \ldots \ldots \quad (4)$$

The vertical force V will be resisted by vertical components at the top of the pile such that

$$V = v_1 + v_2 + \ldots\ldots + v_n \quad \ldots\ldots\ldots\ldots \quad (5)$$

If the axial force in each pile is P_1, P_2, P_3, etc., then

$$V = P_1 \cos \phi_1 + P_2 \cos \phi_2 + \ldots\ldots + P_n \cos \phi_n \quad \ldots\ldots \quad (6)$$

Consider a pile AB inclined at an angle ϕ as shown in Fig. 3(b); when subjected to a vertical force V, the pile moves to AB'.

The vertical displacement (δ_v) can be regarded as a displacement $\delta_v \sin \phi$ (represented by CB') at right angles to AB and a contraction $\delta_v \cos \phi$ (represented by BC). Since the displacements due to load are very small compared with the length of the pile then

$$AB \doteq AC = \frac{h}{\cos \phi} \quad \ldots\ldots\ldots\ldots\ldots\ldots \quad (7)$$

The total contraction of the pile is given by

$$\frac{P}{\cos \phi} \frac{h}{A E} = \frac{P}{\cos \phi} \frac{h}{k} \quad \ldots\ldots\ldots\ldots \quad (8)$$

in which k = AE = the cross-sectional area times the modulus of elasticity.

The vertical displacement at the top of any pile

$$\delta_v = \frac{P}{\cos^2 \phi} \frac{h}{k} \quad \ldots\ldots\ldots\ldots\ldots \quad (9)$$

and since all pile tops are vertically displaced the same then

$$\frac{P_1}{\cos^2 \phi_1} \frac{h}{k} = \frac{P_2}{\cos^2 \phi_2} \frac{h}{k} = \ldots\ldots = \frac{P_n}{\cos^2 \phi_n} \frac{h}{k} \quad \ldots\ldots (10)$$

therefore

$$P_2 = P_1 \frac{\cos^2 \phi_2}{\cos^2 \phi_1} = \ldots\ldots = P_1 \frac{\cos^2 \phi_n}{\cos^2 \phi_1} \quad \ldots\ldots (11)$$

From Eq. 6

$$V = P_1 \left(\cos \phi_1 + \frac{\cos^3 \phi_2}{\cos^2 \phi_1} + \ldots\ldots + \frac{\cos^3 \phi_n}{\cos^2 \phi_1} \right) \quad \ldots\ldots (12)$$

hence

$$P_1 = V \frac{\cos^2 \phi_1}{\cos^3 \phi_1 + \cos^3 \phi_2 + \ldots\ldots + \cos^3 \phi_n} \quad \ldots\ldots (13)$$

and generally the axial force in any pile due to the vertical force V is

$$P_x = V \frac{\cos^2 \phi_x}{\sum_1^n \cos^3 \phi_x} \quad \ldots\ldots\ldots\ldots\ldots\ldots (14)$$

A Pier Subjected to a Horizontal Force H.—If a horizontal force H acts at the deck of the pier as shown in Fig. 4(a) and since the pile deck is rigid

$$\delta_{h_1} = \delta_{h_2} = \ldots\ldots = \delta_{h_n} \quad \ldots\ldots\ldots\ldots\ldots\ldots (15)$$

and the horizontal force H is opposed by horizontal reactions h_1, h_2, h_3, etc., from the top of each pile

$$H = h_1 + h_2 + \ldots\ldots + h_n$$

therefore

$$H = P_1 \sin \phi_1 + P_2 \sin \phi_2 + \ldots\ldots + P_n \sin \phi_n \quad \ldots\ldots (16)$$

In Fig. 4(b) the pile AB, when subjected to a horizontal force H, moves to AB' which could be considered as a displacement $\delta_h \cos \phi$ at right angles to AB and a contraction (or extension if pile is inclined toward the left) $\delta_h \sin \phi$.

The horizontal displacement at the top of any pile

$$\delta_h = \frac{P}{\cos \phi \sin \phi} \frac{h}{k} \quad \ldots\ldots\ldots\ldots\ldots\ldots (17)$$

and from Eq. 15

$$\frac{P_1}{\cos \phi_1 \sin \phi_1} \frac{h}{k} = \frac{P_2}{\cos \phi_2 \sin \phi_2} \frac{h}{k} = \ldots = \frac{P_n}{\cos \phi_n \sin \phi_n} \frac{h}{k} \quad \ldots (18)$$

and by expressing axial pile forces P_2, P_3, etc. in terms of P_1

$$P_2 = P_1 \frac{\cos \phi_2 \sin \phi_2}{\cos \phi_1 \sin \phi_1} \quad \ldots\ldots\ldots\ldots\ldots\ldots (19a)$$

and

$$P_n = P_1 \frac{\cos \phi_n \sin \phi_n}{\cos \phi_1 \sin \phi_1} \quad \ldots\ldots\ldots\ldots\ldots\ldots (19b)$$

By substituting for P_2, P_3 in Eq. 16 the horizontal force

$$H = P_1 \sin \phi_1 + \frac{P_1 \cos \phi_2 \sin^2 \phi_2}{\cos \phi_1 \sin \phi_1} + \ldots\ldots + \frac{P_1 \cos \phi_n \sin^2 \phi_n}{\cos \phi_1 \sin \phi_1} \quad \ldots (20)$$

therefore

$$H = P_1\left(\frac{\cos\phi_1 \sin^2\phi_1 + \cos\phi_2 \sin^2\phi_2 + \ldots + \cos\phi_n \sin^2\phi_n}{\cos\phi_1 \sin\phi_1}\right) \ldots (21)$$

Hence

$$P_1 = H\left(\frac{\cos\phi_1 \sin\phi_1}{\cos\phi_1 \sin^2\phi_1 + \cos\phi_2 \sin^2\phi_2 + \ldots + \cos\phi_n \sin^2\phi_n}\right) \ldots (22)$$

In general the axial force in any pile due to a horizontal force H

$$P_x = H \frac{\cos\phi_x \sin\phi_x}{\sum_1^n \cos\phi_x \sin^2\phi_x} \ldots\ldots\ldots\ldots (23)$$

Axial Forces in Piles Due to a Bending Moment M.—If the deck of a symmetrical pile pier, as shown in Fig. 5(a) is subjected to a bending moment M it will rotate through an angle α. This bending moment may be due to the eccentricity of the acting vertical force V or the horizontal force H. In this case

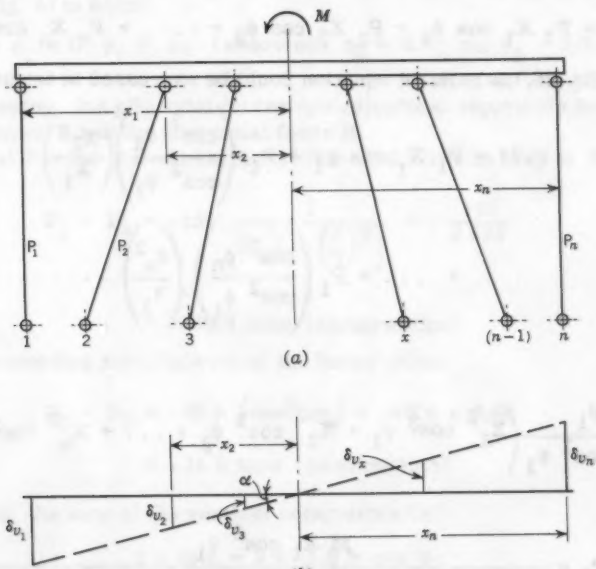

FIG. 5

a counter-clockwise moment will develop a compression on piles of the left-hand group and tension on the right-hand group and vice versa for a clockwise moment. It must be noticed that the sums of the resulting vertical components of the forces on the piles and of the corresponding horizontal components are both zero.

Since the pier deck is rigid in comparison to the piles, the vertical displacement of each pile will be in proportion to its distance from the axis of symmetry.

Referring to Fig. 5(b),

$$\frac{\delta_{v_1}}{\delta_{v_2}} = \frac{X_1}{X_2} \quad \ldots\ldots\ldots\ldots\ldots\ldots (24)$$

By using the expression of the vertical displacement from Eq. 9

$$\frac{P_1}{P_2} \frac{\cos^2 \phi_2}{\cos^2 \phi_1} = \frac{X_1}{X_2} \quad \ldots\ldots\ldots\ldots\ldots\ldots (25)$$

therefore

$$P_2 = P_1 \frac{\cos^2 \phi_2}{\cos^2 \phi_1} \frac{X_2}{X_1} \quad \ldots\ldots\ldots\ldots\ldots\ldots (26)$$

The external moment M will be resisted by the vertical components of the reactions at the top of the piles in such a way that

$$M = P_1 X_1 \cos \phi_1 + P_2 X_2 \cos \phi_2 + \ldots + P_n X_n \cos \phi_n \ldots (27)$$

From Eq. 26, the moment equation could be expressed in terms of P_1 only:

$$M = P_1 X_1 \cos \phi_1 + P_1 \left(\frac{\cos^3 \phi_2}{\cos^2 \phi_1}\right)\left(\frac{X_2^2}{X_1}\right)$$

$$+ \ldots + P_1 \left(\frac{\cos^3 \phi_n}{\cos^2 \phi_1}\right)\left(\frac{x_n^2}{x_1}\right) \quad \ldots\ldots\ldots\ldots (28)$$

therefore

$$M = \frac{P_1}{X_1 \cos^2 \phi_1}\left(X_1^2 \cos^3 \phi_1 + X_2^2 \cos^3 \phi_2 + \ldots + X_n^2 \cos^3 \phi_n\right) \ldots (29)$$

and

$$P_1 = \frac{M X_1 \cos^2 \phi_1}{X_1^2 \cos^3 \phi_1 + X_2^2 \cos^3 \phi_2 + \ldots + X_n^2 \cos^3 \phi_n} \quad \ldots\ldots (30)$$

and, in general, the axial force in any pile due to an external moment M is given by

$$P_x = M \frac{X_x \cos^2 \phi_x}{\sum_1^n X_x^2 \cos^3 \phi_x} \quad \ldots\ldots\ldots\ldots (31)$$

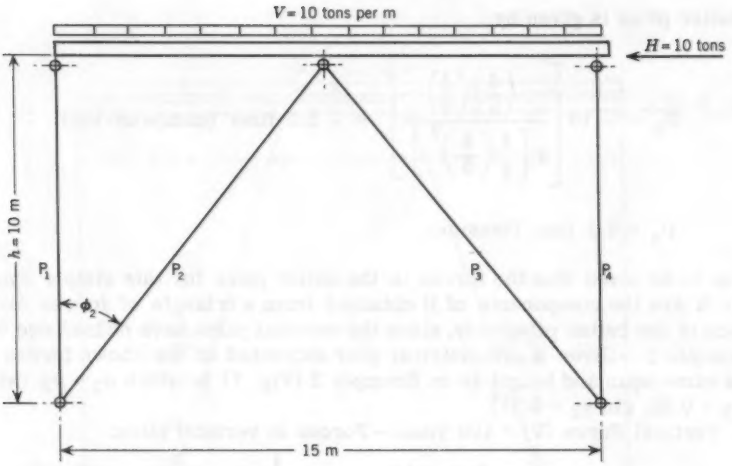

FIG. 6

Example 2.—Given a simple symmetrical pier of a group of batter and vertical piles (Fig. 6) in which

$$\phi_1 = \phi_4 = 0;\ \phi_2 = \phi_3 \quad (\text{where } \cos\phi_2 = 4/5;\ \sin\phi_2 = 3/5)$$

In the following, the pile axial forces are calculated separately for each of the vertical force V and the horizontal force H.

a. Vertical Forces (V).—From Eq. 14 the axial force in each of the vertical piles:

$$P_1 = P_4 = -150\ \frac{1}{2\left[1 + \left(\frac{4}{5}\right)^3\right]} = -\frac{150}{3.024}$$

$$= -49.6 \text{ tons (compression)}$$

The corresponding force in each of the batter piles:

$$P_2 = P_3 = -49.6\left(\cos^2\phi_2\right) = -49.6 \times 0.64$$

$$= -31.8 \text{ tons (compression)}$$

As a check, the sum of the vertical components is:

$$2 \times 49.6 + 2 \times 31.8 \times \cos\phi_2$$

$$= 99.2 + 50.8 = 150 \text{ tons}$$

b. Horizontal Force H = 10 Tons.—There is no force in the vertical piles (P_1, P_4) due to the horizontal force H. From Eq. 23 the axial force in each of

the batter piles is given by

$$P_2 = -10\left[\frac{\left(\frac{4}{5}\right)\left(\frac{3}{5}\right)}{2\left[\frac{4}{5}\left(\frac{3}{5}\right)^2\right]}\right] = -8.3 \text{ tons (compression)}$$

$$P_3 = 8.3 \text{ tons (tension).}$$

It is to be noted that the forces in the batter piles for this simple system due to H are the components of H obtained from a triangle of forces for the junction of the batter piles only, since the vertical piles have no load due to H:

Example 3.—Given a symmetrical pier subjected to the shown forces and of the same span and height as in Example 2 (Fig. 7) in which $\phi_2 = \phi_3$ (where $\cos \phi_2 = 0.95$; $\sin \phi_2 = 0.31$)

a. Vertical Force (V) = 150 Tons.—Forces in vertical piles:

$$P_1 = P_4 = 150 \times \frac{1}{2 + 2 \times 0.857}$$

$$= -40.5 \text{ tons}$$

Forces in batter piles:

$$P_2 = P_3 = 40.5 \times \cos^2 \phi_2$$

$$= 40.5 \times 0.9$$

$$= -36.5 \text{ tons}$$

b. Horizontal Force (H) = 10 Tons.—Forces in vertical piles:

$$P_1 = P_4 = 0.$$

Forces in batter piles:

$$P_2 = -10 \times \frac{0.95 \times 0.31}{2\left[0.95 \times (0.31)^2\right]}$$

$$= -16.1 \text{ tons (compression).}$$

$$P_3 = +16.1 \text{ tons (tension).}$$

Example 4.—Fig. 8 shows a pier of a symmetrical group consisting of two vertical piles and four batter ones:

$$\phi_2 = \phi_5 \text{ (where } \cos \phi_2 = 0.943; \quad \sin \phi_2 = 0.33)$$

$$\phi_3 = \phi_4 \text{ (where } \cos \phi_3 = 0.957; \quad \sin \phi_3 = 0.286)$$

a. Vertical Forces (V).—Forces in vertical piles:

$$P_1 = P_6 = 150 \times \frac{1}{2 + 2 \times 0.827 + 2 \times 0.88}$$

$$= \frac{150}{5.414} = -27.8 \text{ tons}$$

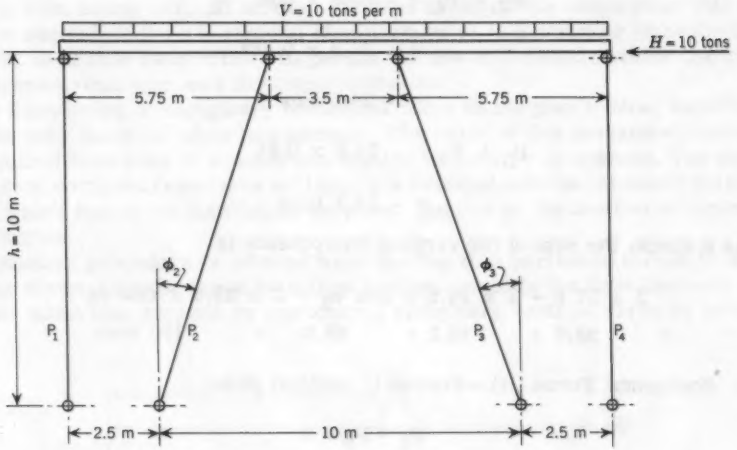
V = 10 tons per m
H = 10 tons
5.75 m
3.5 m
5.75 m
h = 10 m
ϕ2
ϕ3
P1
P2
P3
P4
2.5 m
10 m
2.5 m

FIG. 7

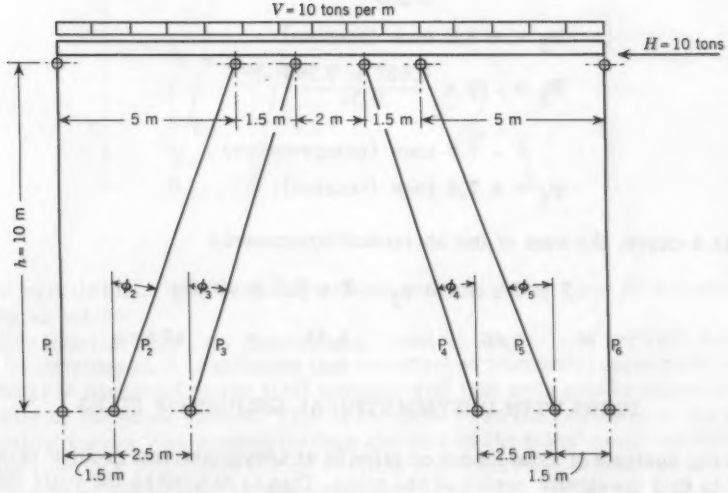
V = 10 tons per m
H = 10 tons
5 m
1.5 m
2 m
1.5 m
5 m
h = 10 m
ϕ2
ϕ3
ϕ4
ϕ5
P1
P2
P3
P4
P5
P6
1.5 m
2.5 m
2.5 m
1.5 m

FIG. 8

Forces in batter piles:

$$P_2 = P_5 = - 27.8 \times \cos^2 \phi_2$$

$$= - 27.8 \times 0.883$$

$$= - 24.5 \text{ tons}$$

$$P_3 = P_4 = - 27.8 \times 0.91$$

$$= - 25.3 \text{ tons}$$

As a check, the sum of the vertical components is

$$2 \times 27.8 + 2 \times 24.5 \times \cos \phi_2 + 2 \times 25.3 \times \cos \phi_3$$

$$= \quad 55.6 + \quad 46.2 + \quad 48.2 \quad = \quad 150 \text{ tons}$$

b. Horizontal Force (H).—Forces in vertical piles:

$$P_1 = P_6 = 0$$

Forces in batter piles:

$$P_2 = -10 \times \frac{0.943 \times 0.33}{2x0.943 \times 0.108 + 2x0.957 \times 0.082}$$

$$= -10 \times \frac{0.312}{0.360} = -8.6 \text{ tons (compression)}$$

$$P_5 = + 8.6 \text{ tons (tension)}$$

$$P_3 = -10 \times \frac{0.957 \times 0.286}{0.36}$$

$$= - 7.6 \text{ tons (compression)}$$

$$P_4 = + 7.6 \text{ tons (tension).}$$

As a check, the sum of the horizontal components

$$2 \times 8.6 \times \sin \phi_2 + 2 \times 7.6 \times \sin \phi_3$$

$$= \quad 5.65 \quad + \quad 4.35 \quad = \quad 10 \text{ tons}$$

PIERS WITH UNSYMMETRICAL GROUPS OF PILES

In the analysis of axial forces on piles in an unsymmetrical group it is necessary to find the elastic center of the piles. This is defined as the point through which a vertical or horizontal force is acting which will cause only translation displacement without rotation. To find this point and the final forces in piles, several equations must be derived and the group of piles must be divided into left hand and right hand groups.

In the following there is determined a simple and practical solution for the problem by considering only the vertical displacement of the pier deck when dealing with acting vertical forces. This is based on the assumption that the deck is restrained from horizontal displacement as in a wharf or by neglecting effect of deck side sway. This will permit the use of the equations for the case of a symmetrical pier as a first approximation.

By introducing an imaginary horizontal force at the pier's deck, the effect of side sway could be taken into account. The value of this horizontal force is determined from laws of equilibrium applied to the pier as a whole. The equilibrium of horizontal reactions will create a residual unbalanced small vertical force which has to be distributed on piles, similar to the method of moment distribution.

A similar procedure is adopted when dealing with horizontal forces by neglecting vertical displacement as a first approximation in the first instance and is then taken into account by introducing imaginary vertical force to satisfy

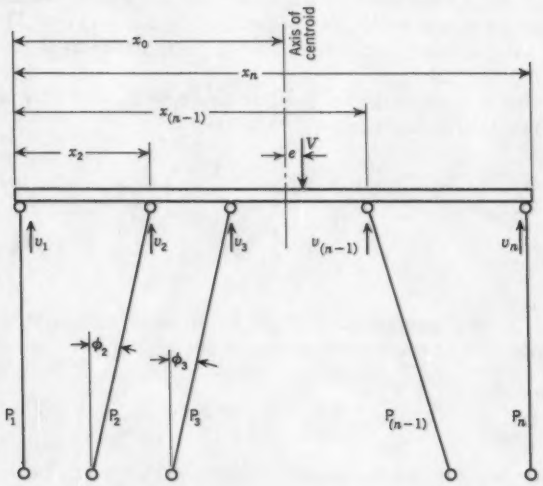

FIG. 9

laws of equilibrium. The resulting unbalanced horizontal force is distributed on piles as before.

Unsymmetrical Pile Pier Subjected to Vertical Forces.—If vertical forces are to be considered, it is assumed that the effect of horizontal movement (deck side sway) is neglected in the first instance and that each pile is compressed vertically by the same amount. This is the case when the resultant of the acting vertical forces V is passing through the axis of the piles' centroid. Otherwise the pile deck will rotate beside vertical movement due to moment M = V e which has to be considered in the calculation (Fig. 9).

Determination of Axis of the Centroid.—It is assumed that the pile deck in Fig. 9 is displaced a unit distance vertically downwards. Referring to Fig. 3(b) the axial deformation of pile AB is cos ϕ and the reaction of the pile is $\cos^2 \phi \frac{k}{h}$ (where k = A E).

The vertical component of the reaction to the top of pile AB is equal to (k/h) ($\cos^3 \phi$). Denoting the distance of the centroid of the vertical components of piles reactions from the left-hand pile by X_0

$$X_0 = \frac{x_1 \cos^3 \phi_1 + x_2 \cos^3 \phi_2 + \ldots + x_n \cos^3 \phi_n}{\cos^3 \phi_1 + \cos^3 \phi_2 + \ldots + \cos^3 \phi_n} \quad \ldots\ldots (32)$$

from which

$$X_0 = \frac{\sum_1^n x \cos^3 \phi_x}{\sum_1^n \cos^3 \phi_x} \quad \ldots\ldots\ldots\ldots\ldots (33)$$

Forces in Piles by Successive Approximation.—Since the effect of deck side sway is neglected at the beginning, we can apply Eqs. 14 and 31 for the case of the symmetrical pile pier to arrive at an approximate value for the pile reactions.

The axial force in any pile inclined at an angle ϕ_x due to V and M (V is not passing through axis of the centroid) will be:

$$P_x = \cos^2 \phi_x \left[\frac{V}{\sum_1^n \cos^3 \phi_x} + \frac{M \quad x}{\sum_1^n x \cos^3 \phi_x} \right] \quad \ldots\ldots (34)$$

From conditions of equilibrium in the vertical direction, it is found that the vertical components of piles reactions are satisfying the condition

$$V = \sum_1^n P_x \cos \phi_x \quad \ldots\ldots\ldots\ldots\ldots (35)$$

On the other hand in the horizontal direction, there will be a residual horizontal force. This means that the system is not in equilibrium in the latter direction and an imaginary horizontal force H must be applied at the pier deck where

$$H = - \sum P_x \sin \phi_x \quad \ldots\ldots\ldots\ldots\ldots (36)$$

This horizontal force will create additional axial forces in the piles.

By considering the effect only of horizontal movement (vertical displacement is neglected) in calculating pile reactions due to the imaginary deck force H, one could apply Eq. 23 as in the case of a symmetrical pile pier. The additional axial force on any pile inclined at an angle ϕ_x due to H will be

$$P_x = H \frac{\cos \phi_x \sin \phi_x}{\sum_1^n \cos \phi_x \sin^2 \phi_x} \quad \ldots\ldots\ldots\ldots (37)$$

A close examination of the algebraic sum of the horizontal components of pile reactions (obtained by adding results from Eqs. 34 and 37 shows that they are equal to the imaginary deck force H while vertical components will not equal the acting force V. This means that we have to repeat the cycle back again with a new imaginary vertical force

$$V = -\sum_{1}^{n} P_x \cos \phi_x \quad \ldots\ldots\ldots\ldots\ldots\ldots (38)$$

Actually this last imaginary force V is small and will create a very small unbalanced horizontal force H, so that it could be neglected. Otherwise the process is repeated until the required precision is attained.

Combining results from all previous acting and imaginary deck forces, the final axial pile reactions are determined for the case of the pier when it is free to sway.

Unsymmetrical Pile Pier Subjected to Horizontal Forces.—The procedure for this case of acting horizontal forces is the same as the previous one. First, the vertical displacement is neglected to get approximate values of pile reactions by treating the system as a symmetrical one.

From Eq. 23 the approximate axial pile reactions will be:

$$P_x = H \frac{\cos \phi_x \sin \phi_x}{\sum_{1}^{n} \cos \phi_x \sin^2 \phi_x} \quad \ldots\ldots\ldots\ldots\ldots\ldots (39)$$

Resolving pile reactions vertically, there will be an unbalanced vertical force which has to be distributed over piles by considering the effect of an imaginary vertical force

$$V = -\sum_{1}^{n} P_x \cos \phi_x \quad \ldots\ldots\ldots\ldots\ldots\ldots (40)$$

This imaginary vertical force will create back an unbalanced horizontal force determined from laws of equilibrium. It must be noticed that the residual unbalanced forces are progressively decreased as the process is repeated. Algebraic summation of results from previous processes will give the final pile reactions.

Example 5.—Given an unsymmetrical pier of two vertical piles and three batter ones (Fig. 10) in which

$$\phi_2 = \phi_4 \quad (\text{where } \cos \phi_2 = 0.943;\ \sin \phi_2 = 0.33;$$
$$\cos \phi_3 = 0.957;\ \sin \phi_3 = 0.286)$$

The loadings, span and height of pier are similar to previous example.

Axis of the Centroid (Fig. 11).—From Eq. 33

$$X_0 = \frac{5 \cos^3 \phi_2 + 6.5 \cos^3 \phi_3 + 10 \cos^3 \phi_4 + 15}{1 + \cos^3 \phi_2 + \cos^3 \phi_3 + \cos^3 \phi_4 + 1}$$

$$= 7.3 \text{ m}$$

Eccentricity, e = 0.20 m

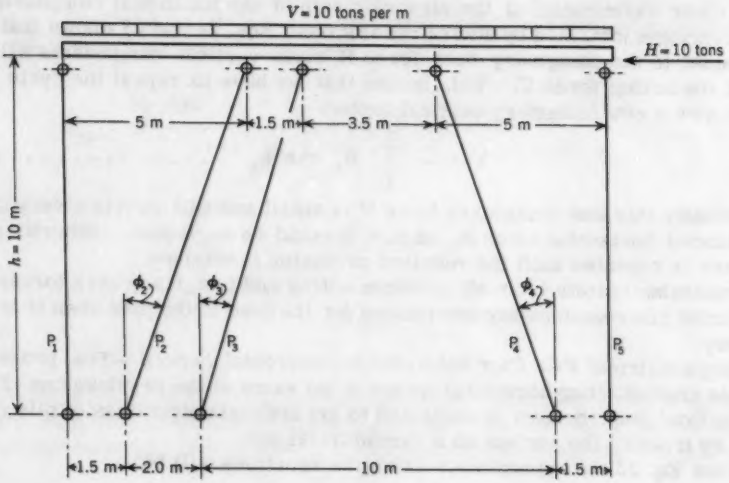

FIG. 10

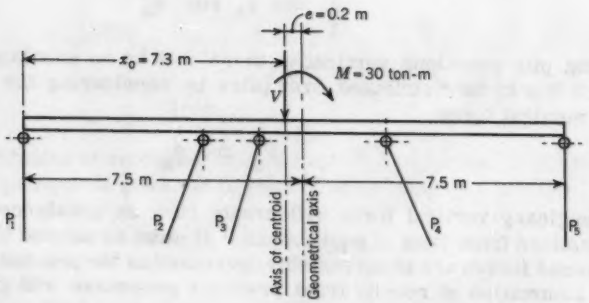

FIG. 11

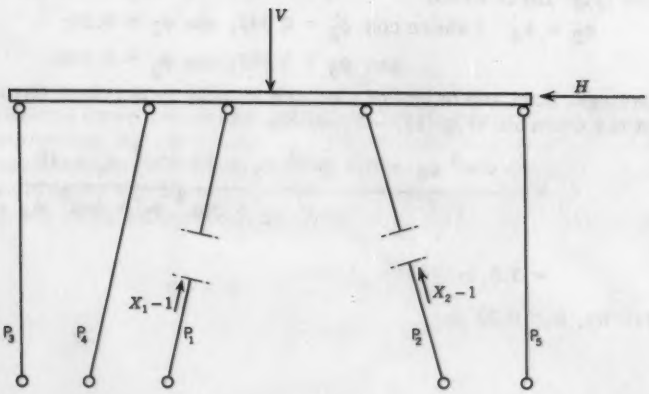

FIG. 12

Thus the pier deck will be subjected to a vertical force (V = 150 tons) and moment (M = 150 x 0.2 = 30 ton-m) passing through axis of centroid as shown in Fig. 11.

a. Forces in Piles Due to V or H or M.--Eqs. 14, 23, and 31 are used to determine the effect of V, H, or M. A solution is presented in Tables 1 and 2.

MORE EXACT SOLUTION

A more exact solution for symmetrical and unsymmetrical groups of piles may be approached by considering the group together with their deck, as a statistically indeterminate system. A main statically determinate system is to be first assumed and then the unknown axial forces in the redundant piles can be calculated by the method of virtual work. This method has the advantage of introducing the bending and axial deformations in the pile deck, as well as the axial deformations of the piles to the solution.

Moreover, this method can be applied to the same degree of accuracy for symmetrical and unsymmetrical groups of piles. As the deck of the pier is always compared to the piles, the assumption of hinged connections between the deck and the piles will help to decrease the statical indeterminacy of the system.

In Fig. 12 the main system is chosen by assuming a cut in piles 1 and 2 and calculating the bending moment M_0 and thrust N_0 diagrams from the equations of statical equilibrium. Virtual loads $X_1 = 1$ and $X_2 = 1$ are then applied along the assumed cuts. Diagrams for M_1, N_1, M_2 and N_2 are then drawn. The redundant axial forces in piles 1 and 2 can be determined from the following equations of deformation at the assumed cuts:

$$\delta_{10} + X_1 \delta_{11} + X_2 \delta_{12} = \frac{X_1 L_1}{A_1 E} \quad \ldots\ldots\ldots\ldots (41)$$

and

$$\delta_{20} + X_1 \delta_{21} + X_2 \delta_{22} = \frac{X_2 L_2}{A_2 E} \quad \ldots\ldots\ldots\ldots (42)$$

where L_1 and L_2 are the lengths of piles P_1 and P_2 and A_1 and A_2 are the areas of piles P_1 and P_2.

The deformations are given by

$$\delta_{10} = \int \frac{M_0 M_1}{I E} \, dl + \sum \frac{N_0 N_1}{A E} \, \Delta l \quad \ldots\ldots\ldots (43)$$

and

$$\delta_{11} = \int \frac{M_1^2}{I E} \, dl + \sum \frac{N_1^2}{A E} \, \Delta l \quad \ldots\ldots\ldots\ldots (44)$$

TABLE 1.—FORCE DISTRIBUTION DUE TO VERTICAL LOAD IN FIG. 10

Loading	Pile	P_V, in tons	P_H, in tons	P_M, in tons	P_{TOTAL}, in tons	Vertical Component, Col. 6 cos ϕ	Horizontal Component, Col. 6 sin ϕ
(1)	(2)	(3)	(4)	(5)	(6)	(7)	(8)
(a) Analysis							
Case I:							
Vertical =	1	-33.1	. . .	1.78	-31.32	31.32 ↑	0
150 tons ↓	2	-29.2	. . .	0.495	-28.705	27.1 ↑	9.45 ←
	3	-30.1	. . .	0.177	-29.923	28.6 ↑	8.55 ←
Moment =	4	-29.2	. . .	-0.582	-29.782	28.1 ↑	9.8 ←
30 ton-m ↷	5	-33.1	. . .	-1.88	-34.98	34.98 ↑	0
					Total	150.1 ↑	8.2 ← Unbalanced
Case II:							
Horizontal =	1	. . .	. . .	. . .	. . .	0	0
8.2 tons →	2	. . .	9	. . .	9	8.5 ↑	2.96 ←
	3	. . .	8	. . .	8	7.62 ↓	2.28 ←
	4	. . .	-9	. . .	-9	8.5 ↑	2.96 ←
	5	. . .	. . .	. . .	. . .	0	0
					Total	7.62 ↓ Unbalanced	8.2 ←
Case III:							
Vertical =	1	-1.69	. . .	. . .	-1.69	1.69 ↑	0
7.62 tons ↓	2	-1.485	. . .	. . .	-1.485	1.4 ↑	0.49 ←
	3	-1.5	. . .	. . .	-1.5	1.4 ↑	0.43 ←
	4	-1.485	. . .	. . .	-1.485	1.4 ↑	0.49 ←
	5	-1.69	. . .	. . .	-1.69	1.69 ↑	0
					Total	7.62 ↑	0.43 ← Unbalanced

(b) Final Pile Forces

Pile	Case I	Case II	Case III	Pile Force, in tons
1	-31.32	0	-1.69	-33.01
2	-28.705	9	-1.485	-21.19
3	-29.923	8	-1.5	-23.423
4	-29.782	-9	-1.485	-40.267
5	-34.98	0	-1.69	-36.67

TABLE 2.—FORCE DISTRIBUTION DUE TO HORIZONTAL LOAD IN FIG. 10

Loading	Pile	P_V, in tons	P_H, in tons	P_M, in tons	P_{TOTAL}, in tons	Vertical Component, Col. 6 cos ϕ	Horizontal Component, Col. 6 sin ϕ
(1)	(2)	(3)	(4)	(5)	(6)	(7)	(8)
(a) Analysis							
Case I: Horizontal = 10 tons ←	1	...	...	...	...	0	0
	2	...	-11.0	...	-11.0	10.4 ↑	3.625 →
	3	...	- 9.7	...	- 9.7	9.3 ↑	2.75 →
	4	...	11.0	...	11.0	10.4 ↓	3.625 →
	5	...	...	...	...		
					Total	9.3 ↑ Unbalanced	10.0 →
Case II: Vertical = 9.3 tons ↑	1	2.06	...	...	2.06	2.06 ↓	0
	2	1.81	...	...	1.81	1.71 ↓	0.6 ←
	3	1.83	...	...	1.83	1.76 ↓	0.525 →
	4	1.81	...	...	1.81	1.71 ↓	0.6 →
	5	2.06	...	...	2.06	2.06 ↓	
					Total	9.3 ↓	0.525 → Unbalanced
Case III: Horizontal = 0.525 ton ←	1	...	...	...	...	0	0
	2	...	-0.58	...	-0.58	0.548 ↑	0.191 →
	3	...	-0.51	...	-0.51	0.486 ↑	0.145 →
	4	...	0.58	...	0.58	0.548 ↓	0.191 →
	5	...	...	...	...		0
					Total	0.486 ↑ Unbalanced	0.527 →

(b) Final Pile Forces

Pile	Case I	Case II	Case III	Pile Force, in tons
1	0	2.06	0	2.06
2	-11.0	1.81	-0.58	-9.77
3	- 9.7	1.83	-0.51	-8.38
4	11.0	1.81	0.58	13.39
5	0	2.06	0	2.06

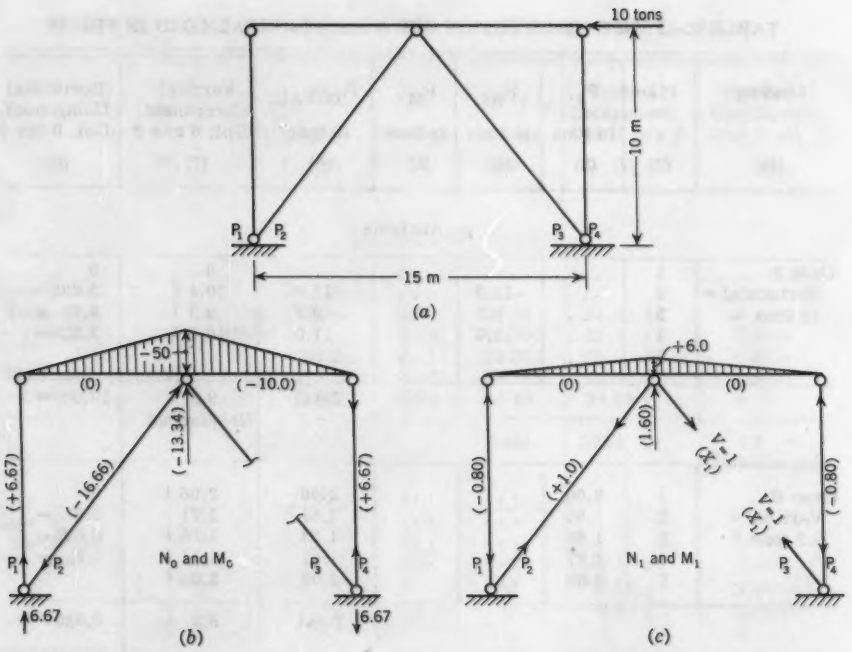

FIG. 13

Example 6.—Using the more exact method, the forces in the piles in Example 2 (Fig. 6) will be determined (Fig. 13).

Assume a deck cross section of 0.4 m by 1.0 m (area = 0.4 sq m and I = 0.033 m^4) and a pile cross section of 0.4 m by 0.4 m (area = 0.16 sq m and I = 0.00213 m^4); thus $I_{deck} = 15\ I_{pile}$.

The axial force in the pile can be determined from

$$\delta_{10} + X_1\ \delta_{11} = -\ X_1\ \frac{L_3}{A_3\ E} \qquad \ldots\ldots\ldots\ldots\ldots\ldots (45)$$

for which

$$\delta_{10} = \sum \frac{M_0\ M_1}{E\ I}\ \Delta L + \sum \frac{N_0\ N_1}{E\ I}\ \Delta L$$

$$= \frac{1}{E}\left[-2\ \frac{(50)(7.5)}{2}\ 4\ \frac{1}{0.033}\right]$$

$$+ \frac{1}{E}\left[-\ 2\ \frac{(6.67)(0.80)(10)}{0.16}\ -\ \frac{(16.66)(1)(12.5)}{0.16}\right]$$

$$= -\ 0.023734\ m/E$$

$$\delta_{11} = \sum \frac{M_1^2}{E\,I}\,\Delta L + \sum \frac{N_1^2}{E\,I}\,\Delta L$$

$$= \frac{1}{E}\left[2\,\frac{(6)(7.5)}{2}\;4\;\frac{1}{0.33}\right]$$

$$+ \frac{1}{E}\left[2\,\frac{(0.8)(0.8)(10)}{0.16} + \frac{(1)(1)(12.5)}{0.16}\right]$$

$$\simeq 0.002814 \text{ m/E}$$

and

$$\frac{L_3}{A_3\,E} = \frac{12.5}{0.16\,E} = \frac{78}{E} = 0.000039 \text{ m/E}$$

Therefore

$$-\,0.023734 + 0.002814\,X_1 = -\,0.000039\,X_1$$

from which

$$X_1 = 8.33 \text{ tons}$$

Thus the axial forces are as follows: For the vertical piles, P_1 and P_4, the force = 0 and for the batter piles, P_2 = -8.33 tons and P_3 = 8.33 tons. In Example 2: $P_1 = P_4 = 0$, P_2 = 8.3 tons, and P_3 = 8.3 tons.

Example 7.—The more exact solution will be used to get the forces in the piles of Example 3 due to a horizontal force of 10 tons (Fig. 14).

The deck and pile data of Example 6 is used in this example. Eq. 45 can be used to determine the axial forces. It is therefore necessary to determine

$$\delta_{10} = \frac{1}{E}\left[-\,\frac{(109)(5.75)}{2}\;3.66 - 3.5\;\frac{(109+67.8)}{2}\;5.48\right.$$

$$\left. -\,\frac{(67.8)(5.75)}{2}\;3.66\right]\frac{1}{0.033} + \frac{1}{E}\left[(-18.90)(0.953)(10)\right.$$

$$\left. -\,(32.30)(1)(10.50) - (11.80)(0.953)(10) - \frac{1}{16}\,(10)(0.31)(3.50)\right]$$

$$= -\,0.05576 \text{ m/E}$$

$$\delta_{11} = \frac{1}{E}\left[2\,\frac{(5.48)(5.75)}{2}\;3.66 + (5.48)(3.5)(5.48)\right]\frac{1}{0.033}$$

$$+ \frac{1}{E}\left[(2)(0.953)(0.953)(10) + (1)(1)(10.5)\right]\frac{1}{0.16}$$

$$= 0.003425 \text{ m/E}$$

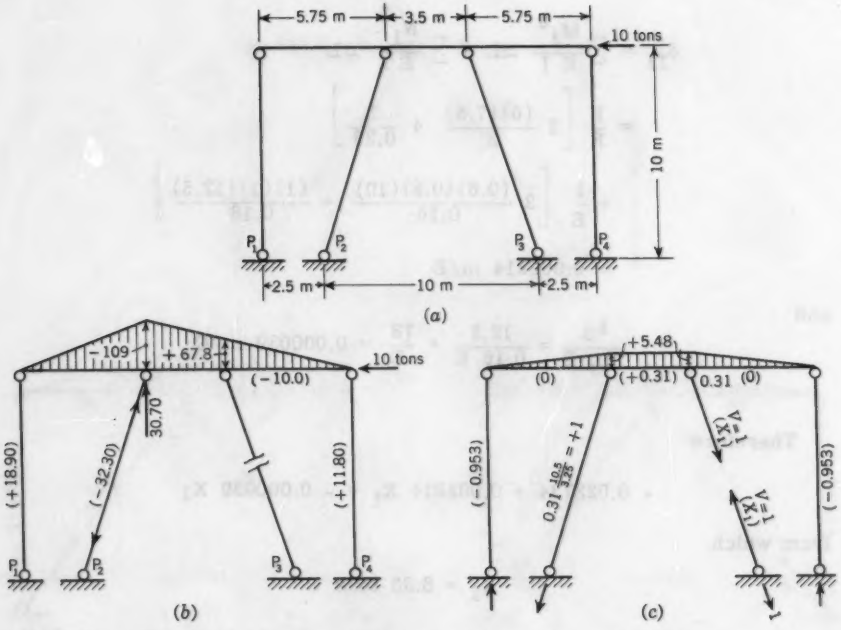

FIG. 14

and

$$\frac{L_3}{A_3 E} = \frac{10.5}{0.16 E}$$

Therefore

$$- 0.05576 + 0.003425 X_1 = - 0.000033 X_1$$

from which

$$X_1 = 16.1 \text{ tons}$$

Thus the axial forces are as follows: For the vertical piles, $P_1 = 3.6$ tons, and $P_4 = -3.6$ tons. For the batter piles, $P_2 = -16.2$ tons and $P_3 = 16.2$ tons. In Example 3 it was found that $P_1 = P_4 = 0$, $P_2 = -16.1$ tons, and $P_3 = 16.1$ tons.

CONCLUSION

Methods of solution presented herein offer simple procedures for the analysis of load distribution in any type of pier or group of piles which can be quickly applied. Difference between results obtained by approximate and exact solutions is small and thus both methods are acceptable.

REFERENCES

1. "Reinforced Concrete Piling," by F. E. Wentworth Sheilds and W. S. Gray.
2. "Maritime Structures," by Minikin.
3. "Reinforced Concrete," by A. L. L. Baker.
4. "An Analysis of Groups of Piles," by S. Jampel, Concrete and Construction Engineering, July, 1952.
5. "Analysis of Groups of Piles," by R. S. Wilkins, Concrete and Construction Engineering, July, 1952.
6. "Loads on Groups of Free-Standing Piles," by Reynolds, Concrete and Construction Engineering, December, 1953.
7. "Docks, Wharves and Piers," by Du-Plat-Taylor.

Journal of the

WATERWAYS AND HARBORS DIVISION

Proceedings of the American Society of Civil Engineers

CONTENTS

DISCUSSION

Page

Engineering Aspects of Coastal Sediment Movement, by Richard Silvester. (September, 1959. Prior discussion: None. Discussion closed.)
by R. G. Dean and P. S. Eagleson 119

Laboratory Investigation of Rubble-Mound Breakwaters, by Robert Y. Hudson. (September, 1959. Prior discussion: December, 1959, March, 1960. Discussion closed.)
by Omar J. Lillevang 121

The Supply and Loss of Sand to the Coast, by J. W. Johnson. (September, 1959. Prior discussion: None. Discussion closed.)
by P. S. Eagleson and R. G. Dean 125

Natural By-Passing of Sand at Coastal Inlets, by P. Bruun and F. Gerritsen. (December, 1959. Prior discussion: None. Discussion closed.)
by J. R. Bowman 131

A Case of Critical Surging of a Moored Ship, by Basil W. Wilson. (December, 1959. Prior discussion: March, 1960. Discussion closed.)
by W. C. Q. Joosting. 133

Note: This paper is a part of the copyrighted Journal of the Waterways and Harbors Division, Proceedings of the American Society of Civil Engineers, Vol. 86, No. WW 2, June, 1960.

ENGINEERING ASPECTS OF COASTAL SEDIMENT MOVEMENT[a]

Discussion by R. G. Dean and P. S. Eagleson

R. G. DEAN,[1] A. M. ASCE and P. S. EAGLESON,[2] A. M. ASCE.—Dealing with and predicting coastal sediment processes presents the coastal engineer with a challenging and difficult problem. As enumerated by the author, the large number of pertinent variables, many of which are not readily measurable, and their affect on coastal physiography has precluded any comprehensive analytical treatment of the problem. The author has, also, presented very clearly in sequential form the interaction of the causative agents of many sediment processes which heretofore were considered only separately. For a given situation, the necessity of considering the meteorological characteristics of the given area as well as following up any modifications or construction with hydrographic surveys was shown.

A logical sequel to the understanding of the qualitative manner in which beach processes are affected by the various factors is the following question: Are these phenomena so involved and complex that they cannot be predicted by analytic means? With the long-range purpose of attempting to relate beach characteristics (that is, slope, median diameter, etc.) to meteorological patterns or ensuing wave conditions, an investigation is being carried out at the Hydrodynamics Laboratory at M.I.T. under the sponsorship of the Beach Erosion Board. This study is concerned with conditions in the offshore zone (seaward of breaker line) and in the initial phases of this program the mechanics of motion of a discrete spherical sediment particle on smooth and roughened sloping beaches was related to the local wave characteristics. It was found that for an equilibrium beach profile, two different types of sediment motion could govern the relationship between beach and wave characteristics. A description of this study and these types of sediment motion is presented elsewhere.[3] A logical query is whether a theory based on a simple model such as the one described therein[3] can be used to predict characteristics of natural beaches. Comparison of predictions based upon this model with natural beach profiles and wave characteristics as provided by the Beach Erosion Board is presented elsewhere.[4] This comparison shows that the trend of the predictions agrees well with measured beach characteristics. It should be stressed that the wave characteristics used for the measured points were estimated and that the theory is valid only for waves advancing normal to a beach. As stressed by Mr.

---

[a] September, 1959, by Richard Silvester.

[1] Asst. Prof. of Hydr., Hydrodynamics Lab., Dept. of Civ. and Sanitary Engrg., Mass. Inst. of Tech. Cambridge, Mass.

[2] Asst Prof. in Hydr. Engrg., Hydrodynamics Lab., Dept. of Civ. and Sanitary Engrg., Mass. Inst. of Tech., Cambridge, Mass.

[3] "Wave Induced Motion of Bottom Sediment Particles," by P. S. Eagleson, and R. G. Dean, Proceedings, ASCE, Vol. 85, No. HY 10, October, 1959.

[4] Ibid., Figure 11.

Silvester, the beach profile may be affected considerably by any longshore effects which, of course, are difficult to include in any laboratory investigation.

In summary, there are presently two basic problems to be reconciled before a comprehensive theory can be developed and used effectively to predict beach processes:

1. The first of these is the development of analytical expressions which includes the many factors brought out so well by the author. On one hand, the use of a laboratory is desirable in order to have better control and measurement of the variables, however, the effects which are feasibly included in a laboratory investigation are limited. For example, the effect of rocky headlands which are essentially fixed boundary points, and longshore currents have not been included in past laboratory investigations. From this point of view it appears that a comprehensive solution must be based on investigations carried out in the field where all possible effects are generally present. Miller and Zeigler[5] are presently (1960) carrying out such a study on the shores of Cape Cod and attempting to correlate their measurements with the theory presented elsewhere.[3] One of the difficulties associated with such a field study is that the presently available techniques for obtaining sediment samples are not completely satisfactory and the necessity of dealing with complex sea conditions raises definite questions in attempting to relate, for example, sediment characteristics to some effective wave height. It seems that any comprehensive solution must then arise from an allied effort of laboratory and field investigations.

2. The second problem, once such a theory has been developed, is that it may involve such a complicated arrangement of a large number of variables that in order to apply the theory, an expensive wave, current and sediment survey of the area may be required.

There are two effects which, with the passage of time, will enhance the development and usage of a comprehensive analytical solution and tend to minimize the objections raised above:

a. The continuing development of oceanographic and sediment sampling instruments and techniques necessary for the establishment and usage of such an analytical solution, and

b. The increasing economic importance associated with the need to quantitatively describe coastal processes.

It is the opinion of the writers, that the development and usage of a comprehensive analytical solution will become a useful and necessary tool available to the coastal engineer.

---

5 "A Model Relating Dynamics and Sediment Pattern in Equilibrium in the Region of Shoaling Waves, Breaker Zone and Foreshore," by R. L. Miller and J. M. Zeigler, Journal of Geology, Vol. 66, No. 4, July, 1958.

LABORATORY INVESTIGATION OF RUBBLE-MOUND BREAKWATERS[a]

Discussion by Omar J. Lillevang

OMAR J. LILLEVANG,[1] M. ASCE.—The engineer who struggles to keep abreast of the growth of knowledge in the field of harbor and coastal engineering can find valuable assistance in Mr. Hudson's paper. The bibliography refers to information which is found in only a few libraries and not many of the references include discussions by reviewers or supplementary contributions. To the reader who finds too little time for study, the discussion by others of the work of technical authors is a great aid to quick evaluation. Wider distribution of information on new work and ideas is needed; it is appreciated that work such as the present paper, originally given limited distribution by the Waterways Experiment Station, is published in the journals of the Society.

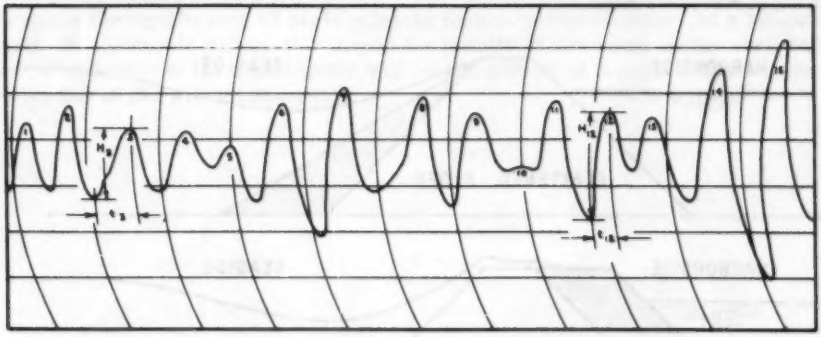

FIG. A.—TYPICAL SECTION OF A WAVE RECORD

Design waves for rubble-mound structures may not be the same for stone size determination as for concerns with uprush of the seas. Where wave statistics are available for a problem site the record normally presents frequency of occurrence of the "Significant" waves and periods, the term being a precise one relating to the average of the highest one-third of the waves in a sample. Other averages within the sample are related by Mr. Hudson, and, in 1952, R. R. Putz[2] published an excerpt from an actual wave record which graphically shows characteristic variations. Fig. A is Putz' illustration, and from it one can clearly appreciate the uncertainty of what may come next in any wave series.

If the major waves were always tightly grouped, any heavy overtopping by uprush on seawalls would be an extremely burdensome problem of water disposal. Some risk can prudently be taken in most instances that the highest

[a] September, 1959, by Robert Y. Hudson.

[1] Senior Engr., Leeds, Hill and Jewett, Inc., Los Angeles, Calif.

[2] From R. R. Putz, AGU, Transactions, ASCE, Vol. 33, No. 5, 1952.

waves do not ordinarily group themselves within the series, and the structure design may, therefore, often be related to some lower average wave. Overtopping by the wave uprush doesn't necessarily mean the design is a failure. Accepting overtopping and providing for it in the design may be the best economic choice in many instances. Fig. B shows three basic variations of a reference cross section which may be considered in treating with the wave runup question. Mr. Hudson's work provides excellent tools for raising the crest of the structure or for flattening the seaward slope to minimize or eliminate overtopping. It is apparent that if one would consider making the crest wider than the minimum width dictated by construction procedures, and drain off the cresting water through the armor voids, then data on the volume of water at any elevation in an uprushing wave would be most helpful. This need for knowledge of volume versus elevation becomes particularly acute if the structure

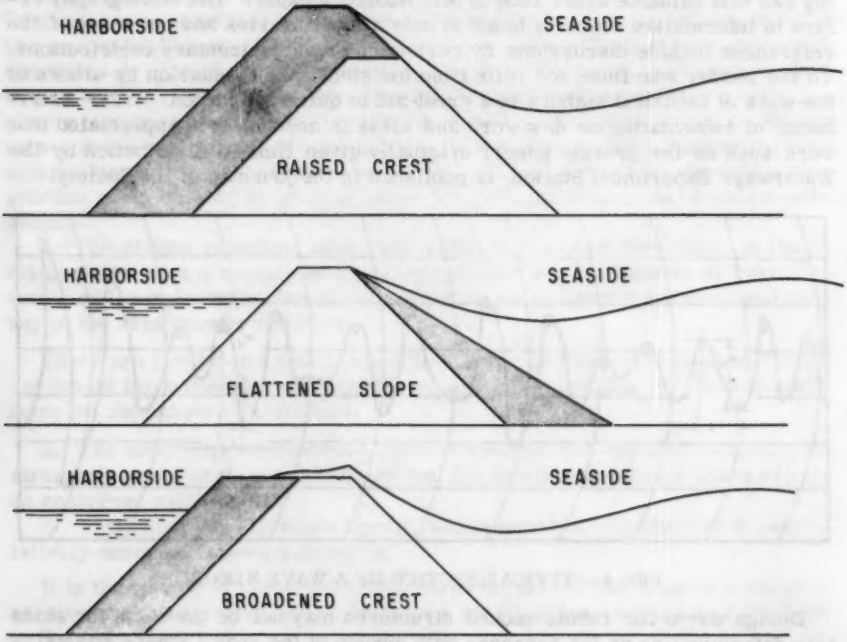

FIG. B.—ALTERNATIVE TREATMENTS FOR WAVE RUNUP

is a seawall of normal crest width, and gutters or storm drains must be proportioned for the area landward of the seawall. If such information exists, its presentation should be sought; if not, it is an area of investigation which could very beneficially be undertaken in one of the research centers active in this field.

Armor stone might be selected of a size to completely resist the maximum wave in a train of waves, but something less is usually acceptable. Armor stone in well built and successfully maintained breakwaters and seawalls are not often as large as would be indicated to be necessary from application of

formulae which neglect interaction between stones (other than friction), or consider the interaction to be a safety factor. "Well built," in this writer's view, requires that armor stone be placed with care, not dumped, and that above the low water line the individual pieces be selected for shape of fit to other stones and laid in juxtaposition with them and in an attitude of optimum stability. Wedging may then be anticipated as the whole structure accepts wave attack, and settles into a coherent unit. Lacking such careful selection and placing of armor stones, the wave-affected slope should be flattened so only friction is relied upon, if maintenance is not to be excessively costly soon after the first heavy storms. Obviously, the variability of dimensions of stones of a given weight, their angularity or blockiness, will affect the degree of stability achieved by careful placement. In essence this is recognized in Mr. Hudson's use of a "Shape Factor." It would be useful if in the author's closing discussion some added data to illustrate the Shape Factor were included.

The writer is intrigued by the author's statement that the effect of nonbreaking wave forces is comparable with that of the forces of breaking waves, though the wave motions are different in characteristics. An elaboration of this statement would be most interesting. Would this view lead one to rational design procedures in determining underwater slopes and stone sizes? For that unseen portion of rubble structures little has been found.

Presumably the tests, under way in the Beach Erosion Board's giant wave flume, on stability of very much larger stones in rubble-mound structures will evaluate the significance of scale effect in Hudson's experiments. As a follow-up of Mr. Hudson's paper, it is hoped the results of the large-scale work and its relationship to the small-scale will be the subject of a paper. The subject is worthy of the wider readership.

THE SUPPLY AND LOSS OF SAND TO THE COAST[a]

Discussion by P. S. Eagleson and R. G. Dean

P. S. EAGLESON,[1] A. M. ASCE and R. G. DEAN,[2] A. M. ASCE.—Mr. Johnson mentions wave-induced onshore-offshore sand movement as being probable means of supply and loss of beach material. In reviewing the present state of knowledge of these factors, however, he concludes that, "The contribution of sand from offshore sources is completely an unknown factor, but it is probably relatively small."

Mr. Johnson appears to have based this conclusion upon the study made by Hall[3] of unsuccessful attempts by the Corps of Engineers to nourish certain beaches by offshore dumping of dredged material.

Work done at the Hydrodynamics Laboratory at M.I.T., over the period 1952 to date (1960), provides both a rational explanation for the failures of the nourishment experiments and a means of quantitatively evaluating the importance of one mechanism of onshore-offshore sediment transportation.

The findings of Ippen and Eagleson[4] may be summarized by the following physical description of wave-induced bed load movement:

As a deep-water oscillatory wave moves into shallow water it produces oscillating pressure gradients and, thus, oscillating fluid velocities near the bottom. The shallower the water becomes, the larger become these oscillating pressure gradients and velocities at any given distance, y, above the bed. As a consequence of this, the instantaneous hydrodynamic forces exerted on individual bed sediment particles will also increase in a shoreward direction.

At some point on the offshore slope these instantaneous hydrodynamic forces may become sufficiently large to cause static instability of bed sediment particles of a given size. This location is called the point of incipient motion for that sediment size for the given bed-particle geometry and beach slope.

Onshore of this point, if the beach slope is the same, that particular sediment size will be in a condition of oscillatory of quasi-oscillatory motion, since for some (increasing) time during each wave cycle, the instantaneous hydrodynamic forces will exceed that value necessary to tip the particle out of its "nest" in the bed.

A bed sediment particle which is in a fluid velocity field stronger than that necessary to produce incipient motion of that size is oscillating in a motion

---

[a] September, 1959, by J. W. Johnson.

[1] Asst. Prof. of Hydr. Engrg., Hydrodynamics Lab., Mass. Inst. of Tech., Cambridge 39, Mass.

[2] Asst. Prof. of Hydr., Hydrodynamics Lab., Mass. Inst. of Tech., Cambridge 39, Mass.

[3] "Artificially Nourished and Constructed Beaches," by J. V. Hall Jr., Tech. Memorandum No. 29, Beach Erosion Bd., Washington, D. C.

[4] "A Study of Sediment Sorting by Waves Shoaling on a Plane Beach," by A. T. Ippen and P. S. Eagleson, Beach Erosion Bd. Tech. Memorandum No. 63, Washington, D. C., 1955.

called established sediment motion. Just as there is a mass transport or "drift" of the oscillating fluid particles so there is a net movement of the oscillating bed sediments.

The direction and magnitude of this net sediment motion depends upon the relative value of the opposing components of the gravitational force, F_G, and the net (over one wave cycle) fluid force, $\bar{F}_F$, in a plane parallel to the beach slope. When $F_G > \bar{F}_F$ the net motion will be offshore and when $F_G < \bar{F}_F$ the particle will move onshore. When $F_G = \bar{F}_F$, the particle oscillates with no net motion. For beaches having positive slopes which increase gradually in the shoreward direction, this latter condition can be shown to be one of stable equilibrium which experiments have shown to play a role in the formation of equilibrium beach profiles.[5]

From considerations of the equation of motion of discrete spherical particles on a plane beach and from additional related experiments Eagleson and Dean[6] presented the earlier data[4] in terms of familiar physical relationships from which extrapolations to natural beaches might justifiably be made. Their findings may be summarized as follows:

Incipient Motion.—For sand in sea water, the size particle just capable of being moved (that is, the incipient size) at any location is given by:

$$D_i = 8.1 \times 10^{-6} \left[\frac{H_i}{T} \frac{\pi}{\sinh \frac{2\pi d}{L}} \right] (1 - \kappa)\, \beta \csc (\alpha + 0.92) \quad \ldots . \quad (1)$$

in which D_i is the incipient sediment size (S.G. = 2.65) in ft, H_i represents the local incident wave height in ft, d is equal to local water depth in ft, L denotes local wave length in ft, T is the wave period in sec, $\beta = \left[\frac{\pi}{\nu T}\right]^{1/2}$, ν is the kinematic fluid viscosity in sq ft per sec, α represents the local beach slope, and κ denotes the wave reflection coefficient.

Established Motion.—The basic relationship governing established motion is the integrated form of the instantaneous equation of bed particle motion.

This integrated form is (details and assumptions have been presented elsewhere[7]):

$$C_D\, \rho_f\, \frac{\pi D^2}{8} \left(\bar{U}_f - \bar{V}_s \right) = F_G \sin \alpha \cos \lambda \quad \ldots \ldots \ldots \quad (2)$$

in which $\bar{V}_s$ is the net sediment velocity, λ represents the angle of wave incidence measured between a normal to the wave crests and the gradient of the beach, $\bar{U}_f$ is the effective fluid mass transport velocity assumed to be given by $\bar{U}(y)$ at y = D, and

$$C_D = \frac{N}{R} = \frac{N \nu}{\left(\bar{U}_f - \bar{V}_s \right) D} \quad \ldots \ldots \ldots \ldots \ldots \quad (3)$$

where N is a constant depending only upon the bed-particle geometry.

---

[5] "Equilibrium Characteristics of Sand Beaches in the Offshore Zone," by P. S. Eagleson, J. Dracup, and B. Glenne, M.I.T. Hydrodynamics Lab. Tech. Report No. 41, April, 1960, (in press).

[6] "Wave-Induced Motion of Bottom Sediment Particles," by P. S. Eagleson and R. G. Dean, Proceedings, ASCE, Vol. 85, No. HY 10, October, 1959.

[7] "The Mechanics of the Motion of Discrete Spherical Bottom Sediment Particles Due to Shoaling Waves," by P. S. Eagleson, L. A. Peralta, and R. G. Dean, Beach Erosion Bd. Tech. Memorandum No. 104, Washington, D. C., 1958.

Using the relationship of Longuet-Higgins[8] for mass-transport velocity distribution within laminar boundary layers, Eq. 2 becomes:

$$\overline{V}_s = 0.92 \left(\frac{\pi H_i}{L}\right)^2 (1 - \kappa^2) \frac{C (\beta D)^{8/7}}{\sinh^2 \frac{2 \pi d}{L}} - \frac{8 F_G \sin \alpha}{\mu \pi D N} \cos \lambda \quad . . \quad (4)$$

in which C is the local wave celerity in ft per sec, and μ is the dynamic fluid viscosity in lb sec per sq ft.

The volumetric rate of bed sediment flow on a sand beach may be written:

$$q_s = A \overline{V}_s t \quad . . . . . \quad (5)$$

in which A is the cross sectional area of moving sediment per unit of beach front, and t is the decimal percentage of time that the given wave conditions prevail.

Assuming that all reflection occurs at the breaker and neglecting dissipation, the familiar considerations of energy flux yield:

$$\left(\frac{H_i}{H_{i_o}}\right)^2 = \frac{2 \cosh^2 \frac{2 \pi d}{L}}{\sinh \frac{4 \pi d}{L} + \frac{4 \pi d}{L}} \quad . . . . . \quad (6)$$

in which the subscript, o, refers to deep water conditions.

Substituting Eqs. 4 and 6 in Eq. 5, and simplifying:

$$q_s = K \frac{\operatorname{ctnh}^2 \frac{2 \pi d}{L}}{\sinh^2 \frac{2 \pi d}{L} + \frac{2 \pi d}{L_o}} - J \sin \alpha \cos \lambda \quad . . . . . \quad (7)$$

in which:

$$K = 0.92 \ \pi^2 \ (1 - \kappa^2) \left(\frac{H_{i_o}}{L_o}\right)^2 C_o (\beta D)^{8/7} A t \quad . . . . . \quad (8)$$

and

$$J = \frac{4}{3} \frac{g D^2}{N \nu} \left(\frac{S_s}{S_f} - 1\right) A t \quad . . . . . \quad (9)$$

The rate of sediment transport by this mechanism can be seen in the general case to be a function of position on the beach, a fact which, due to continuity considerations, requires a time varying beach profile.

The value of N has been determined experimentally[7] to be 19.2 for a ratio of sediment diameter to bed roughness, D/k = 1.

Using this value, and for $\kappa = 0$ and $\lambda = 0$, the equilibrium condition of established motion ($q_s = 0$) becomes:

$$D_e^{6/7} = 7.6 \times 10^{-6} \beta^{8/7} \overline{U}_o \csc \alpha \quad . . . . . \quad (10)$$

---

8 "Mass Transport in Water Waves," by M. S. Longuet-Higgins, Phil. Trans. Roy. Soc. London Series A., No. 903, Vol. 245, March 31, 1953, pp. 535-581.

in which

$$\overline{U}_o = \frac{1}{2}\left(\pi \frac{H}{L}\right)^2 \frac{C}{\sinh^2 \frac{2\pi d}{L}} \quad \ldots\ldots\ldots\ldots (11)$$

Applications. A. Beach Nourishment.—When attempting to nourish a beach by offshore dumping of sand the above development indicates that the diameter of the greater part of the sand chosen should be smaller than D_i or it will not be moved at all and should also be smaller than D_e or it will move only in the offshore direction.

From available data,[9,10] the following field conditions for the Long Branch, N. J. nourishment test were determined: mean diameter of dumped sand = 0.34 mm, depth in which sand was dumped = 38 ft, and mean slope in spoil area α = 0.0067.

The most severe wave recorded (although it occurred only 0.1% of the time) had the approximate characteristics at the site: H = 10 ft, and T = 10 sec.

From Eq. 1 then D_i = 0.21 mm.

Since the incipient size, D_i, is only about two-thirds the mean diameter of the dumped sand, it is logical that the spoil was not moved.

B. Quantitative Estimate of Onshore Transport.—From published data on beach slopes and significant waves for Southern California,[11,12] the following estimates are made for the section of California coast dealt with by Mr. Johnson: average beach slope α = 0.014, median sediment diameter D = 0.30 mm, and annual average deep-water wave characteristics H_o = 1.5 ft and T = 13 sec. For purposes of this rough estimate the beach slope will be assumed constant at the above average value and the entire beach, including the moving sand, will be assumed to be of the above size.

As was pointed out previously (and elsewhere[6]), q_s will vary from zero where $D = D_i$ to a maximum at the point on the offshore slope at which backrush from the breaker begins to exert forces on the moving sediment. Eqs. 7, 8, and 9 are not applicable outside this range. An average q_s for this range will be calculated and the fact that the profile is probably changing with time will be ignored.

For zero reflection and normal incidence of the given wave, the position of incipient motion of the given sediment may be calculated from Eq. 1 to be:

$$\left(d/L_o\right)_{\text{incipient}} = 0.064$$

This defines the point at which $q_s = 0$.

The breaker is estimated from the work of Keulegan[13] to be located at

$$\left(d/L_o\right)_{\text{breaker}} = 0.004$$

---

9 "Test of Nourishment of the Shore by Offshore Deposition of Sand," by J. V. Hall Jr. and W. J. Herron, Beach Erosion Bd. Tech. Memorandum No. 17, Washington, D. C., 1950.

10 "Restudy of Test-Shore Nourishment by Offshore Deposition of Sand, Long Branch, New Jersey," by R. L. Harris, Beach Erosion Bd. Tech. Memorandum No. 62, Washington, D. C., 1954.

11 "Movement of Sand Around Southern California Promontories," by P. D. Trask, Beach Erosion Bd. Tech. Memorandum No. 76, Washington, D. C., 1955.

12 "Beach Erosion Board Control Report on Cooperative Study of Orange County California," Appendix V, Phase I, June 15, 1959.

13 "Wave Motion," by G. H. Keulegan, Engineering Hydraulics, John Wiley and Sons, Inc., New York, 1950.

Since the point of initial breaker influence on the sediment motion is unknown, this last value will be used to define the point at which $q_s = q_{s_{max}}$.

The average of these two values will be used to calculate $q_{s_{avg.}}$:

$$\left(\frac{d}{L_o}\right)_{average} = \frac{0.064 + 0.004}{2} = 0.034$$

Evaluating Eq. 7 then yields:

$$q_s = 3.4 \times 10^3 \; A \; t \text{ tons per sq ft}^2 \text{ per year}$$

in which the submerged unit weight of transported solids is assumed to be 100 lb per cu ft.

If the sediment moves only to a depth of one particle diameter, the area, A in sq ft per ft, can be expressed:

$$A = n \; D \quad \ldots\ldots\ldots\ldots\ldots\ldots (12)$$

in which n is the porosity or the decimal percentage of a linear dimension parallel to the beach which is occupied by moving sediment at any instant.

Suppose $n = 0.1$ and $t = 0.3$, which seems reasonable. Then $q_s = 0.1$ tons per ft of shoreline per year or $q_s = 528$ tons per miles of shoreline per year.

For the 245 miles of coastline considered by Mr. Johnson, the total annual sediment supply by this means is, thus, only 130,000 tons or slightly more than 17% of the bed material estimated by Mr. Johnson to be delivered annually by the Santa Ynez River alone.

It must be pointed out that mechanisms, other than those considered here, enter the onshore-offshore transport process. In particular, the lighter sediments are put into suspension especially in the breaker region and are carried offshore near mid-depth by the return fluid mass-transport or are carried along-shore to be returned to sea by localized rip currents.

It should also be remembered that Eqs. 1 and 4 were developed using theoretical laminar near-bottom velocity distributions. Field conditions will almost certainly be turbulent in which case one would expect higher velocities of both fluid and sediment.

The foregoing analysis shows that useful quantitative estimates of wave-induced bed load sediment transport can now be made.

NATURAL BY-PASSING OF SAND AT COASTAL INLETS[a]

Discussion by J. R. Bowman

J. R. BOWMAN,[1] M. ASCE.—The authors have made a significant contribution to the better understanding of littoral drift problems associated with the improvement of coastal inlets. Although a remedy for every case obviously is not within the scope of the paper, the recognition and classification of the natural processes involved offer clues to methods adaptable to many coastal inlets that heretofore have been considered hopeless.

Of the several inlets treated in the paper, the writer is most appreciative of the problems associated with the ultimate stabilization and improvement of Oregon Inlet in eastern North Carolina. This inlet is situated near the northeastern end of Pamlico Sound, a sound which has a surface area of nearly 2,000 sq miles, and which drains an area of some 25,000 sq miles in North Carolina and Virginia. The principal outlets to the Atlantic Ocean are provided by three relatively narrow and shallow inlets, one of which is Oregon Inlet.

The writer takes exception to the authors' statements regarding the longevity of this inlet. A 20-mile reach of sand barrier reefs, in which Oregon Inlet is situated, has long been regarded as "inlet prone"; it is not unlikely that the "English maps of the sixteenth century" depicted only the earliest recorded of several inlets, known to have opened and closed in this vicinity between 1585 and 1845. Other historical sources indicate that the present inlet was opened by a seiche generated in Pamlico Sound during the passage of a tropical storm in September, 1846; the name of the inlet is believed to have been derived from the destination of the first cargo schooner to utilize the newly opened passage.

Oregon Inlet has migrated some two miles southward since 1846, as noted by the authors. The erosion of its south bank has long ago engulfed the sites of the first Bodie Island lighthouse, the original Oregon Inlet lifesaving station, and a fort built by troops of the Confederacy during the Civil War. Although the present Oregon Inlet lifeboat station was built well south of the inlet, a scant mile now separates the two; considerable encroachment has taken place as the result of hurricanes and severe winter storms during the past decade.

The authors' stated tide range of 5 ft is somewhat misleading, inasmuch as it appears to include storm tides, and thereby precludes a proper differentiation between the effects of storm and normal tidal action on sand by-passing processes. Tide gage records for Oregon Inlet are indicative of a mean tide range of 2 ft and a spring tide range only a fraction of a foot greater. At Hatteras Inlet, one of the other principal inlets to Pamlico Sound, mean tide ranges of 2 ft outside and 0.5 ft inside the inlet have been recorded.

---

[a] December, 1959, by P. Bruun and F. Gerritsen.

[1] Engr., Tidewater Constr. Corp., Norfolk, Va.

Inasmuch as the general arrangement of Oregon Inlet, in relation to its land and water environs, is not greatly dissimilar to that of Hatteras Inlet, it appears feasible to consider it as an inlet of the inadequate entrance type, in accordance with a system of inlet classification suggested by Caldwell.[2] Caldwell assumes that this type of inlet "is so inadequate that the tide range in the bay (sound) is only a small fraction of the tide range in the ocean." Moreover, "the time of strength of current in the inlet will tend to coincide with the times of high and low tide because the maximum hydraulic gradient will exist through the inlet at these times." Current velocities of about 4 fps have been measured in Hatteras Inlet under head differentials averaging 0.75 ft; it is not unreasonable to assume that velocities of similar magnitude occur in Oregon Inlet under normal tidal conditions.

During stormy periods, the tidal characteristics of the two inlets are similar, but they differ in the direction of winds to which they are most responsive. Whereas Hatteras Inlet is particularly responsive to southeast and northwest gales, the winds that produce the greater head differentials at Oregon Inlet are the more frequent northeast and southwest gales. Critical winds generated by tropical storms can be expected to occur at both inlets once every 2 or 3 years, on the average, but "hairy northeasters" are expected at least once each winter. The critical wind directions at Oregon Inlet are aligned with the longest fetch in Pamlico Sound, a distance of nearly 70 miles. During northeast storms at Oregon Inlet, heavy surf action is observed on the outer bar and along the shore, and tides at the entrance probably reach stages of 2 ft or 3 ft above normal; simultaneously, the waters of the sound are driven southwestward away from the inlet, exposing shoals that ordinarily are submerged by 2 ft or 3 ft. After the passage of a small hurricane in August, 1953, during which the sound was subjected to southwesterly gales for several hours, the writer observed high-water marks along the sound near Oregon Inlet estimated at 10 ft to 12 ft above normal sound levels. The steep hydraulic gradients and heavy surf action accompanying such storms have been responsible for the more aggravating occurrences of bank erosion and of shifting and shoaling of navigation channels at the inlet.

Oregon Inlet has been referred to as the gateway to Pamlico Sound and to the Outer Banks south of the inlet, a region that has become increasingly attractive by virtue of its commercial fishing and recreational opportunities. Exploitation of these potentials is hampered by the lack of adequate facilities for transportation into the region. Federal and state agencies have undertaken immediate remedial measures involving the dredging of a deeper channel through the inlet and outer bar (a project under way at this writing, and possibly the same one mentioned by the authors); and a bridge spanning the inlet to replace the present inadequate ferry system. The writer is not aware of any measures, in conjunction with either project, for preventing further migration of the inlet, or for ultimate stabilization of the navigation channel. The conclusions of the authors as to the instability of dredged channels as a sole means of improvement of certain types of inlets apply fully to Oregon Inlet; and the authors' predictions as to consequent events are verified by the amount of redredging that is required to complete the current channel improvement project.

---

[2] "Tidal Currents at Inlets in the United States," by Joseph M. Caldwell, ASCE, Proceedings, June, 1955.

A CASE OF CRITICAL SURGING OF A MOORED SHIP[a]

Discussion by W. C. Q. Joosting

W. C. Q. JOOSTING.[1]—The author is to be commended for having made a comprehensive application of surge theory, as far as developed to date, to the case of a particular ship. He arrives finally at the conclusion that the fifth harmonic (period 22 sec) of the known fundamental seiche across the harbour basin in question must have been responsible for the parting of the ropes of an 18,000 ton tanker.

The writer has been intimately connected with this occasion and would like to put forward some remarks on the details of the author's theory and some of the assumptions made, in the light of the more detailed knowledge available locally as regards the conditions in the harbour in question. As a result, he also wishes to present a different possible explanation of the cause of the ship breaking loose; in the writer's view, it is quite likely that the excessive movement of the ship was caused by the combined action of some 7 or 8 seiches with periods in the band of about 35 sec to 120 sec, which two different models have shown to exist in that part of the harbour.

Author's Theory and Application.—The general theory of the surging of a ship moored at a quay, along which a seiche is active, is now well established and explains clearly the principles involved in the motion of the ship, and the author has presented a very interesting and able application of this theory. However, there are some points of major and minor importance which call for clarification. It is hoped that the author will not take amiss the rather large number of questions raised. This is done to bring the theory nearer to its fully correct solution. The points will be treated in the order in which they appear in the paper.

a. In Table 1 the author gives a list of the harmonics of the transverse seiche in the harbour basin. On the tide gauge in that basin, only the fundamental period of about 110 sec is clearly visible, due to the small time scale and throttling of the water duct. This seiche is already not pure as it contains two nodes, one along and one across the middle of the rectangular basin. In his previous work, the author[2] had already found, in addition, another strong seiche, at about 99 sec (uncorrected), which was found to have one node along but two across the basin, and he, also, gave a formula with which the periods of seiches with various numbers of nodes in either direction could be calculated. Later model work by the writer, and confirmed by similar tests by a French firm, has shown that the main combinations given in Table 1 exist in this basin.

---

[a] December, 1959, by Basil W. Wilson.

[1] Dist. Engr., Research, South African Railways.

[2] "Origin and Effects of Long Period Waves in Ports," by B. W. Wilson, XIXth International Navigation Congress, 1957, Sect. II, Communication 1, Chapter 11, pp. 35-36, Fig. 13.

Thus, the seiches active in this basin are more numerous and of different constitution than those assumed to exist by the author.

b. The author states that he has conjectured the amplitudes of the various harmonic waves as shown in Fig. 7(b). Here two matters arise:

The amplitudes of the fundamental 110 sec seiche appear to be those indicated by the tide gauge. However, this gauge is located at a distance of several hundred feet from the corner of the basin, the wave height at which would be a measure of the seiches at the berth in question. Now, the model tests have shown that the wave height in that corner is about 40% greater than that at the tide gauge position, in respect of the 110 sec seiche. Accordingly, the wave height used in the calculations should be taken larger by that amount.

TABLE 1.—MAIN RESONANT SEICHES IN HARBOUR BASIN

Number of nodes	along	1	1	1	1	2	2	2	3	3	4	5
	across	1	2	3	4	1	2	4	3	4-5	4-5	5-6
Period, in seconds		106	94	80	69	59	54	49	36	34	27	21

On the other hand, it would seem to the writer that the wave heights assumed for the harmonic seiches are a little on the high side. The author gives, in Fig. 7(b), a ratio of the fundamental and 2nd and 5th harmonics of about 1 : 0.75 : 0.55. It is not stated on what basis these heights were adopted; the South African and French model tests show that operation with a constant input wave height at the wave generator results, due to the layout of the harbour, its protection by the breakwater and the position of the entrance to the basin, in approximate direct proportionality between the heights of the main resonance peaks and the wave period. Consequently, it is thought that a ratio of 1 : 0.5 : 0.2 would have been more appropriate as a likely assumption.

But in that case, the fifth harmonic would become too small to be responsible for excessive movement of the ship so that the author's conclusion would be invalidated.

c. The author's geometrical deductions as to the tension-extension characteristics of the moorings have been accepted though not checked. However, in Fig. 4, it would seem that the markings of the lines for moorings (1), (2), and (3) have been inadvertently interchanged.

In the same figure, it is seen that at the time of docking, due to the assumptions made in respect of the relative slacks at the three mooring positions, the back-springs (4) take almost all the strain consequent on movement of the ship. Would not the ropes be made fast in such a way that they would be subject to approximately equal stresses at the relatively small movement of the ship at docking? This would reverse the author's assumptions as to the relative slacks: (1) and (2) would have the least and (4) the greatest slack instead of vice-versa; all three curves would intersect at a point of equal stress, say 4 tons, at a ship deflection of, say, 1.3 ft.

d. In the development of the equations of motion (Eq. 12), the author uses the mathematical contraction ζ which has the dimension of a velocity and, as such, has little meaning. A real convenient physical quantity would have been

obtained by using the factor $\zeta/\sigma = -H'$. In that case, Eq. 16 would become, with $\sigma \simeq \sqrt{gd}$:

$$-\frac{\zeta}{\sigma} = H' = H \frac{\sinh kd - \sinh ks}{kD \cosh kd} \frac{\sin k\,l}{k\,l} \sin kb \quad \ldots\ldots (16a)$$

in which H is the amplitude of the horizontal water movement at the node of the seiche, and H', consequently, denotes the actual horizontal "driving" amplitude, corrected for depth of immersion of the ship, its length and its position in the seiche.

e. The writer considers that, to be fully correct, another correction factor should be added to Eq. 16(a) in order to account for the fact that the seiche is disturbed by the proximity of the ship to the quay and the seabed; however, no suitable values seem to be available as yet for this factor which can only be determined experimentally.

f. As regards the influence of the ship's length, the author's factor $\frac{\sin k\,l}{k\,l}$ relates to the influence of the acceleration of the water past the ship only. But this influence is small ($C_M - 1 \simeq 0.16$) as compared with that of the slope of the wave on which the ship rides down, which is the main driving force. With a ship as long as the wave ($k\,l = \pi$), this factor would become zero, which is obviously impossible as, with such a ship at the node of the wave, one half of the ship is pushed upwards while the other half is pulled down so that it cannot lie in the horizontal plane. This is shown clearly in Fig. 1.

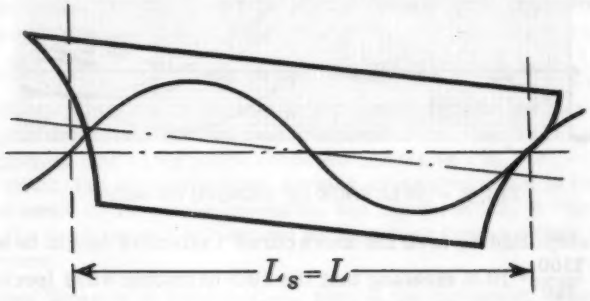

FIG. 1.—SLOPE OF SHIP AT NODE OF SEICHE.

The horizontal position is only reached with a ship that is considerably longer than the seiche wave. The full formula was published elsewhere[3] by the writer 3 years ago. However, the acceleration of the water had then been taken at full value ($C_M = 2$) while later developments have shown that it only acts to the extent of ($C_M - 1 \simeq 0.16$). The correct factor for the influence of the length of the ship is therefore:

$$c_l = \frac{\left(C_M - 1\right)\frac{\sin k\,l}{k\,l} + 3\left[\frac{\sin k\,l - k\,l \cos k\,l}{(k\,l)^3}\right]}{C_M} \quad \ldots\ldots (1)$$

[3] "Investigation into Long Period Waves in Ports," by W. C. Q. Joosting; XIXth International Navigation Congress, 1957, Section II, Communication 1, Eqs. (17) and (21), pp. 225-226.

The length 2l of the ship used in the calculations must, of course, be the "effective" length which is slightly less than the overall length due to the shape of stern and bow. The difference will be of the order of 10% to 15% so that in this case an effective length of about 420 ft should be reasonable. Using this length with a ship as long as the wave and the author's value $C_M = 1.16$, the factor becomes $c_1 = 0.262$ which is anything but zero. Similarly, the horizontal position of the ship is obtained when the effective length of the ship is 1.362 times that of the wave.

This factor is represented in Fig. 2, as a function of the ratio between the effective length of the ship and that of the wave, with $C_M = 1.38$, which includes the effect of the proximity to quay and seabed and would seem to cover most cases well.

h. The author puts forward Eqs. 19 to prove that the ship was inevitably prone to surging. In Eq. 19(i), apart from the fact that this condition would have to be revised according to the writer's Eq. 1, the author uses the overall

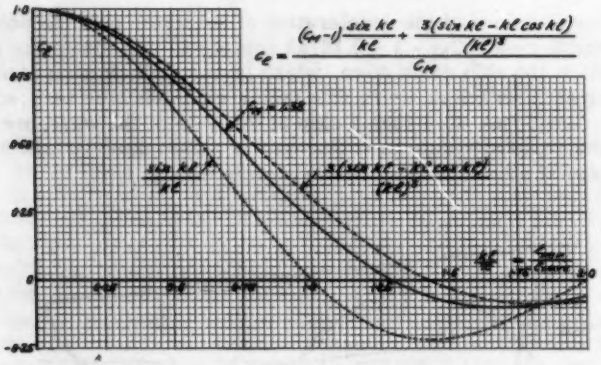

FIG. 2.—INFLUENCE OF LENGTH OF SHIP.

length of the ship. Had he used the more correct effective length he would have obtained $\frac{B}{l} = \frac{2100}{210} = 10.0$, meaning that the 10th harmonic wave (period 11 sec) would not contribute to surging of the ship. In the writer's opinion the statement should rather be that "ships are inevitably prone to surging, except at those periods for which Eq. 19 give a value in the vicinity of an integer number."

i. Eq. 20(i) would have to be corrected to fit the writer's Eq. 1. Values of p greater than unity need hardly be considered as then k l becomes large so that $\frac{\sin/kl}{kl}$ becomes small with, consequently, little action on the ship.

j. It is not clear how the author obtained a cosine function in Eq. 21. The original differential equation leads naturally to:

$$X = X_1 \sin(\phi - \alpha) \quad \ldots\ldots\ldots\ldots\ldots\ldots \quad (2)$$

The cosine function leads to an unnatural phase angle which has to be corrected by 90° to get the correct relationship between the ship movement and that of the water.

k. Had the author used, in Eq. 22(i), the writer's factor $-\frac{\zeta}{\sigma} = H'$, this equation would have reduced to

$$X_1^n \Delta(n) \left(\frac{\omega}{\sigma}\right)^2 - X_1 = H' \quad \ldots\ldots\ldots\ldots \quad (3)$$

which would then have constituted a physically clear relationship between the properties of the ship, the moorings and the water.

l. Eq. 22, apart from the prior-mentioned shift by 90°, seems to contain an error; as given, the phase angle is permanently tan $\alpha = -\infty$, when the damping is neglected ($2\beta \to 0$), as is done in the remaining calculations. The expression should read:

$$\tan \alpha = \frac{\sigma}{2\beta\ \omega} \quad \frac{(2\beta)^2 + \left(\frac{\sigma}{\omega}\right)^2}{X_1^{n-1} \Delta(n)} - 1 \quad \ldots\ldots\ldots\ldots \quad (4)$$

However, with the sine function (Eq. 2), the correct phase angle—that between the horizontal movements of the ship and water—is given by:

$$\tan \alpha \quad \frac{\left(\frac{2\beta\ \omega}{\sigma}\right) X_1^{n-1} \Delta(n)}{(2\beta)^2 + \left(\frac{\sigma}{\omega}\right)^2 - X_1^{n-1} \Delta(n)} \quad \ldots\ldots\ldots\ldots \quad (5)$$

This is in agreement with the phase angles for normal linear spring systems.

m. From Fig. 7(a), the amplitude of the 110 second seiche, at the time of maximum response at noon, was 8 in. At the corner of the basin, as explained above, its amplitude would be 1.4 x 8 = 11.2 in. The fifth harmonic, as stated by the writer, would possibly have an amplitude at that position of $\frac{11.2}{5 \times 12} = 0.187$ ft. If, further, this wave amplitude is corrected for the position of the ship and its length, the effective wave amplitude will be A' = 0.187 x 0.96 x 0.755 = 0.136 ft. Applying this value to the response curves of Fig. 7(d), it is seen that at no time could the ship have been surging excessively due to the effects of the fifth harmonic of the seiche unless the sea wave exciting it was about twice as high as the fundamental 110 second wave, which seems highly unlikely for various reasons.

Alternative Solution to Problem.—In view of the foregoing, supported by the writer's experience that ship surging, generally, does not seem to contain much movement at periods of less than about 30 sec, the problem has been examined again and it has been found that, in this particular case, it may well be that the ship broke loose due to the combined action of several of the longer period water oscillations listed in Table 1.

Of course, once a few ropes had parted, the maximum response of the ship shifted to slightly larger periods with an increase in the maximum tension per rope, so that then only one or two periods, probably between 30 sec and 40 sec, may have been responsible for the inability to re-moor the ship.

For clarity, the basic response Eq. 3 is given here once more, using the various physical factors involved:

$$\frac{R_x}{c_n\ c_b\ C_M\ M} - \sigma^2 X_1 = H' = - c_1\ c_p\ \sigma\ A \sqrt{\frac{g}{d}} \quad \ldots\ldots \quad (6)$$

where, in addition to the author's notation c_n denotes the factor for exponential response = $1/\Delta(n)$, c_b is the factor for proximity to quay and seabed $\simeq 1.2$, c_l is the factor for length of ship = Eq. 1, c_p represents the factor for position of ship = sin kb, A is the amplitude of seiche in corner of basin, and H' denotes the effective amplitude of horizontal water movement.

Strictly speaking, the proximity of the ship to quay and seabed will have a different influence on the water acceleration and wave slope, respectively, but no separate values are available. It would seem that $c_b = 1.2$ could be accepted as a reasonable approximation.

Furthermore, as previously mentioned, it was found that, in the basin in question, the amplitudes of the resonant seiches could be considered to be proportional to their periods so that the quantity σ A can be replaced by the factor $2\pi c_a A_o/\tau_o$, where A_o is the amplitude of the 106 sec seiche discernible on the tide gauge, τ_o its period and $c_a = 1.4$ to account for the difference in height of the waves indicated on the gauge and in the corner of the basin. This gives $\sigma A = 0.083 A_o$.

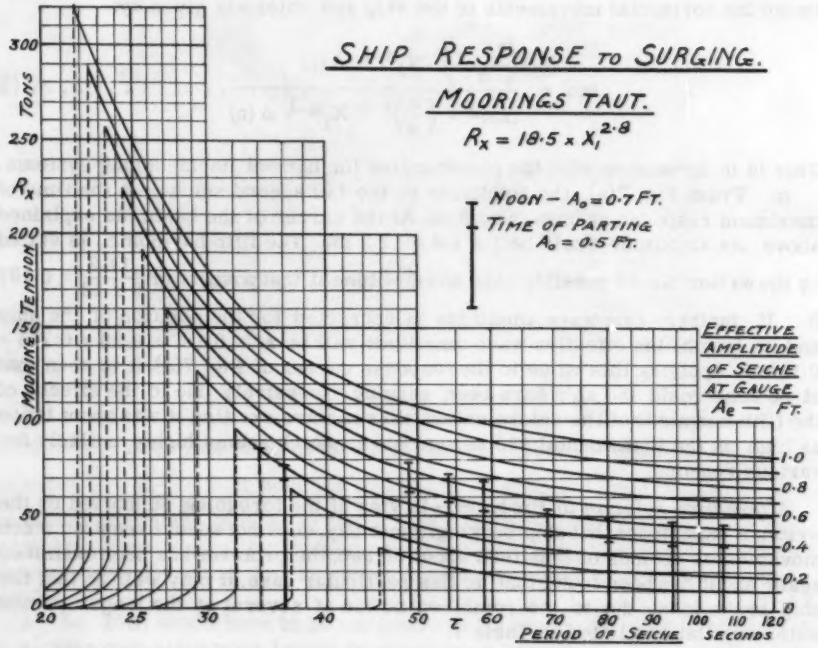

FIG. 3.—SHIP RESPONSE CURVES.

The value of $\Delta(n)$ can be obtained from a rather cumbersome integration. However, the factor $c_n = \frac{1}{\Delta(n)}$ can be very closely represented by $c_n = 1 + 0.2$ (n - 1).

The values of the other quantities are, as given by the author: $C_M = 1.16$; d = 43 ft; g = 32.14 ft per sq sec at the latitude of the harbour, and M = 560 tons sq sec per ft. The values c_l and c_p have to be obtained from their respective equations for each seiche.

The solution will be developed for the conditions at the time the ropes began parting, that is 10:30 a.m. From the author's Figs. 4 and 5 the mooring force—ship amplitude relation—can be assessed at approximately:

$$R_x = C\ X_1^n = 18.5\ X_1^{2.8} \quad \ldots\ldots\ldots\ldots\ldots\ (7)$$

Inserting the Eq. 7 into Eq. 6 and using only mooring tensions results in

$$R_x - \frac{14763\ R_x^{1/2.8}}{\tau^2} = -\ 76.38\ A_e \quad \ldots\ldots\ldots\ (8)$$

in which $A_e = c\ c_p\ A_o$ is now the effective water amplitude indicated by the tide gauge in respect of the fundamental 106 sec seiche, corrected for length and position of the ship.

Fig. 3 shows the relationship between the mooring forces R_x and the period τ of the seiche at various effective seiche amplitudes A_e from 0 ft to 1 ft.

Now, the effective water amplitude A_e can be found from the fact that, at the time of parting of the ropes, the fundamental seiche indicated on the tide gauge had an amplitude of about $A_o = 0.5$ ft, as shown in Fig. 7(b). The corrections to be applied for the various seiches are listed in Table 2 as well as the resulting effective amplitudes A_e:

TABLE 2.—EFFECTIVE SEICHE AMPLITUDES

Period, in Seconds	Nodality		c_1	c_p	A_o, in feet	A_e, in feet
	m	n				
106, 94, 80, 69	1	1,2,3,4	0.988	0.773	0.5	0.381
59, 54, 49	2	1,2,4	0.955	0.981	0.5	0.468
36, 34	3	3, 4-5	0.900	0.473	0.5	0.213
27	4	4-5	0.825	0.381	0.5	0.157
21	5	5-6	0.737	0.956	0.5	0.352

Plotting these values of A_e as vertical lines in Fig. 3 at their corresponding periods gives the various mooring forces which would be obtained if each seiche were acting alone. It is seen that only the longer periods cause relatively large forces; the short periods lie below the maximum response conditions.

If the forces, due to the various seiches, are added together, a total force of about 390 tons is obtained. However, it must be considered that all the component movements are hardly ever in phase with each other. It would seem reasonable to expect that surges on the moorings of about half this maximum, or 195 tons, can be expected fairly frequently at the appropriate moments. Now, since there are the equivalent of 12 coir ropes of 18 in. holding the ship in each direction, the average surge force per rope would be about 16 tons.

Considering the influence of age, distribution and unequal response of the moorings, a mean breaking strength of 15 tons can be taken as reasonable, as stated by the author under the heading "Elastic Properties of the Mooring Ropes," so that it seems quite possible that parting of the ropes was initiated in this manner.

Subsequently, surging increased to reach a maximum, at noon, of $A_o = 0.7$ ft. The mooring forces increased correspondingly, and an additional force, at a period of 34 sec, overcame the jump-period, so that at noon, if all the moorings had still been present, the 50% total force would have reached 288 tons, or 24 tons per rope. In addition, the moving liquid load of the tanker may have assisted the surging.

As a matter of interest Fig. 4 has been compiled, giving the response conditions with the same basic values except that the moorings are assumed to have 1 ft more slack, so that $R_x = 6.9\ X_1^{3.5}$ represents the approximate mooring characteristics.

It is seen that the periods of maximum response now lie at somewhat higher values, and that the mooring forces at the periods beyond the maximum

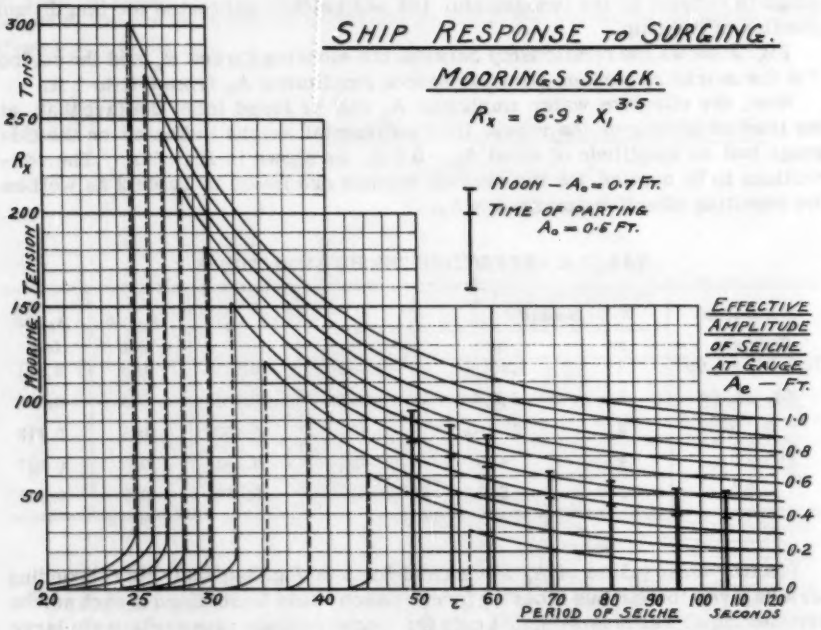

FIG. 4.—RESPONSE CURVES WITH EXTRA SLACK.

response are a little greater, while the maximum response forces have decreased a little. The effect of the shift in the maximum response periods is that the 34 sec and 36 sec periods do not contribute any more. At the same time, the movement at the longer periods leads to slightly higher mooring forces. The net result is that the 50% total force is about the same as before—192 tons or 16 tons per rope—at the time of parting.

At noon, the time of maximum surge conditions, the water amplitudes were still not high enough to cause any shorter periods to have any influence; the total 50% force then became 245 tons or 20 tons per rope which is some improvement on the 24 tons with tauter moorings. Under certain conditions, it may, therefore, be of advantage to slacken the ropes.

Better results could be obtained by providing moorings which all have the same tension - extension characteristics. An approach to this requirement could be made by moving, especially, the back springs to some other position, or by making them more elastic by inserting longer coir springs.

The technical papers published in the past year are identified by number below. Technical-division sponsorship is indicated by an abbreviation at the end of each Paper Number, the symbols referring to: Air Transport (AT), City Planning (CP), Construction (CO), Engineering Mechanics (EM), Highway (HW), Hydraulics (HY), Irrigation and Drainage (IR), Pipeline (PL), Power (PO), Sanitary Engineering (SA), Soil Mechanics and Foundations (SM), Structural (ST), Surveying and Mapping (SU), and Waterways and Harbors (WW), divisions. Papers sponsored by the Department of Conditions of Practice are identified by the symbols (PP). For titles and order coupons, refer to the appropriate issue of "Civil Engineering." Beginning with Volume 33 (January 1956) papers were published in Journals of the various Technical Divisions. To locate papers in the Journals, the symbols after the paper number are followed by a numeral designating the issue of a particular Journal in which the paper appeared. For example, Paper 2290 is identified as 2290(ST9) which indicates that the paper is contained in the Journal of the Structural Division during 1956.

VOLUME 85 (1959)

JUNE: 2049(CP1), 2049(CP1), 2050(CP1), 2051(CP1), 2052(CP1), 2053(CP1), 2054(CP1), 2055(CP1), 2056(HY6), 2057(HY6), 2058(HY6), 2059(IR3), 2060(IR2), 2061(PO2), 2062(SM3), 2063(SM3), 2064(SM3), 2065(ST6), 2066(WW2), 2067(WW2), 2068(WW2), 2069(WW2), 2070(WW2), 2071(WW2), 2072(CP1)[c], 2073(IR2)[c], 2074(PO3)[c], 2075(ST6)[c], 2076(HY6)[c], 2077(EM3)[c], 2078(WW2)[c].

JULY: 2079(HY7), 2080(HY7), 2081(HY7), 2082(HY7), 2083(HY7), 2084(HY7), 2085(HY7), 2086(SA4), 2087(SA4), 2088(SA4), 2089(SA4), 2090(SA4), 2091(EM3), 2092(EM3), 2093(EM3), 2094(EM3), 2095(EM3), 2096(EM3), 2097(HY7)[c], 2098(SA4)[c], 2099(EM3)[c], 2100(AT3), 2101(AT3), 2102(AT3), 2103(AT3), 2104(AT3), 2105(AT3), 2106(AT3), 2107(AT3), 2108(AT3), 2109(AT3), 2110(AT3), 2111(AT3), 2112(AT3), 2113(AT3), 2114(AT3), 2115(AT3), 2116(AT3), 2117(AT3), 2118(AT3), 2119(AT3), 2120(AT3), 2121(AT3), 2122(AT3), 2123(AT3), 2124(AT3), 2125(AT3).

AUGUST: 2126(HY8), 2127(HY8), 2128(HY8), 2129(HY8), 2130(PO4), 2131(PO4), 2132(PO4), 2133(PO4), 2134(SM4), 2135(SM4), 2136(SM4), 2137(SM4), 2138(HY8)[c], 2139(PO4)[c] 2140(SM4)[c].

SEPTEMBER: 2141(CO2), 2142(CO2), 2143(CO2), 2144(HW3), 2145(HW3), 2146(HW3), 2147(HY9), 2148(HY9), 2149(HY9), 2150(HY9), 2151(IR3), 2152(ST7)[c], 2153(IR3), 2154(IR3), 2155(IR3), 2156(IR3), 2157(IR3), 2158(IR3), 2159(IR3), 2160(IR3), 2161(SA5), 2162(SA5), 2163(ST7), 2164(ST7), 2165(SU1), 2166(SU1), 2167(WW3), 2168(WW3), 2169(WW3), 2170(WW3), 2171(WW3), 2172(WW3), 2173(WW3), 2174(WW3), 2175(WW3), 2176(WW3), 2177(WW3), 2178(CO2)[c], 2179(IR3)[c], 2180(HW3)[c], 2181(SA5)[c], 2182(HY9)[c], 2183(SU1)[c], 2184(WW3)[c], 2185(PP2)[c], 2186(ST7)[c], 2187(PP2), 2188(PP2).

OCTOBER: 2189(AT4), 2190(AT4), 2191(AT4), 2192(AT4), 2193(AT4), 2194(EM4), 2195(EM4), 2196(EM4), 2197(EM4), 2198(EM4), 2199(EM4), 2200(HY10), 2201(HY10), 2202(HY10), 2203(PL3), 2204(PL3), 2205(PL3), 2206(PO5), 2207(PO5), 2208(PO5), 2209(PO5), 2210(SM5), 2211(SM5), 2212(SM5), 2213(SM5), 2214(SM5), 2215(SM5), 2216(SM5), 2217(SM5), 2218(ST8), 2219(ST8), 2220(EM4), 2221(ST8), 2222(ST8), 2223(ST8), 2224(HY10), 2225(HY10), 2226(PO5), 2227(PO5), 2228(PO5), 2229(ST8), 2230(EM4), 2231(EM4), 2232(AT4)[c], 2233(PL3)[c], 2234(EM4)[c], 2235(HY10)[c], 2236(SM5)[c], 2237(ST8)[c], 2238(PO5)[c], 2239(ST8), 2240(PL3).

NOVEMBER: 2241(HY11), 2242(HY11), 2243(HY11), 2244(HY11), 2245(HY11), 2246(SA6), 2247(SA6), 2248(SA6), 2249(SA6), 2250(SA6), 2251(SA6), 2252(SA6), 2253(SA6), 2254(SA6), 2255(SA6), 2256(ST9), 2257(ST9), 2258(ST9), 2259(ST9), 2260(HY11), 2261(ST9)[c], 2262(ST9), 2263(HY11), 2264(ST8), 2265(HY11), 2266(SA6), 2267(SA6), 2268(SA6), 2269(HY11)[c], 2270(ST9).

DECEMBER: 2271(HY12)[c], 2272(CP2), 2273(HW4), 2274(HW4), 2275(HW4), 2276(HW4), 2277(HW4), 2278(HW4), 2279(HW4), 2280(HW4), 2281(IR4), 2282(IR4), 2283(IR4), 2284(IR4), 2285(PO6), 2286(PO6), 2287(PO6), 2288(PO6), 2289(PO6), 2290(PO6), 2291(PO6), 2292(SM6), 2293(SM6), 2294(SM6), 2295(SM6), 2296(SM6), 2297(WW4), 2298(WW4), 2299(WW4), 2300(WW4), 2301(WW4), 2302(WW4), 2303(WW4), 2304(HW4), 2305(ST10), 2306(CP2), 2307(CP2), 2308(ST10), 2309(CP2), 2310(HY12), 2311(HY12), 2312(PO6), 2313(PO6), 2314(ST10), 2315(HY12), 2316(HY12), 2317(HY12), 2318(WW4), 2319(SM6), 2320(SM6), 2321(ST10), 2322(ST10), 2323(HW4)[c], 2324(CP2)[c], 2325(SM6)[c], 2326(WW4)[c], 2327(IR4)[c], 2328(PO6)[c], 2329(ST10)[c], 2330(CP2).

VOLUME 86 (1960)

JANUARY: 2331(EM1), 2332(EM1), 2333(EM1), 2334(EM1), 2335(HY1), 2336(HY1), 2337(EM1), 2338(EM1), 2339(HY1), 2340(HY1), 2341(SA1), 2342(EM1), 2343(SA1), 2344(ST1), 2345(ST1), 2346(ST1), 2347(ST1), 2348(EM1)[c], 2349(HY1)[c], 2350(ST1), 2351(ST1), 2352(SA1)[c], 2353(ST1)[c], 2354(ST1).

FEBRUARY: 2355(CO1), 2356(CO1), 2357(CO1), 2358(CO1), 2359(CO1), 2360(CO1), 2361(PO1), 2362(HY2), 2363(ST2), 2364(HY2), 2365(SU1), 2366(HY2), 2367(SU1), 2368(SM1), 2369(HY2), 2370(SU1), 2371(HY2), 2372(PO1), 2373(SM1), 2374(HY2), 2375(PO1), 2376(HY2), 2377(CO1)[c], 2378(SU1), 2379(SU1), 2380(SU1), 2381(HY2)[c], 2382(ST2), 2383(SU1), 2384(ST2), 2385(SU1)[c], 2386(SU1), 2387(SU1), 2388(SU1), 2389(SM1), 2390(ST2)[c], 2391(SM1)[c], 2392(PO1)[c].

MARCH: 2393(IR1), 2394(IR1), 2395(IR1), 2396(IR1), 2397(IR1), 2398(IR1), 2399(IR1), 2400(IR1), 2401(IR1), 2402(IR1), 2403(IR1), 2404(IR1), 2405(IR1), 2406(IR1), 2407(SA2), 2408(SA2), 2409(HY3), 2410(ST3), 2411(SA2), 2412(HW1), 2413(WW1), 2414(WW1), 2415(HY3), 2416(HW1), 2417(HW3), 2418(HW1)[c], 2419(WW1)[c], 2420(WW1), 2421(WW1), 2422(WW1), 2423(WW1), 2424(SA2), 2425(SA2)[c], 2426(HY3)[c], 2427(ST3)[c].

APRIL: 2428(ST4), 2429(HY4), 2430(PO2), 2431(SM2), 2432(PO2), 2433(ST4), 2434(EM2), 2435(PO2), 2436(ST4), 2437(ST4), 2438(HY4), 2439(EM2), 2440(EM2), 2441(ST4), 2442(SM2), 2443(HY4), 2444(ST4), 2445(EM2), 2446(ST4), 2447(EM2), 2448(SM2), 2449(HY4), 2450(ST4), 2451(HY4), 2452(HY4), 2453(EM2), 2454(EM2), 2455(EM2)[c], 2456(HY4)[c], 2457(PO2)[c], 2458(ST4)[c], 2459(SM2)[c].

MAY: 2460(AT1), 2461(ST6), 2462(AT1), 2463(AT1), 2464(CP1), 2465(CP1), 2466(AT1), 2467(AT1), 2468(SA3), 2469(HY5), 2470(ST5), 2471(SA3), 2472(SA3), 2473(ST5), 2474(SA3), 2475(ST5), 2476(SA3), 2477(ST5), 2478(HY5), 2479(SA3), 2480(ST5), 2481(SA3), 2482(CO2), 2483(CO2), 2484(HY5), 2485(HY5), 2486(AT1)[c], 2487(CP1)[c], 2488(CO2)[c], 2489(CP1)[c], 2490(SA3)[c], 2491(ST5)[c], 2492(CP1), 2493(CO2).

JUNE: 2494(IR2), 2495(IR2), 2496(ST9), 2497(EM3), 2498(EM3), 2499(EM3), 2500(EM3), 2501(SM3), 2502(EM3), 2503(PO3), 2504(WW2), 2505(EM3), 2506(HY6), 2507(WW2), 2508(PO3), 2509(ST6), 2510(EM3), 2511(EM3), 2512(ST6), 2513(HY6), 2514(HY6), 2515(PO3), 2516(EM3), 2517(WW2), 2518(WW2), 2519(EM3), 2520(PO3), 2521(ST6), 2522(SM3), 2523(ST9), 2524(HY6), 2525(HY6), 2526(HY6), 2527(IR2), 2528(ST9), 2529(HW2), 2530(IR2), 2531(HY6), 2532(EM3)[c], 2533(WW2)[c], 2534(WW2), 2535(HY6)[c], 2536(IR2)[c], 2537(PO3)[c], 2538(SM3)[c], 2539(ST6)[c], 2540(WW2)[c].

c. Discussion of several papers, grouped by divisions.

AMERICAN SOCIETY OF CIVIL ENGINEERS

OFFICERS FOR 1960

PRESIDENT

FRANK A. MARSTON

VICE-PRESIDENTS

Term expires October, 1960:
PAUL L. HOLLAND
LLOYD D. KNAPP

Term expires October, 1961:
CHARLES B. MOLINEAUX
LAWRENCE A. ELSENER

DIRECTORS

Term expires October, 1960:
PHILIP C. RUTLEDGE
WESTON S. EVANS
TILTON E. SHELBURNE
CRAIG P. HAZELET
DONALD H. MATTERN
JOHN E. RIBNE

Term expires October, 1961:
THOMAS J. FRATAR
EARL F. O'BRIEN
DANIEL B. VENTRES
CHARLES W. BRITZIUS
WAYNE G. O'HARRA
FRED H. RHODES, JR.
N. T. VEATCH

Term expires October, 1962:
ELMER K. TIMBY
SAMUEL S. BAXTER
THOMAS M. NILES
TRENT R. DAMES
WOODROW W. BAKER
BERNHARD DORNBLATT

PAST PRESIDENTS

Members of the Board

LOUIS R. HOWSON
FRANCIS S. FRIEL

EXECUTIVE SECRETARY
WILLIAM H. WISELY

TREASURER
E. LAWRENCE CHANDLER

ASSISTANT TREASURER
ENOCH R. NEEDLES

PROCEEDINGS OF THE SOCIETY

HAROLD T. LARSEN
Manager of Technical Publications

PAUL A. PARISI
Editor of Technical Publications

MARVIN L. SCHECHTER
Associate Editor of Technical Publications

IRVIN J. SCHWARTZ
Assistant Editor of Technical Publications

COMMITTEE ON PUBLICATIONS

PHILIP C. RUTLEDGE, *Chairman*

THOMAS M. NILES, *Vice-Chairman*

TILTON E. SHELBURNE
WESTON S. EVANS
WAYNE G. O'HARRA
BERNHARD DORNBLATT